



Review

Trends in Satellite Earth Observation for Permafrost Related Analyses—A Review

Marius Philipp ^{1,2,*}, **Andreas Dietz** ², **Sebastian Buchelt** ³ and **Claudia Kuenzer** ^{1,2}¹ Department of Remote Sensing, Institute of Geography and Geology, University of Wuerzburg, D-97074 Wuerzburg, Germany; Claudia.Kuenzer@dlr.de² German Remote Sensing Data Center (DFD), German Aerospace Center (DLR), Muenchner Strasse 20, D-82234 Wessling, Germany; Andreas.Dietz@dlr.de³ Department of Physical Geography, Institute of Geography and Geology, University of Wuerzburg, D-97074 Wuerzburg, Germany; sebastian.buchelt@uni-wuerzburg.de

* Correspondence: marius.philipp@uni-wuerzburg.de

Abstract: Climate change and associated Arctic amplification cause a degradation of permafrost which in turn has major implications for the environment. The potential turnover of frozen ground from a carbon sink to a carbon source, eroding coastlines, landslides, amplified surface deformation and endangerment of human infrastructure are some of the consequences connected with thawing permafrost. Satellite remote sensing is hereby a powerful tool to identify and monitor these features and processes on a spatially explicit, cheap, operational, long-term basis and up to circum-Arctic scale. By filtering after a selection of relevant keywords, a total of 325 articles from 30 international journals published during the last two decades were analyzed based on study location, spatio-temporal resolution of applied remote sensing data, platform, sensor combination and studied environmental focus for a comprehensive overview of past achievements, current efforts, together with future challenges and opportunities. The temporal development of publication frequency, utilized platforms/sensors and the addressed environmental topic is thereby highlighted. The total number of publications more than doubled since 2015. Distinct geographical study hot spots were revealed, while at the same time large portions of the continuous permafrost zone are still only sparsely covered by satellite remote sensing investigations. Moreover, studies related to Arctic greenhouse gas emissions in the context of permafrost degradation appear heavily underrepresented. New tools (e.g., Google Earth Engine (GEE)), methodologies (e.g., deep learning or data fusion etc.) and satellite data (e.g., the Methane Remote Sensing LiDAR Mission (Merlin) and the Sentinel-fleet) will thereby enable future studies to further investigate the distribution of permafrost, its thermal state and its implications on the environment such as thermokarst features and greenhouse gas emission rates on increasingly larger spatial and temporal scales.



Citation: Philipp, M.; Dietz, A.; Buchelt, S.; Kuenzer, C. Trends in Satellite Earth Observation for Permafrost Related Analyses—A Review. *Remote Sens.* **2021**, *13*, 1217. <https://doi.org/10.3390/rs13061217>

Academic Editor: Magaly Koch

Received: 22 January 2021

Accepted: 18 March 2021

Published: 23 March 2021

Publisher's Note: MDPI stays neutral with regard to jurisdictional claims in published maps and institutional affiliations.



Copyright: © 2021 by the authors. Licensee MDPI, Basel, Switzerland. This article is an open access article distributed under the terms and conditions of the Creative Commons Attribution (CC BY) license (<https://creativecommons.org/licenses/by/4.0/>).

1. Introduction

1.1. Permafrost in a Warming World

Permafrost covers approximately one quarter of exposed land on the Northern Hemisphere and is therefore an essential component of the cryosphere [1]. Almost twice the amount of carbon is stored in its frozen masses compared to the carbon content in the atmosphere [2,3]. A thawing of permafrost causes the release of said carbon stocks to the atmosphere as greenhouse gases, which could accelerate climate change even faster than projected by current Earth system models [2]. Without mitigating action, abrupt methane releases associated with permafrost thaw are hereby predicted to cause trillions of dollars in global economic damage [4]. Thus, a widespread degradation of permafrost has substantial consequences for the environment and human society. The development of geohazards [5], a deepening of the active layer [6], amplified surface deformation rates [7–9] as well as

coastal erosion [10–12] and emerging greenhouse gases [13–15] are thereby just some of the implications of thawing permafrost driven by climate change.

Temperatures in the Arctic increased more than twice as fast as the global average, which is commonly referred to as Arctic amplification [16]. Weather stations across the Northern High Latitudes (NHL) revealed annual mean surface air temperatures to have risen by nearly 2 °C since 1900, with the largest part of warming taking place during the autumn and winter months [17]. The extent of snow cover on the Northern Hemisphere has decreased by 7–11% during the 1970–2010 period compared to pre-1970 values in March and April [18]. Earlier and prolonged non-frozen seasons in recent years have been identified as a major driver for Arctic greening [19]. Moreover, projections of future vegetation cover based on various climate change scenarios and the Circumpolar Arctic Vegetation Map (CAVM) suggest at least half of vegetated areas in the Arctic will shift to a different class by the 2050s [20].

A crucial component of the Arctic and also subjected to climate change is the distribution and thermal state of permafrost. Permafrost is defined as ground material, which remains frozen for at least two consecutive years [21]. The importance of permafrost becomes all the more prevalent, when considering that roughly 24% of exposed land on the Northern Hemisphere and more than 65% of terrestrial area above 60° N is underlain by permanently frozen ground (Figure 5) [22,23]. The uppermost ground layer of varying thickness that seasonally freezes and thaws in areas underlain by permafrost is called the active layer [24]. Understanding the thermal state of permafrost and the associated dynamics in the active layer thickness are hereby crucial characteristics for the assessment of permafrost degradation [25,26]. Within permafrost, also layers and bodies of unfrozen ground can be present in the form of taliks and cryopegs [21]. Taliks are hereby divided into open taliks which completely penetrate the permafrost layer and therefore connecting supra- and sub-permafrost water, whereas closed taliks refer to a depression in the permafrost table below rivers and lakes [21,27]. Cryopegs on the other hand are defined as perennially cryotic (<0 °C) soils that remain unfrozen due to the presence of dissolved-solids in the pore water [21]. Increasing temperatures of permafrost are reported for most regions with frozen ground [28]. As stated in the Intergovernmental Panel on Climate Change (IPCC) Special Report on the Ocean and Cryosphere in Changing Climate (2019), temperatures of permafrost have reached a record high since the 1980s with recent warming numbers of $0.29\text{ °C} \pm 0.12\text{ °C}$ from 2007–2016 as a global average across high-mountain and polar regions [3]. Consequently, future projections on the distribution of permafrost are consistently predicting a drastic reduction of permafrost extent [29–31].

Definition of Permafrost:

Permafrost, also described as permanently frozen ground, is defined as ground (sediment, soil, or rock) which remains continuously frozen for at least two consecutive years [32]. Permafrost is commonly divided into different zones depending on the percentage of frozen ground in a given area [1]:

Continuous: 100–90%; Discontinuous: 90–50%; Sporadic: 50–10%; Isolated: <10%

The degradation of permafrost has major implications for the environment. A variety of related landscape features and processes are visualized by the infographic in Figure 1, such as emerging greenhouse gas emissions [33–38], coastal erosion [39–42], amplified surface deformation rates due to frost heave or thaw settlement [43–46], landslides [47–49], increasing depths of the active layer [50–52], thermokarst lakes and ponds [53–56], wild fires [57–59], changing rock glacier kinematics [47,60,61], patterned ground [62,63], and thaw slump activities [64–66]. The reorganization of hydrological flowpaths, soil carbon stocks and vegetation composition are also consequences of thawing permafrost [67]. Surface water areas underlain by permafrost are highly dynamic, resulting in both the expansion of lakes and ponds due to thermoerosion as well as in subsurface drainage and thus in shrinking or complete disappearance of lakes [68,69].

A thinning of permafrost will therefore lead to increased inputs from groundwater to streams and consequently alter the temperature and chemical properties of rivers and lakes [70]. Warming and thawing of frozen ground impairs its physical stability, causing dramatic changes for the overlaying ecosystem as well as the reduction of load capacities for human infrastructure, such as buildings, pipelines or railroads [70–72]. Moreover, deformation of the ground surface such as active-layer detachments and increased frequency of mass movements may develop as geohazards and therefore impose risks to exposed infrastructure [5]. Approximately 30–34% of coastlines on the Earth are influenced by permafrost [73]. The lengthening of the open water season, rising sea- and air-temperatures, higher storm frequencies and warming permafrost are hereby drivers for greater erosion rates [12]. Arctic coastal erosion in return causes carbon release to oceans, changes in the Arctic ecosystem, alter wildlife and fish habitats and endanger human settlements and infrastructure [12,74–76].

Infrastructure engineering in permafrost areas is particularly challenging due to the increased risk of structural damage caused by warming of frozen soils [77]. It is hereby expected that 70% of Arctic infrastructure will be located in areas considered at risk from thawing permafrost and ground subsidence by the year 2050 [78]. Rising ground temperatures of frozen soils reduce the load capacity and increase the deformation rates and risks for foundation failure [79,80]. As stated by Schnabel et al. [77], this is especially relevant for heated structures such as heated buildings or warm pipelines which have to be separated from the ground via pilings and ventilated space in order to avoid an accelerated thawing through heat exchange. However, simply putting unheated structures on or in permafrost can already cause an increase in ground temperatures caused by the replacement of native surface cover with warmer surface materials such as asphalt roads [77]. Therefore, proactive cooling of the present frozen ground is commonly recommended in order to reduce maintenance costs on infrastructures related to warming permafrost [71,77,79,81].

Another very important aspect of permafrost is the previously mentioned amount of organic carbon which is stored in its frozen masses. According to current estimates, permafrost stores around 1460–1600 billion tonnes of organic carbon, which is almost twice the amount of carbon in the atmosphere [2,3]. A continued degradation of permafrost could cause its release to the atmosphere as greenhouse gases, creating a positive feedback and thus accelerate climate change even further [2,82]. Although the Arctic greening could act as a carbon sink to a certain degree, there is little consensus on the vegetation uptake of CO₂ in the NHL from different models [23,83,84]. As mentioned in an expert assessment by Abbott et al. [84], an increase of organic carbon release of up to 75% from collapsing coastlines and Arctic rivers can be expected by the year 2100, with carbon emissions caused by fire activities even multiplying by a factor of four. The authors further indicate permafrost regions to become carbon sources by the end of the century, regardless of the warming scenario. However, 65–85% of permafrost carbon release could potentially still be avoided by reducing human emission rates [84]. Future permafrost carbon emissions are hereby often modelled based on Representative Concentration Pathways (RCP) scenarios, as the fate permafrost carbon is closely linked to these pathways [85]. RCPs, which were developed as a basis for near- and long-term climate modelling experiments, represent thereby four pathways for the trajectory of greenhouse gas concentrations with each pathway being labeled after different potential radiative forcing values (2.6, 4.5, 6.0, 8.5 W/m²) in the year 2100 [86]. An estimated emission of 23–174 Pg carbon under the strong warming scenario RCP8.5 and 6–33 Pg carbon under the moderate warming scenario RCP4.5 are expected by 2100 [2,37,87,88]. As mentioned by Schaefer et al. [89], a substantial warming of frozen soils and the associated long-term carbon releases would increase global temperatures by 0.29 ± 0.21 °C in 2100 (under RCP8.5), which in turn poses the risk to exceed the desired warming target of maximum 2 °C above pre-industrial temperatures by the year 2100. The authors further warn about the absence of such permafrost carbon emission trajectories in climate projections within the IPCC's Fifth Assessment Report (AR5) [89].

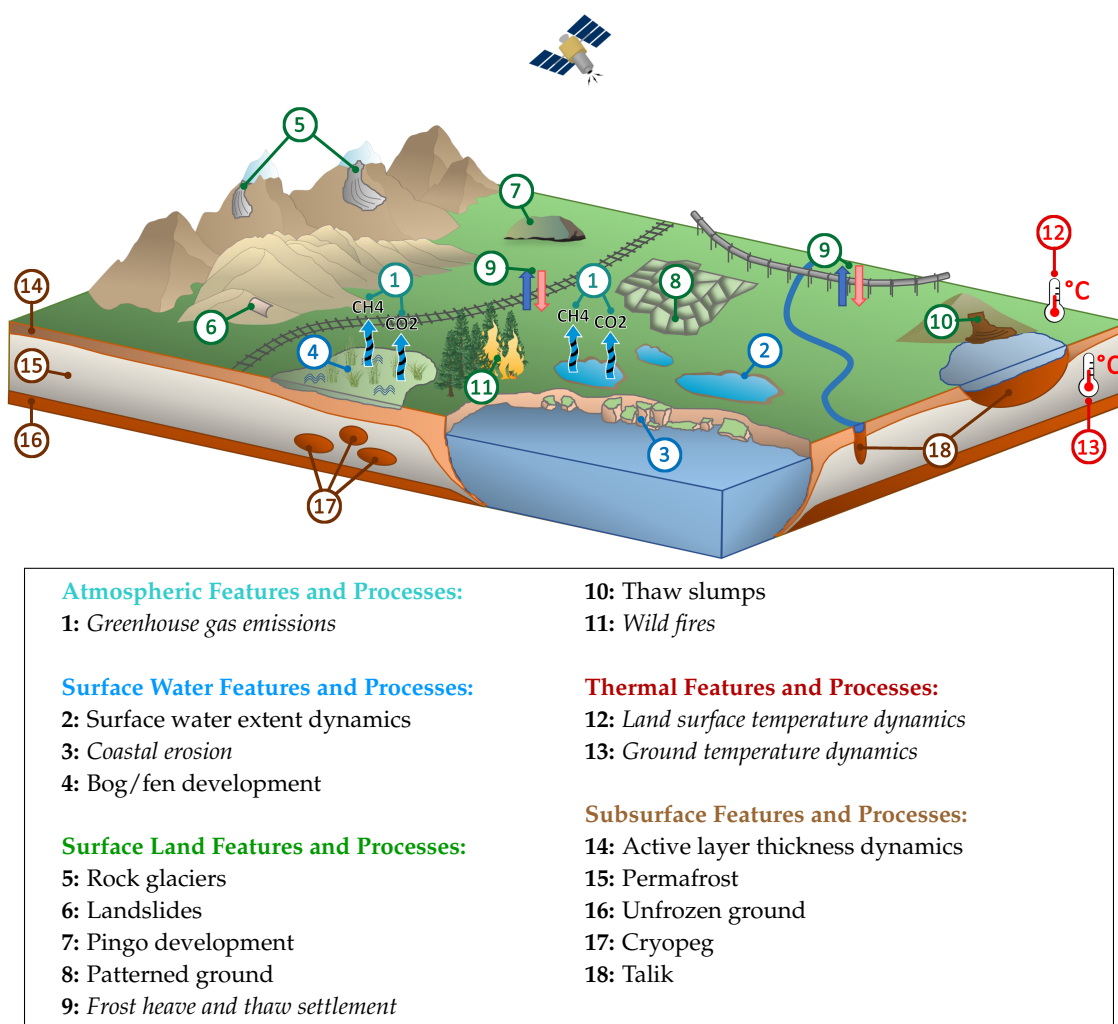


Figure 1. The info-graphic illustrates a variety of common permafrost related features and processes. Processes are hereby written in italics. Several symbols, which were used to generate the infographic, were adopted or modified according to courtesy of the Integration and Application Network, University of Maryland Center for Environmental Science [90].

1.2. Efforts in Satellite Earth Observation for Monitoring Permafrost and Permafrost-Affected Landscapes

Recognized by its importance, permafrost was added as one of the 50 Essential Climate Variables (ECV) as defined by the Global Climate Observing System (GCOS) of the World Meteorological Organization (WMO) [23,52]. Both “Depth of active layer (m)” and “Permafrost temperature (K)” are hereby the required and associated parameters by GCOS for the ECV permafrost [91]. In this context permafrost was also added to the European Space Agency (ESA) Climate Change Initiative (CCI) program lineup, next to ongoing projects for example, ESA Snow_cci or LST_cci [91,92]. A list containing some recent and ongoing permafrost related programs and networks which are commonly mentioned in literature is provided in Table 1.

Since permafrost is a subsurface feature, it cannot directly be measured from space. However, the presence and degradation of permafrost is accompanied by various land surface characteristics and processes (Figure 1), which can be detected and analyzed over space and time via satellite imagery. These target characteristics are thereby means to indirectly derive the state of permafrost [26]. Nevertheless, Earth observation analyses of frozen ground and related land surface features remain challenging due to unfavorable environmental conditions, such as persistent cloud coverage, low light intensities (including polar night) and steep sun angles [93] as well as technical limitations such as decorrelation

between Synthetic Aperture RADAR (SAR) scenes [26,94], as described in more detail in the following paragraph. A handful of satellite remote sensing of permafrost associated review articles were published during the last 20 years (Table 2).

Table 1. A variety of recent and ongoing permafrost related programs and networks.

Name	Objective	Runtime
Global Terrestrial Network for Permafrost (GTN-P) [95,96]	Organization and management of permafrost data.	since 1998
Swiss Permafrost Monitoring Network (PERMOS) [97,98]	Documentation of the state and changes of mountain permafrost in the Swiss Alps.	since 2000
PermaNET—Permafrost Long-Term Monitoring Network [99,100]	Alpine-wide permafrost monitoring.	2007–2013
Permafrost Carbon Network [101]	Quantifying the role of permafrost on future climate change.	since 2011
ArcticNet [102,103]	Studying the impacts of climate change in the Canadian North.	since 2003
Cooperative Global Air Sampling Network [104]	International effort in gathering regular discrete air flask samples.	since 1967
PAGE21 [105]	Studying the vulnerability of permafrost environments and feedback mechanisms associated with rising greenhouse gas emissions.	2011–2015
Circumpolar Active Layer Monitoring (CALM) [106,107]	Observing the response of near-surface permafrost and the active layer to climate change over long (multi-decadal) time scales.	since 1991
Thermal State of Permafrost (TSP) [28,108]	Database for assessing the changes in temperatures and distribution of permafrost.	since 2007
ESA Atmosphere-Land Interactions Study (ALANIS) [109,110]	Interaction and contribution of boreal Eurasia to greenhouse gas concentration.	2010–2012
ESA Data User Element (DUE) Permafrost [111,112]	Establishment of a satellite based systematic permafrost monitoring program.	2009–2012
ESA GlobPermafrost [113,114]	Development, validation and implementation of permafrost related products by integrating Earth observation data.	2016–2019
ESA CCI Permafrost [91,92]	Development of permafrost maps as Essential Climate Variables (ECV) products via satellite measurements.	2018–2021
Arctic-Boreal Vulnerability Experiment (ABOVE) [115,116]	Major field campaign in Alaska and western Canada to help understand and predict ecosystem responses of climate change in Boreal regions and the Arctic.	since 2015
Climate and Cryosphere (CliC) [117,118]	Improve our understanding of the cryosphere and its interactions with the global climate system as well as to strengthen the utilization of cryospheric observations for climate change detection.	since 2001
Next-Generation Ecosystem Experiments (NGEE) Arctic [119,120]	Improving our predictive understanding of carbon-rich Arctic system feedbacks and processes to the climate.	2012–2022
Study of Environmental Arctic Change (SEARCH) [121,122]	Understanding the impact of degrading permafrost and shrinking land/sea ice on the Arctic and global systems.	since 2001

Table 1. *Cont.*

Name	Objective	Runtime
PermaSAR [123]	Development of methodologies to detect subsidence through remote sensing analysis in permafrost regions.	2015–2019
SatPerm-Satellite-based Permafrost Modeling across a Range of Scales [124]	Investigating the feasibility of satellite data sets as input for permafrost modeling.	2015–2018
COmbining remote sensing and field studies for assessment of Landform Dynamics and permafrost state on Yamal (COLD Yamal) [125]	Development of methodologies for monitoring permafrost and related land surface features on the Yamal peninsula.	2013–2016
Horizon 2020 Nunataryuk [126,127]	Analysing the impacts of thawing subsea and coastal permafrost and developing mitigation strategies for the Arctic coastal population.	2017–2022
Modular Observation Solutions for Earth Systems (MOSES) [128]	A joint observing system that primarily targets four events: hydrological extreme events, ocean eddies, heat waves and the thawing of permafrost.	2017–2021
PETA-CARB [129]	Quantification of the distribution, amount and vulnerability of deep carbon stocks in permafrost deposits. Investigations in the formation, turnover and the release of organic carbon stored in northern Siberian permafrost landscapes.	2013–2018
CARBOPERM [130]	Joint research project dedicated to examine carbon dynamics in permafrost-affected northeastern Siberian landscapes via mathematical models and field observations.	2013–2016
KoPf [131]	Quantifying the effects of thawing terrestrial permafrost and changing freshwater exports of organic matter to Arctic coastal waters.	2017–2020
Changing Arctic Carbon cycle in the cOastal Ocean Near-shore (CACOON) [132]		2018–2021

Table 2. Some remote sensing of permafrost related review articles during the last 20 years.

Author	Year	Title
Zhang et al. [133]	2004	Application of Satellite Remote Sensing Techniques to Frozen Ground Studies
Kääb et al. [134]	2005	Remote sensing of glacier- and permafrost-related hazards in high mountains: an overview
Kääb [135]	2008	Remote sensing of permafrost-related problems and hazards
National Research Council [136]	2014	Opportunities to use remote sensing in understanding permafrost and related ecological characteristics: Report of a workshop
Arenson et al. [137]	2016	Detection and analysis of ground deformation in permafrost environments
Jorgenson and Grosse [76]	2016	Remote Sensing of Landscape Change in Permafrost Regions
Bartsch et al. [22]	2016	Land Cover Mapping in Northern High Latitude Permafrost Regions with Satellite Data: Achievements and Remaining Challenges
Trofaier et al. [23]	2017	Progress in space-borne studies of permafrost for climate science: Towards a multi-ECV approach
Duncan et al. [93]	2020	Space-Based Observations for Understanding Changes in the Arctic-Boreal Zone

Optical imagery from for example, Landsat enables time series analyses of surface changes since 1972 [133]. However, a major limitation of all Landsat-based analyses is the sparse data availability for 1989–1998 for much of the Arctic region [22]. Thermal

imagery derived from Moderate Resolution Imaging Spectroradiometer (MODIS) and Advanced Very High Resolution Radiometer (AVHRR) can be implemented for estimating thawing indices or modelling active layer thickness [133]. That said, both thermal and optical data are heavily influenced by their cloud contamination, resulting in data gaps and therefore limiting their usability [23,133]. Radio Detection and Ranging (RADAR) data in the form of SAR on the other hand has the potential to overcome limitations of optical and thermal imagery, due to its ability to gather information independent of the weather condition (e.g., clouds) or sun illumination [134,135]. The application of Differential Interferometric Synthetic Aperture Radar (D-InSAR) allows for surface displacement analyses with high precision [46]. A major constraint of D-InSAR based analyses is the decorrelation between scenes due to changing surface properties such as snow, soil moisture or vegetation cover [26,94]. SAR and optical data are in general highly complementary in the context of permafrost-related feature analyses, with optical data approaches might work where SAR fails and the other way round [26]. Another potent data source are passive RADAR sensors such as the Special Sensor Microwave/Imager (SSM/I) that provides continuous, sub-daily and global coverage since 1987, which can be used to detect for example, surface soil freeze/thaw conditions [133]. However, the very high temporal resolution comes at the cost of a very coarse spatial resolution of several tens of kilometers [138]. High spatial resolution satellite imagery, or rather the lack thereof, is a commonly mentioned limitation factor for current spaceborne studies in the context of permafrost analyses [22,76,134]. While high-resolution images from IKONOS, QuickBird or WorldView have shown to be valuable data sources for analysing small scale processes and features (e.g., Jones et al. [12], Ulrich et al. [139], Godin et al. [140]), they are oftentimes still expensive and difficult to acquire [134,141]. Next to higher spatial resolution, there is a demand for long-term and frequent observations to monitor highly dynamic processes [22,23]. The combination of remotely sensed data from different sensors is thereby especially promising in overcoming sensor and/or platform specific limitations for analysing the large variety of permafrost related features and processes such as emerging greenhouse gas emissions, coastal erosion, vegetation cover dynamics or the distribution of permafrost on high spatio-temporal resolutions and large scales [76,142].

1.3. Objectives of This Review

While other review articles dedicated their investigations on satellite technologies and methods in relation to how well they can answer permafrost-related research questions (e.g., [23,76]), this study focuses on a detailed bibliographic analysis of recent trends in the frequency of investigated environmental topics, the spatial distribution of the study areas and the applied spatio-temporal resolution of satellite data for studying permafrost-related features and processes over a range of scales. The aim of this review is to provide a comprehensive overview of past achievements, current efforts as well as future challenges and possibilities for satellite remote sensing of permafrost related analyses. To achieve this, a total of 325 articles published in 30 international journals during the last two decades were analyzed. In addition, a variety of relevant and open source data sets for permafrost related analyses are presented. Trends in satellite remote sensing of permafrost features were observed, research gaps identified and recommendations for future work and an outlook on the potential of new data and methodologies are given.

2. Review Methodology

A visualisation of the review methodology can be found in Figure 2. The Web of Science (WoS) (formerly known as ISI Web of Knowledge) platform was used to search for permafrost and remote sensing related Science Citation Index (SCI) papers. A search string was defined to filter the literature based on the following conditions. The term “Permafrost” and at least one of the following terms “Earth Observation”, “Satellite” or “Remote Sensing” have to appear in either the title, abstract or keywords. If a one of the following keywords “Earth Observation”, “Satellite” or “Remote Sensing” occurs in the name of a journal, only

the term “Permafrost” has to appear in either the title, abstract or keywords. Furthermore, the document type was set to “Article” and the language was set to “English”. Articles with a publication date between January 2000 and February 2020 were considered, thus a time span of two decades is covered within this review. This initial filtering resulted in over 700 articles which met the defined requirements.

Since the focus of this review lies on the potential of satellite Earth observation for monitoring permafrost landscapes, the literature was further reduced to eleven international journals with a thematic focus on remote sensing. In addition, 19 renowned non-remote sensing specific international journals were also included in order to keep the analysis as representative as possible. This led to a total number of 536 articles.

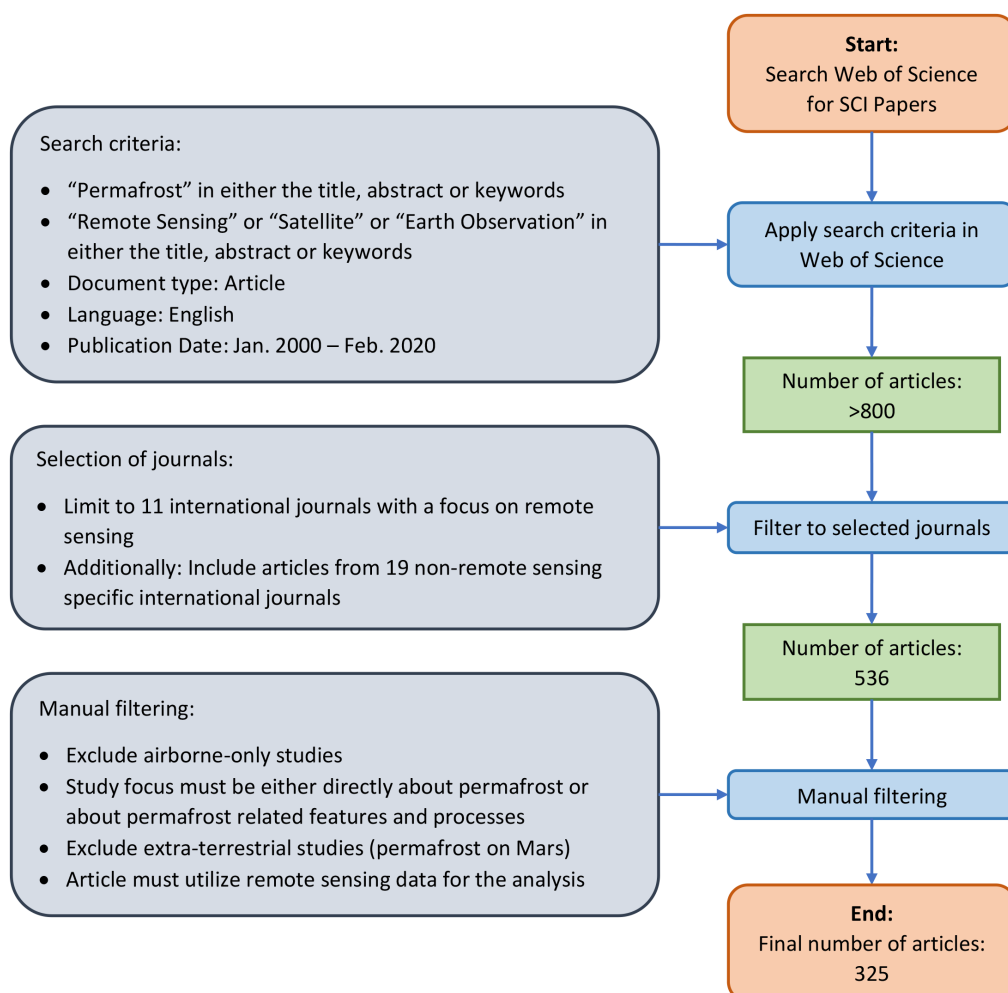


Figure 2. Overview of the selection process for relevant articles within this review.

The last stage of the literature selection comprised of a manual screening process of the articles based on the following criteria: (1) Studies that used only airborne remote sensing were excluded, since this review major focus lies on satellite earth observation of permafrost and related features/processes; (2) No extra-terrestrial studies (permafrost on Mars) were included in this review; (3) The study must utilize remote sensing for their analysis; (4) The study focus must be either about or directly connected to permafrost. Therefore, studies that for example, mentioned the term “permafrost” once in the abstract but do not actually investigate permafrost or any of its associated features and processes were excluded from the review process. The remaining 325 articles from 30 international journals were analyzed based on relevant parameters for this review, including:

- The number of published articles per year

- The number of studies per country
- The nationality of the first authors institution
- Frequently investigated study regions across the globe
- The frequency of investigated environmental categories
- The frequency of investigated research foci
- Applied spatio-temporal resolutions of remote sensing data
- Observed temporal coverage of time series analyses
- Studied spatial scales
- Frequencies of remote sensing platforms
- Utilized sensor types and sensor combinations

The number of reviewed articles per journal are listed in Table 3. We are aware that by applying the described filtering methodology, some relevant articles from other journals may have been excluded. However, the inclusion of more journals would go beyond the scope of this review. For the same reason, no non-English articles were considered in the review process. Given diminishing returns, we consider this approach to be a reasonable compromise for a representative overview of the current state and recent trends in satellite earth observation for permafrost related analyses.

Within the context of this review, all research articles were categorized into the five environmental categories “Atmospheric Features and Processes”, “Surface Water Features and Processes”, “Surface Land Features and Processes”, “Thermal Features and Processes” and “Subsurface Features and Processes”. The category “Atmospheric Features and Processes” covers all environmental topics related to the atmosphere, such as greenhouse gas emissions or evapotranspiration. “Surface Water Features and Processes” encompasses topics related to the surface water, including lake extent dynamics, coastal erosion or lake ice extents. The category “Surface Land Features and Processes” includes all land surface related topics, such as vegetation cover dynamics, surface movements (e.g., frost heave/thaw settlement) or snow cover. Dynamics in the land surface temperature or ground temperature, as well as heat fluxes are covered by the category “Thermal Features and Processes”. Lastly, the category “Subsurface Features and Processes” comprises of features and processes which occur below the surface, including the distribution of permafrost, dynamics in the thickness of the active layer or freeze/thaw dynamics of the soil. Each environmental research focus per study was therefore identified as a sub-category of these spheres. Some articles covered several research topics from multiple categories. For each category, the findings of some representative and highly cited articles are presented.

Another relevant parameter during this review process is the spatio-temporal resolution of applied satellite data. The temporal resolution was hereby divided into the four categories “Unitemporal”, “Bitemporal”, “Multitemporal” and “Time Series”. In the context of this review, studies are considered to be multitemporal, if 3–9 time steps are used for analyzing the temporal development, whereas a “Time Series” study is defined to cover at least 10 time steps. The spatial resolution was categorized into the four classes high (<10 m), medium high (10–100 m), medium low (100–1000 m) or low (>1000 m). Furthermore, in this study the different scales are defined as local ($<10,000\text{ km}^2$), regional small (10,000–250,000 km^2), regional large ($>250,000\text{ km}^2$), national or circum-Arctic.

Even though this review focuses on studies that utilized satellite Earth observation, “aerial” was also considered for the platform frequency analysis since many articles employed aerial imagery either as a historical reference, for validation or other complementary use with satellite data and is therefore included for completeness. Lastly, permafrost-related and openly available data sets which were commonly applied across the reviewed articles are presented.

Table 3. List of reviewed journals, the number of articles per journal covered in this review and their respective impact factor for the year 2019 as well as the 5-year impact factor according the Web of Science [143] (rounded to the first decimal place).

Journal Name	Number of Reviewed Articles	Impact Factor 2019	Impact Factor 5 Year
Remote Sensing	60	4.5	5
Remote Sensing of Environment	34	9.1	9.6
Permafrost and Periglacial Processes	29	2.7	2.7
Environmental Research Letters	28	6.1	6.7
The Cryosphere	21	4.7	4.9
Geomorphology	17	3.8	3.9
Journal of Geophysical Research: Biogeosciences	15	3.4	4.2
Biogeosciences	14	3.5	4.2
Global Change Biology	14	8.6	9.8
Journal of Geophysical Research: Earth Surface	10	3.6	4
Hydrological Processes	10	3.3	3.6
International Journal of Remote Sensing	8	3	2.7
Journal of Geophysical Research: Atmospheres	8	3.8	4.3
IEEE Journal of Selected Topics in Applied Earth Observations and Remote Sensing	7	3.8	3.9
Science of the Total Environment	7	6.6	6.4
Scientific Reports	6	4	4.6
IEEE Transactions on Geoscience and Remote Sensing	5	5.9	6
Water Resources Research	5	4.3	5
Nature Communications	4	12.1	13.6
Nature Geoscience	3	13.6	16.1
Journal of Applied Remote Sensing	3	1.4	1.3
GIScience & Remote Sensing	3	6	4.2
Global and Planetary Change	3	4.4	5.1
Remote Sensing Letters	2	2.3	2.4
International Journal of Applied Earth Observation and Geoinformation	2	4.7	5.4
Frontiers in Earth Science	2	2.7	NA
ISPRS Journal of Photogrammetry and Remote Sensing	2	7.3	8.6
IEEE Geoscience and Remote Sensing Letters	1	3.8	3.7
Earth System Science Data	1	9.2	9.6
Palaeogeography, Palaeoclimatology, Palaeoecology	1	2.8	3
Total	325		

3. Results

The following section provides details and key findings about the number of satellite Earth observation of permafrost related articles per year, followed by the spatial distribution of the study area and the author countries. Subsequently, the proportions and temporal development of environmental research foci are analyzed. Afterwards, the applied spatio-temporal resolutions over time and per environmental topic are elaborated.

Lastly, the frequency of platform and sensor combinations which are applied in the context of permafrost analysis are presented.

3.1. Temporal Development of Permafrost Related Studies

The degradation of permafrost and its effects on the environment gained increasing attention over the past years [23,52]. This increase in attention can be observed in the number of satellite based studies of permafrost and its associated land features, which grew over the course of the last two decades (Figure 3). Especially during the last decade a higher frequency of articles can be observed, with 2018 featuring the most (62) articles published per year within the scope of this review. In 2018 permafrost was added to the ESA CCI program lineup as an ECV, which could have been a potential driver for the sudden increase in publication frequency [91,92]. For the year 2020 only 12 articles are shown, however this review also only considered articles which were published until February 2020. Therefore, based on the trend of the last 20 years, a growing number of satellite Earth observation of permafrost related studies can be expected in future years.

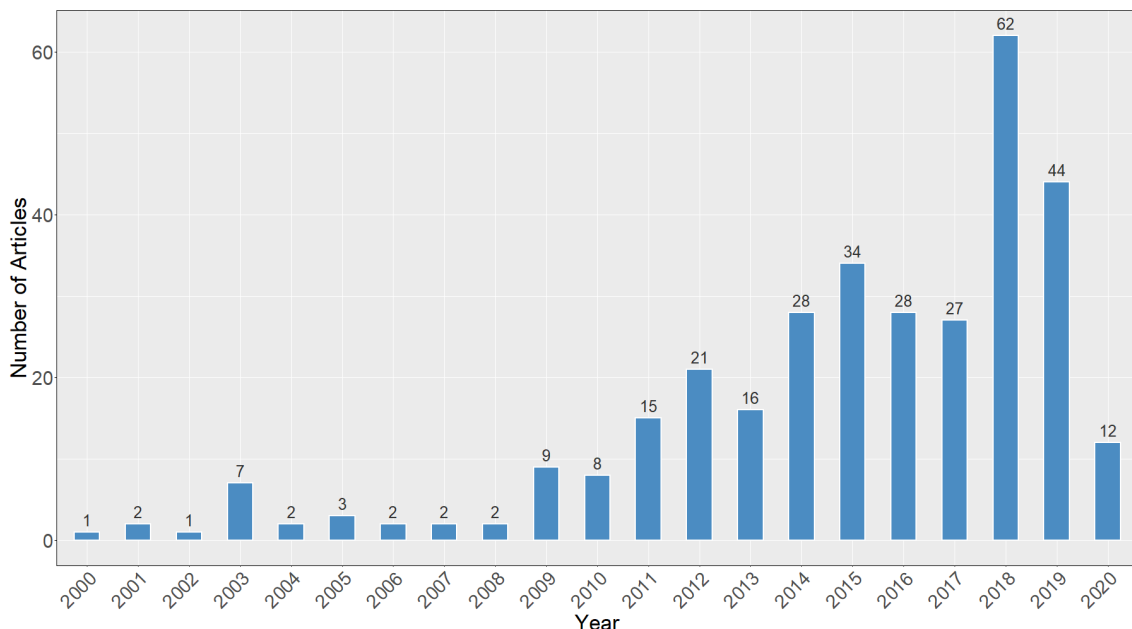


Figure 3. Number of permafrost related satellite Earth observation studies per year based on the reviewed articles.

3.2. Distribution of Study Countries and First Author Institution Nationalities

The frequency of studied countries and the nationality of the first authors institutions are visualized in Figure 4. The most frequent nationality of the first authors institution is hereby the United States with 91 articles, followed by China (57), Germany (48) and Canada (47) (Figure 4a,b). On the other hand, the most studied countries are Russia with 75 articles, followed by Canada (71), the United States (68) and China (54) (Figure 4c,d). The three countries United States, Canada and China feature major permafrost occurrences (Figure 5), which explains their positions as both highly investigated countries and the most common author countries. Russia, however, appears to be underrepresented within the author distribution, since it is the most frequently researched country across all reviewed articles and features the greatest spatial coverage of permafrost out of any country based on the circum-Arctic permafrost map by Brown et al. [1]. As already mentioned in Section 2, only English articles were considered for this review, therefore no Russian publications were included. In contrast, Germany stands out by being one of the top authors, despite of its lack of permafrost with local exceptions for example, mountain permafrost at the Zugspitze [144].

The relationships between the author and study countries reveal a trend for authors to investigate the same country as the nationality of the first authors institution, given that permafrost is present within the corresponding country. 80% of all studies carried out in the USA were conducted by American institutions, followed by Canadian institutions (7%). In case of Canadian studies, 58% are associated with Canadian institutions and 21% with German institutions. China is almost exclusively studied by Chinese institutions with 93%. Russia on the other hand features a more heterogeneous distribution of the author nationality, with 36% of studies carried out by German institutions, 21% by the United States, 10% by Russian and 6% by Austrian institutions. Germany as a major author country studies mainly in Russia (48%), with additional common study countries such as Canada (26%) and the United States (9%). A visualization of the author nationality and study country relationship can be found in the supplementary materials under Figure S1.

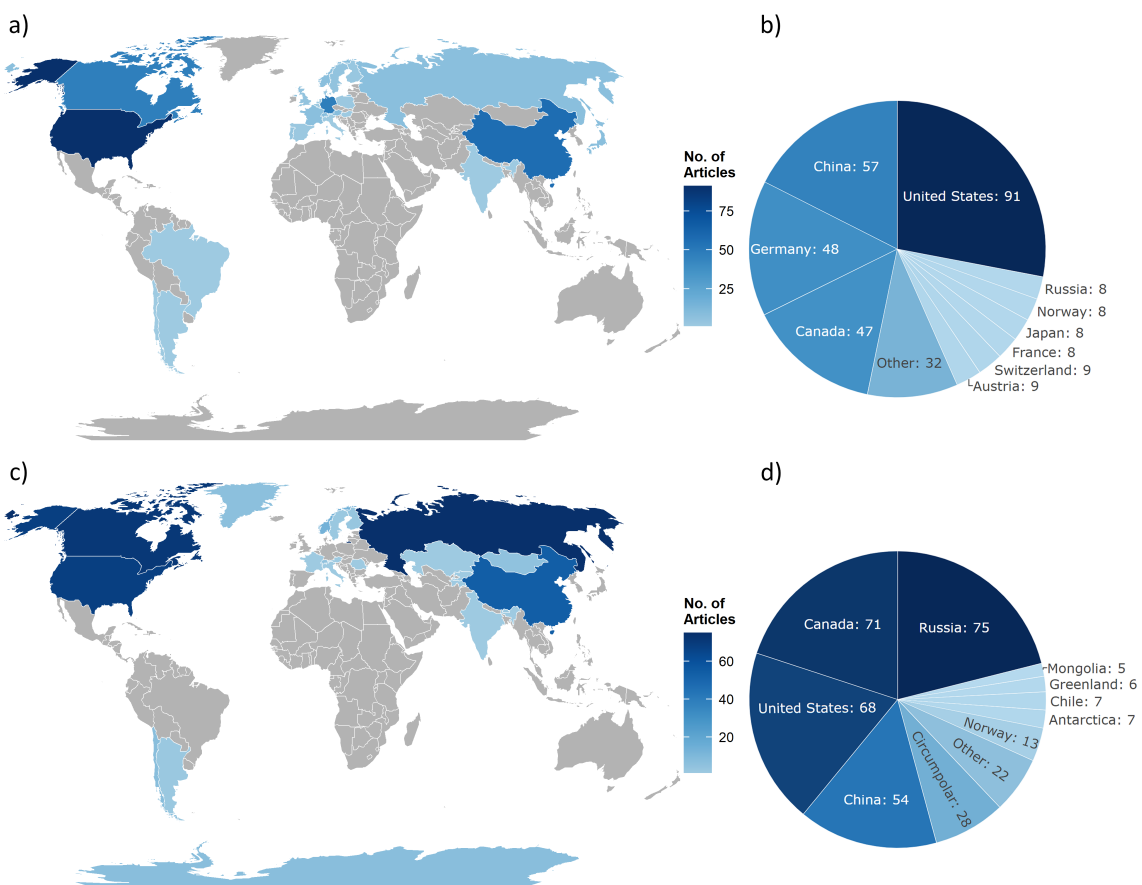
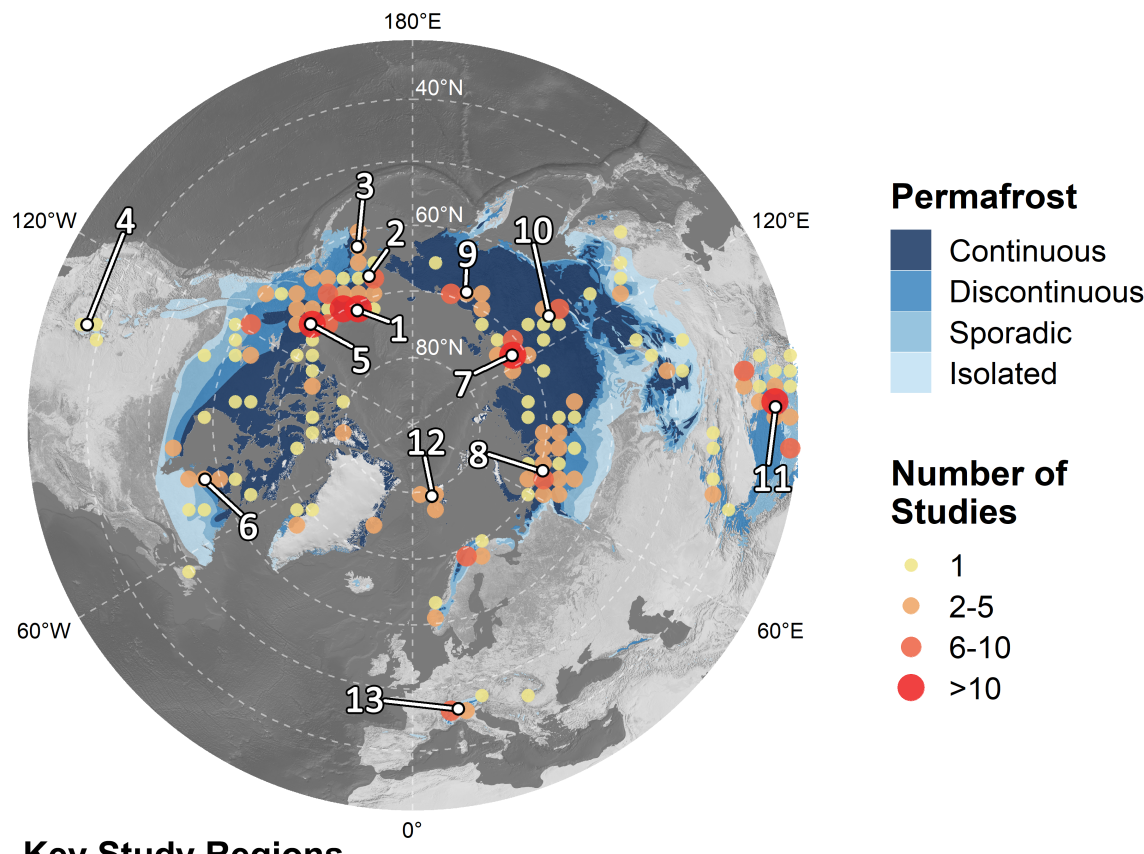


Figure 4. Map showing the frequency of first author institution nationalities (a) and the relative distribution (b). Next to the first author institution, the frequency of study countries are displayed via a map (c) and the relative distribution as a pie chart (d). Circumpolar studies are hereby excluded from the map (c). Some articles featured study areas in multiple countries.

3.3. Spatial Distribution of Reviewed Articles

Out of the 325 articles analyzed in this review, only 9% of studies were conducted on a circum-Arctic scale [14,33,39,51,138,145–166]. Figure 5 displays the distribution and frequency of study locations across the Northern Hemisphere from non-circumpolar studies. Distinct key study regions within the four major study countries United States, Canada, Russia and China can be observed. Permafrost related features and processes in the United States are almost exclusively researched in Alaska. In particular across the North Slope Borough and its Arctic Coastal Plain [12,27,36,37,43,55,167–193] (Figure 5 key region 1), Seward Peninsula [36,139,168,193–196] (Figure 5 key region 2) and the Yukon-Kuskokwim Delta [183,184,197–199] (Figure 5 key region 3). The only studies within the

United States but outside of Alaska are located in the Rocky Mountains in southwestern Colorado [200,201] (Figure 5 key region 4), as well as one study by Zhang et al. [202] who studied freeze-thaw dynamics across the contiguous United States.



Key Study Regions

- | | | |
|--------------------------|-------------------------------|--------------------|
| 1. North Slope Borough | 6. Umiujaq | 11. Beiluhe region |
| 2. Seward Peninsula | 7. Lena River Delta | 12. Svalbard |
| 3. Yukon–Kuskokwim Delta | 8. Yamal and Gydan Peninsulas | 13. European Alps |
| 4. Rocky Mountains | 9. Kolyma Lowland | |
| 5. Mackenzie Delta | 10. Central Yakutia Lowland | |

Figure 5. The study area distribution of the reviewed articles for the Northern Hemisphere together with the circum-Arctic permafrost map by Brown et al. [1] (bluish coloured areas). One study may have several study areas. A shaded relief by Natural Earth [203] was utilized as a background map. All data is visualized in a polar Lambert azimuthal equal area projection. Circum-Arctic studies were excluded from this visualization. Thirteen key regions with study clusters are marked and labeled.

In Canada, most research efforts are concentrated around the Mackenzie Delta and Tuktoyaktuk Coastlands within the Northwest Territories [66,177,183,184,204–219] (Figure 5 key region 5). Several more studies are also distributed across the Northwest Territories [58,177,211,220–230]. Other geographical hotspots are Herschel Island in the Yukon territory [11,231–237] (also Figure 5 key region 5) and the eastern shore of Hudson Bay around the Inuit village of Umiujaq in Northern Quebec [238–242] (Figure 5 key region 6). Especially the territory Nunavut features sparse study coverage both on the Canadian mainland as well as the Arctic islands, despite being largely underlain by continuous permafrost.

The Lena River Delta is one of the key study regions in Russia [42–44,94,139,142,183,184,206,209,243–258] (Figure 5 key region 7), followed by the Yamal and Gydan Peninsulas and the surrounding regions [40,179,184,193,229,259–271] (Figure 5 key region 8) as well as the Kolyma Lowland [15,36,42,55,183,184,266,272–276] (Figure 5 key region 9). There are

also some additional clusters in the Central Yakutia Lowland [55,142,277–279] (Figure 5 key region 10). Despite being the most examined country within this review, large areas of Russia underlain by continuous permafrost are still under-explored.

Permafrost related studies in China mostly concentrate inside the Qinghai–Tibet Plateau (QTP), with a focus on the Beiluhe region [9,64,71,280–294] (Figure 5 key region 11). The 1.956 km long Qinghai–Tibet Railway (QTR) and the Qinghai–Tibet Highway (QTH) are hereby major research interests inside the Qinghai–Tibet Engineering Corridor (QTEC) [7,9,71,280,283,284,286–289,291,293,295,296].

Other common study regions in the Northern Hemisphere are Svalbard in Norway [63,297–303] (Figure 5 key region 12) and the European Alps [47,60,304–309] (Figure 5 key region 13). Also, a noteworthy amount of studies were conducted within Scandinavia [34,94,271,310–314] and Greenland [35,43,60,315–317].

While the majority of permafrost is distributed over the Northern Hemisphere and so are most of the research articles (94%), some authors also investigated permafrost related features and processes on the Southern Hemisphere (Figure 6). One of the geographical research hotspots are hereby the Andes with a focus on rock glacier kinematics and mountain permafrost distribution [60,61,318–323] (Figure 6 key region 1). Moreover, the Antarctic features a noteworthy amount of permafrost related research. Studies are almost entirely located across the South Shetland Islands with a focus on Byers Peninsula on Livingston Island [43,324–328] (Figure 6 key region 2), whereas a single article examined rock glaciers in the McMurdo Dry Valleys [329] (Figure 6 key region 3). Lastly, in a recent study by Obu et al. [163] near-surface permafrost temperatures were modelled for the entire Antarctic. The lowest temperature was hereby modelled to be -36°C , which marks the lowest permafrost temperature worldwide according to global modelling efforts [163].

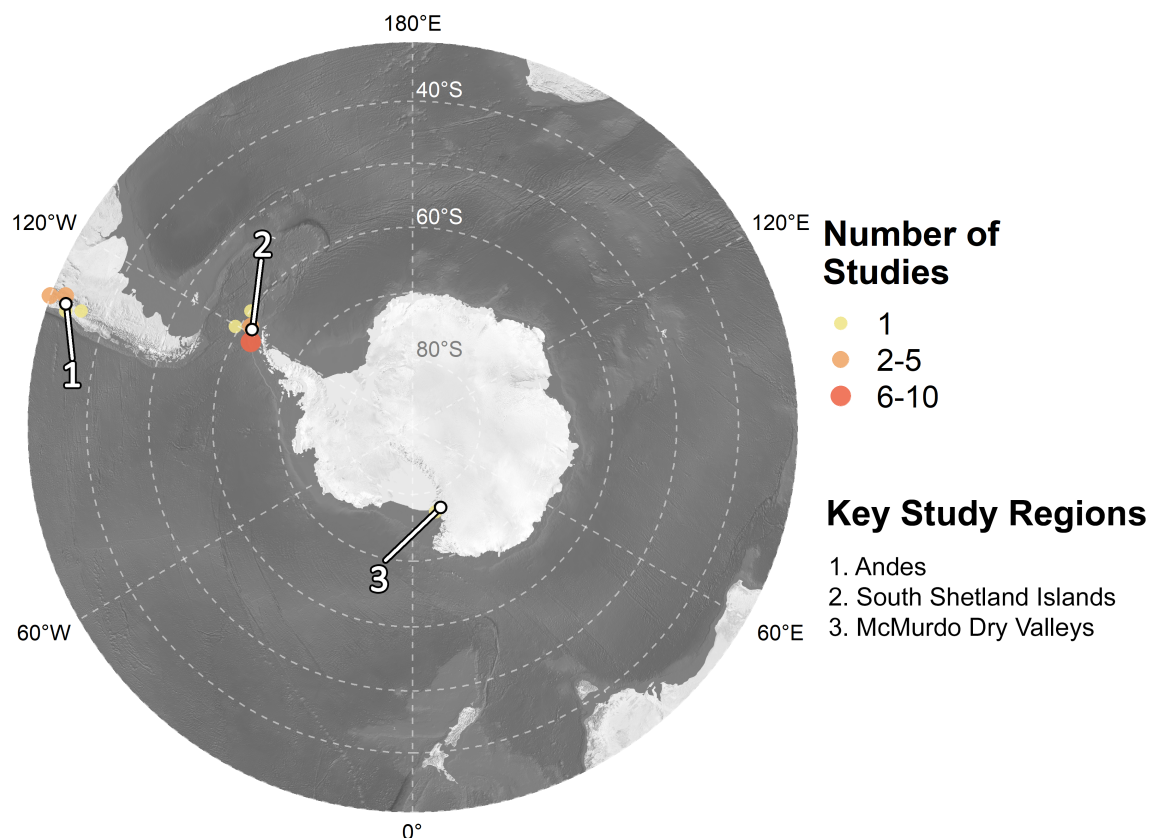


Figure 6. The study area distribution of the reviewed articles for the Southern Hemisphere. One study may have several study areas. A shaded relief by Natural Earth [203] was utilized as a background map. All data is visualized in a polar Lambert azimuthal equal area projection. Circum-Antarctic studies were excluded from this visualization. Three key regions with study clusters are marked and labeled.

3.4. Categorization of Environmental Research Foci

The distribution of categories and research foci are visualized in Figure 7. Almost half (~43%) of all articles conducted their research within the “Surface Land Features and Processes” category. The top environmental research foci are hereby “Vegetation Cover (Dynamics)” (~12% in total and ~27% in category), followed by “Frost Heave/Thaw Settlement” (~7% in total and ~16% in category), “Rock Glacier Mapping/Dynamics” (~4% in total and ~10% in category), “Thaw Slump Mapping/Dynamics” (~4% in total and ~10% in category) and “Wild Fires” (~4% in total and ~10% in category).

The second most common category is “Surface Water Features and Processes” with ~25%. Here, most studies concentrated their research effort on “Lake Extent/Dynamics” (~12% in total and ~47% in category). The following topics, for example, “Coastal Erosion” (~4% in total and ~14% in category), “Ocean Colour” (~1% in total and ~7% in category) and “Wetland Dynamics” (~1% in total and ~6% in category) already feature significantly lower numbers of occurrences.

Similar but slightly lower in frequency is the category “Subsurface Features and Processes” with ~21%. Within this category, “Permafrost Distribution” (~7% in total and ~32% in category), “Active Layer Thickness (Dynamics) (~4% in total and ~21% in category) and “Freeze/Thaw Dynamics” (~4% in total and ~18% in category) are the most frequent research foci.

The two least studied categories are “Thermal Features and Processes” with ~7% and “Atmospheric Features and Processes” with ~4% of the share across all studies reviewed in this paper. Within the category “Thermal Features and Processes”, the research focus “Land Surface Temperature (Dynamics) (~3% in total and ~50% in category) is slightly more researched than “Ground Temperature (Dynamics)” (~3% in total and ~43% in category). Studies associated with the category “Atmospheric Features and Processes” mostly focused their analyses on “Methane/Carbon Dioxide Emissions” (~3% in total and 75% in class).

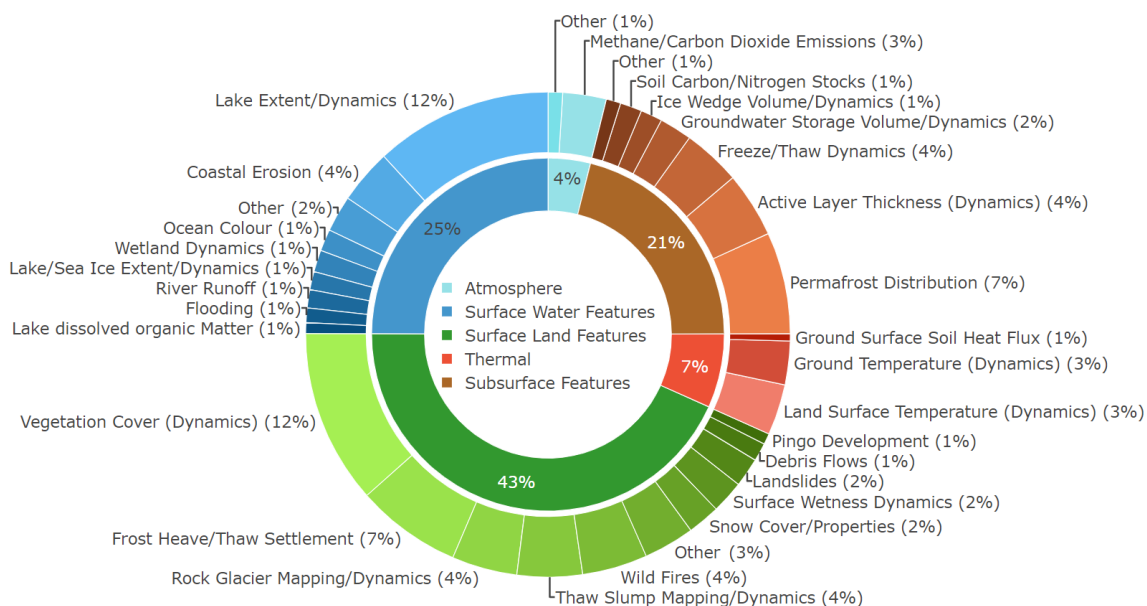


Figure 7. Distribution of the study focus frequency across the reviewed articles. Research foci are categorized into the five spheres “Atmospheric Features and Processes”, “Surface Water Features and Processes”, “Surface Land Features and Processes”, “Thermal Features and Processes” and “Subsurface Features and Processes”.

The temporal distribution of the top 15 environmental foci is displayed in Figure 8a. Accompanied with the higher publication frequency, a general increase in the number of studies per topic can be observed, especially during the last decade. Methane and carbon dioxide emissions, as part of the the category “Atmospheric Features and Processes”, was

first investigated in 2008 in the context of this review. Strongest research effort in this field can be observed for the year 2015.

As part of the “Surface Water Features and Processes” category, the dynamics and extent of lakes was regularly studied throughout the last 20 years, with peaks in 2013 and 2018. Within the framework of this review, first efforts in studying coastal erosion using satellite remote sensing data and linked to permafrost degradation were conducted in 2008, but the topic did not gain increasing attention before 2018.

Looking at topics related to “Surface Land Features and Processes”, vegetation cover and dynamics were mainly studied during the last decade, with 2018 featuring the most related publications. Articles that focused on frost heave and thaw settlement began in 2010 and feature an increase in the publication rate since 2014. Research efforts on rock glacier dynamics are generally sparse, but temporally distributed rather evenly with peaks in 2012 and 2019. Investigations on the influence of snow cover and associated properties on permafrost is overall also sparsely distributed, even though first analyses already began in 2006. Publication rates on thaw slumps were highest for the years 2014 and 2018. Lastly, effects of wild fires on permafrost landscapes were first investigated in 2009, with a growing study interest since 2016.

Within the environmental category “Thermal Features and Processes”, stronger efforts in land surface temperature related studies can be observed for the year 2012, whereas research of ground temperature dynamics already started in 2003, but reached its peak not before 2018, followed by 2015 and 2019.

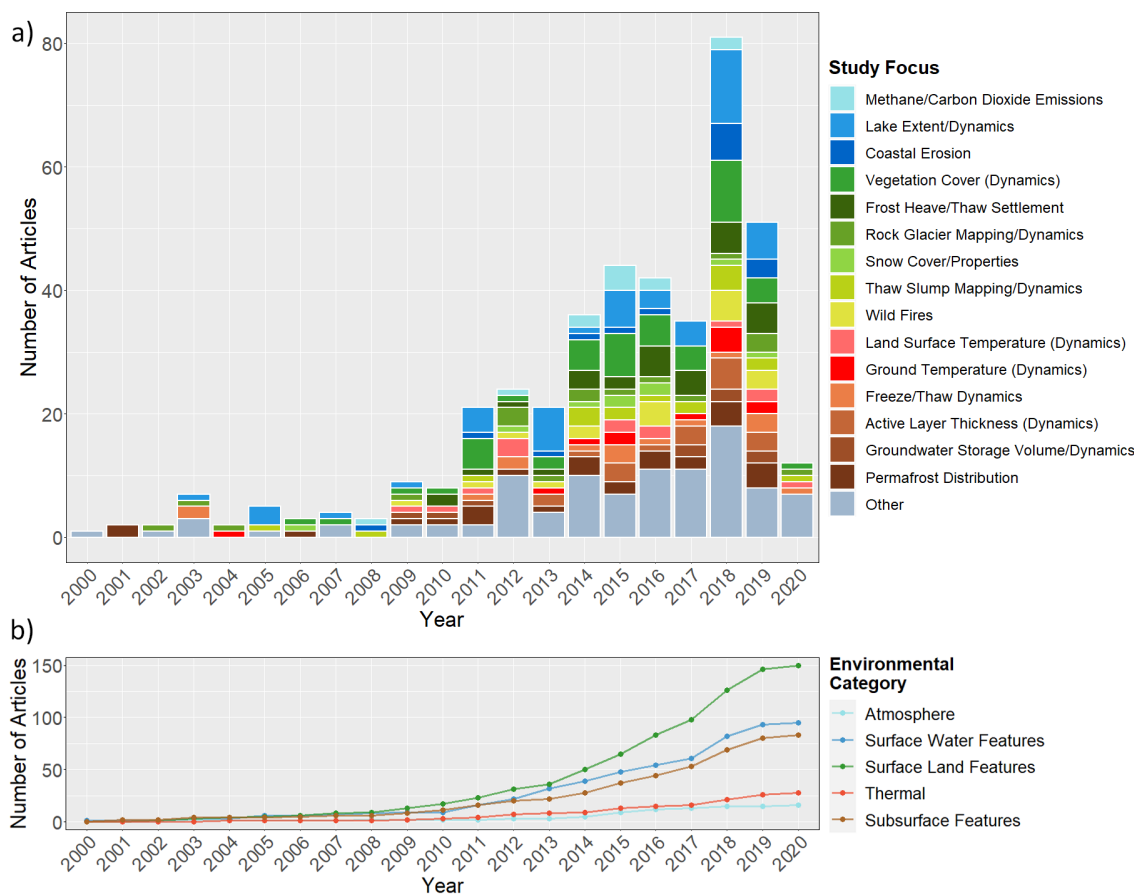


Figure 8. (a) Frequency of the top 15 most common and permafrost related environmental foci across the reviewed articles per year. Several articles covered multiple environmental foci. (b) The cumulative sum of articles per environmental category.

As for the “Subsurface Features and Processes”, freeze/thaw dynamics were mainly investigated during the last decade (except for the year 2003), with the largest number of publications reached in 2015 and 2019. The thickness and dynamics of the active layer

gained an overall growing interest since 2013. Similar to other topics, investigations on groundwater storage and dynamics peaked in 2018. Mapping the actual distribution of permafrost is part of the earliest applications of permafrost related research using satellite remote sensing. Although first studies go back as far as 2001, the topic did not regain major attention until the last decade, with 2018 and 2019 featuring the most articles.

Figure 8b gives a more general overview of the environmental categories “Atmospheric Features and Processes”, “Surface Water Features and Processes”, “Surface Land Features and Processes”, “Thermal Features and Processes” and “Subsurface Features and Processes” and their distribution over time. The cumulative sum per year clearly shows a growing discrepancy between the five categories since the last decade. The category “Surface Land Features and Processes” features hereby the strongest increase in number of articles per year out of all categories. Both “Surface Water Features and Processes” and “Subsurface Features and Processes” show a similar development over the years. In contrast, the categories “Thermal Features and Processes” and “Atmospheric Features and Processes” are revealed to display relatively slow growing rates.

During the review process, a spatial variability in the locations of study foci could be observed. Therefore, the distribution of research frequencies for permafrost related environmental topics vary across different countries. Mentioned distribution for the top four study countries as well as for studies that applied their analysis on a circum-Arctic scale is visualized in Figure 9.

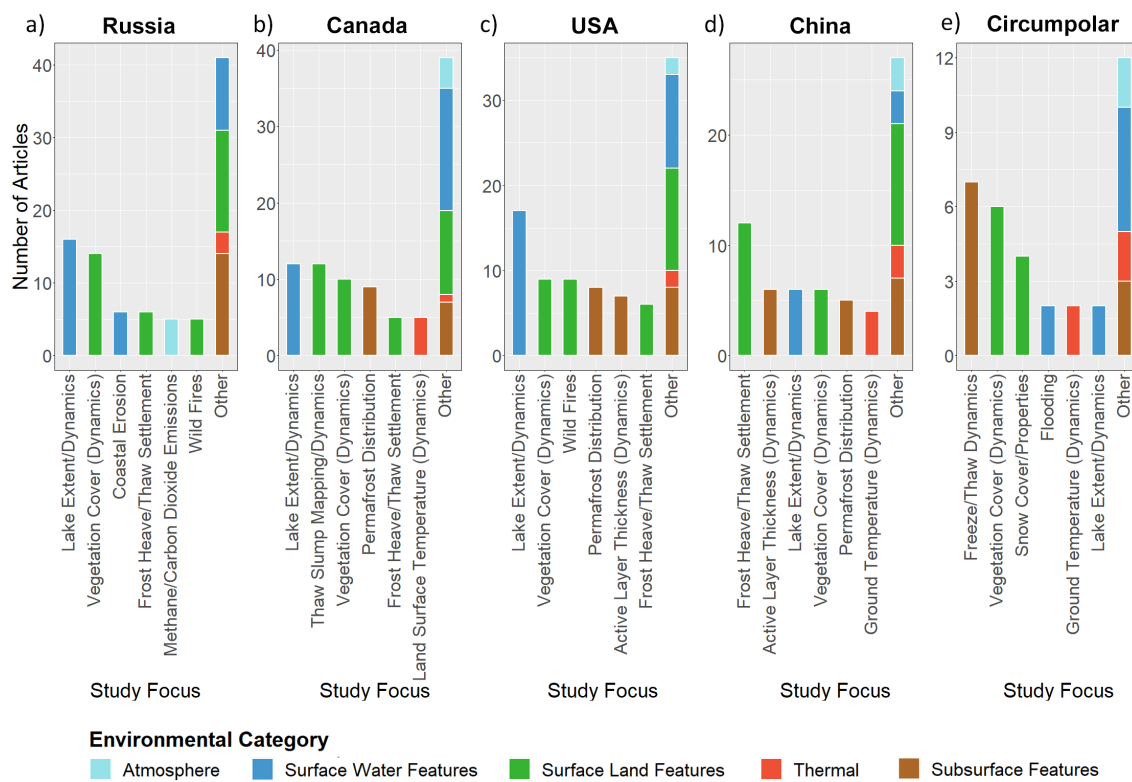


Figure 9. Study focus distribution for the top four most studied countries and circum-Arctic studies. Featured countries are Russia (a), Canada (b), United States (c), China (d) and circum-polar studies (e).

In Russia, 43% of articles studied “Surface Land Features and Processes”, followed by 34% “Surface Water Features and Processes”, 15% “Subsurface Features and Processes”, 5% “Atmospheric Features and Processes” and 3% “Thermal Features and Processes”. The most common research topics are lake extent (dynamics), vegetation cover (dynamics), coastal erosion and frost heave/thaw settlement observations.

Canadian studies are again mainly associated with “Surface Land Features and Processes” by 40%. “Surface Water Features and Processes” make up 33%, followed by 17%

“Subsurface Features and Processes”, 6% “Thermal Features and Processes” and 4% “Atmospheric Features and Processes”. Both lake extent (dynamics) and the analysis of thaw slumps were hereby the most popular research topics. Other frequent environmental subjects are vegetation cover (dynamics) and the distribution of permafrost.

As for the United States, while the category “Surface Land Features and Processes” is again the most studied sphere with 39%, “Surface Water Features and Processes” and “Subsurface Features and Processes” are also frequently investigated with 32% and 25%, respectively. On the other hand, both “Thermal Features and Processes” and “Atmospheric Features and Processes” make up only 2% each. Major efforts were put into lake extent (dynamics), followed by vegetation cover (dynamics), wild fires and the distribution of permafrost.

Articles with a study focus in China investigated once more for the most part “Surface Land Features and Processes” (43%). The relative distribution of other categories were 27% “Subsurface Features and Processes”, 14% “Surface Water Features and Processes” and 10% “Thermal Features and Processes” as well as 5% “Atmospheric Features and Processes”. With twice as many studies as the second most researched topic, frost heave/thaw settlement (dynamics) is the major investigation subject in China, followed by active layer thickness (dynamics), lake extent (dynamics) and vegetation cover (dynamics).

Lastly, there were a total of 28 articles which applied their analyses on a circum-Arctic or circum-Antarctic scale. Unlike the top four most studied countries, both categories “Subsurface Features and Processes” and “Surface Land Features and Processes” are equally distributed with 29% each, followed by 26% “Surface Water Features and Processes”, 11% “Thermal Features and Processes” and 6% “Atmospheric Features and Processes”. The most common permafrost related topic analyzed on a circumpolar level was thereby freeze/thaw dynamics. Next to that, vegetation cover (dynamics) as well as the influence of snow cover and associated properties on permafrost were hereby common study subjects, as well.

3.4.1. Environmental Research Focus: Atmospheric Features and Processes

Although several studies dedicated their research to a topic within the category “Atmospheric Features and Processes” (e.g., [13–15,33,33–37,213,226,268–270,330–333]), it still proved to be the least common environmental category in the context of this review. This relative shortage in permafrost-atmosphere-related studies highlights the need for satellite remote sensing research dedicated to investigate the effect of permafrost degradation on current and future greenhouse gas emissions. Song et al. [13] studied atmospheric methane release due to spring thawing effects of natural wetlands. In their research, extremely high CH₄ emissions via bubbling over the spring season were observed in addition to the methane emissions from thaw lakes. The authors further stress the importance of including this spring thawing effect into permafrost carbon-climate models, since the mentioned thawing process potentially becomes stronger in the face of climate change [13]. Another study by Watts et al. [14] investigated the effect of surface temperature and surface moisture on Arctic wetland methane release. The authors recommend future studies to consider potential impacts of fractional water scaling for regional modeling due to the highly dynamic surface water in northern high latitudes. They further warn about potential overestimation of modeled methane emission rates caused by insufficient resolution of satellite data which cannot account for small scale heterogeneity of soil temperature and moisture. However, new remote sensing data with higher temporal and/or spatial capabilities based on for example, Soil Moisture Active Passive (SMAP) may reduce uncertainties for regional and global modelling [14]. Curasi et al. [15] linked in their study the distribution of subsurface water tracks to carbon dioxide emissions in a Siberian tundra landscape. Since water tracks provide favourable conditions for increased shrub expansion, understanding the distribution of such water tracks may hereby improve our knowledge of the spatial variability in present and future tundra carbon cycling [15].

Contrary to lower latitudes (<60° N), Arctic methane emissions showed no significant increase in 2017 compared to the average value for 2000–2006 according to a study done by

Jackson et al. [334]. Dlugokencky et al. [335] observed similar results and suggested the Arctic has yet to reach the turning point of a sustained increase in CH₄ emissions cased by permafrost melt. However, the authors also state that there is a clear potential for increasing methane emissions in the future due to permafrost degradation [335].

In a recent publication, Anthony et al. [36] investigated methane emissions from thawing lakes in the Arctic. Emissions from expanding thermokarst lakes were hereby directly proportional to the eroded soil carbon caused by thawing permafrost [36]. Another study by Anthony et al. [37] revealed further insights into the acceleration of carbon emissions through abrupt permafrost thaw beneath Arctic lakes [37]. Additional study efforts were recently made by Elder et al. [336] who analysed CH₄ hotspots over Alaska and northwestern Canada via an airborne campaign covering ~30,000 km². The authors identified 2 Million methane hotspots which are concentrated in a radius of ~40 m around lakes [336].

The transatlantic National Aeronautics and Space Administration (NASA) and ESA collaborative community initiative Arctic Methane and Permafrost Challenge (AMPAC) aims to address the challenge of analysing the Arctic methane release and permafrost thawing through interdisciplinary research [337,338]. Furthermore, new satellites including the Sentinel-5P mission and the Methane Remote Sensing LiDAR Mission (Merlin) are hereby promising data sources for future analyses of permafrost related Arctic emissions. The ESA Sentinel-5P is a satellite mission for monitoring key atmospheric components, including CO, CH₄, CH₂O, NO₂, SO₂ and O₃ via the TROPOspheric Monitoring Instrument (TROPOMI) [339]. The mission extends data records from previous instruments such as the Global Ozone Monitoring Experiment (GOME), Scanning Imaging Absorption Spectrometer for Atmospheric Chartography (SCIAMACHY) or the Ozone Monitoring Instrument (OMI) [340]. Since its launch in February 2017, several studies employed Sentinel-5P data to investigate atmospheric methane concentrations [341–344]. As mentioned in a review by Duncan et al. [93], the TROPOspheric Monitoring Instrument (TROPOMI) instrument on board Sentinel-5P provides a better signal-to-noise ratio, a larger spectral range and higher spatial resolution relative to similar current satellite systems which in term allow for improved detection of trace gas concentrations. Nevertheless, the authors also identify arctic conditions such as bright surfaces (e.g., snow), steep sun angles, low light intensities and persistent cloud coverage to continue being major challenges for passive satellite systems such as Sentinel-5P [93]. These limitations can, however, be overcome to a certain degree by utilizing active satellite sensors such as the Light Detection and Ranging (LiDAR) instrument on the upcoming Merlin mission. Merlin is a joint German and French space mission by the German Aerospace Center (DLR) and the French National Centre for Space Studies (CNES), dedicated to generate spaceborne measurements of atmospheric methane concentration for regional to global scales [345]. Merlin will hereby be the first mission to utilize Integrated Path Differential Absorption (IPDA) LiDAR for monitoring methane from space [346]. Contrary to passive satellite missions, the active LiDAR sensor allows for retrieval of methane fluxes independent of season or sun illumination and at all latitudes [347]. The active nature of the instrument even allows for the penetration through thin cirrus clouds and therefore increases the observation capabilities [348]. A joint use of active and passive sensors could thereby overcome current challenges and improve our understanding of arctic emission rates [93].

3.4.2. Environmental Research Focus: Surface Water Features and Processes

Roughly one quarter of all articles was assigned to the category “Surface Water Features and Processes” (e.g., [349–368]). Overall, the majority of related studies are located in northern Alaska across the North Slope and its Arctic Coastal Plain, followed by the Mackenzie Delta, Gydan and Yamal Peninsula and the Lena Delta. As already visualized in Figure 7, the most common environmental focus within the category “Surface Water Features” is “Lake Extent/Dynamics”, covering roughly half of all studies connected to this category. A study by Morgenstern et al. [243] analyzed hereby the

spatial distribution of thermokarst basins and lakes in the Yedoma uplands around the Lena River Delta. The authors report large parts of the researched area to be affected by thermokarst, with thermokarst basins covering four times the total area as thermokarst lakes. Morgenstern et al. [243] further explained that 33.7% of the surface area on Kurungnakh Island is vulnerable to future thermokarst processes. Nevertheless, past thermokarst activities led to a severe degradation of original Yedoma landscapes, thus future erosion and lake extension due to thawing deposits may be limited [243]. Another study by Lyons et al. [170] dedicated their research to the error quantification of lake mapping by using Landsat data. Seven scenes were thereby analyzed based on the two sensors Multi Spectral Scanner (MSS) and Thematic Mapper (TM). The authors report an increasing error in lake area mapping with decreasing lake sizes. Lyons et al. [170] further described spectral properties to be highly variable due to the depth, vegetation and suspended sediments in lakes, making a threshold analysis difficult. Lastly, seasonal effects should be reduced as much as possible for long-term trends and inter-annual changes [170]. A recent study by Rey et al. [53] investigated the dynamics of lake area changes via a Landsat time-series analysis coupled with airborne electromagnetic surveys. The authors hereby observed relatively synchronous lake extent dynamics in continuous permafrost landscapes, whereas the lake area dynamics in discontinuous permafrost areas appeared more asynchronous. Rey et al. [53] argue these differences may be explained by a stronger subsurface-connectivity in discontinuous permafrost regions caused by differential thawing, while lake dynamics in continuous permafrost zones are primarily controlled by hydroclimatic factors. The authors further hypothesis that an ongoing degradation of permafrost in discontinuous permafrost regions could result in an ubiquitous connectivity and therefore again lead to synchronous lake dynamics. Similar to Morgenstern et al. [243], a decrease in lake extent dynamics is predicted, since the thawing of the subsurface functions as a low-pass filter for the variability in hydroclimatic processes [53].

The second most common topic but already significantly less in frequency is “Coastal Erosion”. In a study done by Lantuit and Pollard [233], coastal erosion rates on Herschel Island which is located in the western Canadian Arctic were analyzed over a time-span of 50 years using historical airphotos and IKONOS imagery. Although an overall decreasing trend in coastal erosion (0.61 m/yr from 1950–1970 and 0.45 m/yr from 1970–2000) can be depicted in this research, shorelines featuring high ice-contents and ground-ice related surface features for example, thaw slumps have increased erosion rates [233]. Barnhart et al. [39] studied the effect of changing sea ice on Arctic coastlines on a panarctic scale by using passive RADAR data with a 25 km spatial resolution. According to Barnhart et al. [39], the duration of open-water conditions was revealed to have doubled since 1979 and therefore increasing the vulnerability of Arctic coasts since sea ice acts as a limiter for wave-based fluvial erosion. However, understanding the relationship between coastal erosion and dynamics in the open water seasons is further complicated by for example, the present geomorphological conditions, storm climate, orientation, ice content and dynamics as well as the lithology [39]. A more recently published article by Isaev et al. [10] covers the retreat of cliffs along a permafrost coast in the south-western Baydaratskaya Bay in Russia by using handheld Differential Global Positioning System (DGPS) and high resolution QuickBird-2 satellite data. In agreement with Barnhart et al. [39], wind-driven waves during the open-water season are identified to be of higher relevance for coastal erosion in permafrost landscapes compared to increases in air temperature alone [10].

Several articles also dedicated their research to other surface water related features and processes, such as ocean colour (e.g., [219,258]), wetland dynamics (e.g., [250,312]) or lake/sea ice extent/dynamics (e.g., [39,168,369]).

3.4.3. Environmental Research Focus: Surface Land Features and Processes

With 43%, the category “Surface Land Features and Processes” featured the most articles out of all environmental categories (e.g., [45,370–405]). Analogous to “Surface Water Features and Processes”, study hotspots are also located in northern Alaska, the Mackenzie

Delta, Gydan and Yamal Peninsula as well as the Lena Delta. However, additional study clusters are concentrated inside the QTP, mountainous regions including the European Alps and the Andes, along with the South Shetland Islands in the Antarctic.

“Vegetation Cover (Dynamics)” is hereby the most common research focus. Epstein et al. [148] applied a Normalized Difference Vegetation Index (NDVI) time series analysis (1982–2010) on AVHRR data coupled with extensive in-situ measurements for estimating phytobiomass changes in the Arctic tundra on a circum-Arctic scale. The study revealed an average increase in above-ground biomass of 19.8%, resulting in major implications for a vast variety of tundra ecosystem aspects, such as the distribution of permafrost, depth of the active layer, hydrology, wildlife and human land use. The authors further stress the importance of future continuous and extensive field campaigns as a means for validation [148]. Kharuk et al. [406] investigated the growth response of larch trees in the central Siberian permafrost zone by using in-situ tree-ring samples, climate data as well as optical remote sensing imagery from Aqua and gravimetric satellite data from the Gravity Recovery And Climate Experiment (GRACE). The authors reported an increased productivity in larch stands at the beginning of the 21st century. The growth of tree rings correlated thereby for example, with water from snow- and permafrost melt, early summer air temperatures and drought conditions [406]. Changes in the vegetation cover along the QTP engineering corridor were observed in an article by Song et al. [281] through a time-series analysis based on Enhanced Vegetation Index (EVI) MODIS data spanning from 2000–2016. The study revealed a decreasing trend for roughly one-fifth of the vegetation caused by overgrazing and permafrost degradation. The degradation of permafrost resulted in increased water infiltration which forced the shallow rooted alpine meadows to retreat [281].

The second most common research topic within the category “Land Surface Features and Processes” is “Frost Heave/Thaw Settlement”. Chen et al. [71] for example, applied Persistent Scatterer Interferometry (PSI) on C- and L-band SAR imagery to investigate surface deformation along the QTR. Results of this study revealed significant deformation rates of ± 20 mm/yr along the embankment. The authors further stress the need for proactive cooling methods by using for example, block stone or crushed stone in the face of climate change, instead of relying only on permafrost-protecting techniques along the embankment of the QTR. Another study by Short et al. [231] investigated the applicability of X-, C- and L-band SAR data based on TerraSAR-X, RADARSAT-2 and Advanced Land Observing Satellite (ALOS)-Phased Array L-Band Synthetic Aperture Radar (PALSAR) for surface displacement observations on Herschel Island. The authors state that the high temporal and spatial resolution of TerraSAR-X makes the data suitable for detecting thaw slumps, however long-term movement observations are limited due to a high amount of noise even after stacking. Short et al. [231] further classify C-band data to be more reliable, whereas L-Band data provided overall best results. In the context of permafrost stability, long-term changes are of most interest and therefore showcasing the potential of C-band and L-band SAR data [231]. In a paper published by Strozzi et al. [43], Sentinel-1 interferometry analysis was conducted for low-land permafrost areas in both the Arctic and Antarctic. Results suggested high coherence during the snow-free summer-months, enabling one year interferograms and thus long-term analyses of deformation. However, the authors also reported only small deformation magnitudes and thereby limitations for the estimation of annual movement rates. Both, longer time-series as well as specific in-situ data for validating the Interferometric Synthetic Aperture Radar (InSAR) measurements are needed in future studies [43].

Early efforts in remote sensing and mountain permafrost were conducted by Kääb [47] who applied photogrammetry on airborne and space-born (Advanced Spaceborne Thermal Emission and Reflection Radiometer (ASTER)) optical data and therefore generating a Digital Elevation Model (DEM) for each stereo-pair of images. Kääb [47] subsequently calculated the difference between DEMs from multiple time steps in order to identify and quantify movements of for example, landslides and rock glaciers in the Swiss Alps. The

accuracy of horizontal displacement was hereby estimated to be roughly the size of one pixel [47]. A recent study by Strozzi et al. [60] dedicated their focus on monitoring rock glacier kinematics by the means of SAR data in the Swiss Alps, Greenland and the Andes. In their study, SAR interferometry analysis on Sentinel-1, TerraSAR-X, Constellation of small Satellites for Mediterranean basin Observation (COSMO-Skymed) and the Japanese Earth Resources Satellite 1 (JERS-1) was applied. Strozzi et al. [60] identified Sentinel-1 data to provide good performance next to very high resolution SAR images from the other platforms. Future long-term observations of rock glacier movements via Sentinel-1 are expected to be valuable indicators for assessing mountain permafrost conditions [60].

Both “Thaw Slump Mapping/Dynamics” and “Wild Fires” also feature a significant amount of research in the context of permafrost. Huang et al. [294] for example published one of the few permafrost-related articles which incorporated deep learning for their analysis. A total of 220 thaw slumps within an area of 5200 km² in the Beiluhe region of the QTP could hereby be mapped with CubeSat images [294]. Another study by Brown et al. [407] investigated the effects of wild fires on the distribution of permafrost for a 100 km² study area in the White Mountains National Recreation Area in Alaska. Higher burn severities were identified to strongly affect the extent of permafrost degradation and therefore the drainage conditions, which caused a drying of the soils [407].

3.4.4. Environmental Research Focus: Thermal Features and Processes

Being second to last in terms of article frequency, the category “Thermal Features and Processes” features overall sparser study distribution (e.g., [408–412]), with a cluster on the QTP, isolated studies in Alaska, Canada, Greenland, Norway and the Lena Delta as well as a handful of circumpolar studies. A number of articles focused on the potential of Land Surface Temperature (LST) as a proxy for the thermal state of permafrost. Hachem et al. [175] for example, compared MODIS LST data with ground and air temperature measurements for Northern Quebec in Canada and the North Slope of Alaska. The study demonstrated stronger correlation for air temperature (1–3 m above ground) vs. ground temperature (3–5 cm below surface). The authors suggest the variety of different materials on the ground as well as snow cover to be sources of uncertainty when correlating LST with ground temperature data. Furthermore, Hachem et al. [175] mention the lack of available data over the Arctic due to the abundance of cloud coverage and therefore limiting the potential for freeze/thaw analyses. However, by incorporating imagery from both Terra and Aqua LST in combination with temporal interpolation techniques, existing gaps could be filled [175]. The applicability of LST was further investigated in a recent study by Batbaatar et al. [323] who mapped permafrost distribution in an area around the volcano Ojos del Salado in Chile. Batbaatar et al. [323] used hereby ASTER and MODIS LST time-series data to map the so called “zero curtain”, which describes a slowed phase transition from water to ice caused by latent heat release, in order to delineate permafrost boundaries. The authors promote the potential for this approach over arid regions, however similar to Hachem et al. [175], snow cover, surface heterogeneity and cloud cover were identified to be limiting factors [323].

A total of 14 studies dedicated their research focus on “Ground Temperature (Dynamics)”. Gisnås et al. [313] applied CryoGRID 1.0 which is an equilibrium model based on the Temperature at the Top of Permafrost (TTOP) model originally developed by Smith and Riseborough [413]. The CryoGRID 1.0 model was hereby applied for estimating permafrost distribution and Mean Annual Ground Temperature (MAGT) in Norway at a 1 km² spatial resolution. The modelled MAGT showed good agreement with in-situ ground measurements. According to this study, lowest MAGT observed were –3.5 °C and therefore relatively warm for most areas in Norway. In the case of severe permafrost degradation after the IPCC Special Report on Emission Scenarios (SRES) A2 scenario for 2071–2100, only 0.2% of the mainland permafrost in Norway is expected to remain stable [313]. Westermann et al. [414] developed the CryoGRID 1.0 model even further and applied it on the North Atlantic permafrost region for MAGT estimation. However, the

authors highlight the need for investigating uncertainties in land cover maps and other associated parameters required for modelling [414]. Circumpolar modelling efforts based on CryoGRID were eventually conducted by Obu et al. [415] for the entire Northern Hemisphere at a 1 km² spatial resolution. The study employed satellite-derived land surface temperature data, ERA-Interim climate reanalysis data and land cover information from the ESA CCI project. Comparing the modelled MAGT values to borehole measurements revealed an accuracy of ± 2 °C [415]. As previously mentioned, in another recent study by Obu et al. [163] the CryoGRID 1.0 model was also applied to estimate MAGT for the entire Antarctic [163].

3.4.5. Environmental Research Focus: Subsurface Features and Processes

A considerable amount (21%) of reviewed articles investigated subsurface features and processes (e.g., [416–440]). Study clusters for this category are again located in Alaska, Mackenzie Delta, Lena Delta and the QTP, together with a few additional circum-Arctic studies. The environmental topic “Permafrost Distribution” was thereby the most common research focus of articles linked to this category. Including satellite derived information can lead to improved accuracies for modelling the distribution of permafrost [441]. The two previously mentioned studies by Westermann et al. [414] and Obu et al. [415] also developed permafrost zonation maps with the help of satellite imagery, in addition to the MAGT analyses for the North Atlantic permafrost region and the Northern Hemisphere, respectively. According to Obu et al. [415], 22% of exposed land area on the Northern Hemisphere are underlain by permafrost, which is roughly 2×10^6 km² less compared to previous estimations. Both the circumpolar MAGT and permafrost distribution maps are openly available as listed in Table 4. Another study by Zhang et al. [220] mapped the distribution of permafrost on a 20 m resolution scale for an area covering ~ 8836 km² in the Canadian Northwest Territories. The incorporation of satellite derived land cover maps hereby enabled Zhang et al. [220] to map permafrost on a higher spatial resolution compared to existing maps. However, the coarser resolution of available soil and ground condition data were a major limitation for high-resolution mapping of frozen ground [220].

The second most frequent topic in this category and closely related to the underlying permafrost is “Active Layer Thickness (Dynamics)”. Pastick et al. [442] combined airborne electromagnetic surveys with satellite remote sensing imagery from Landsat and other spatial data to model Active Layer Thickness (ALT) on a 30 m spatial resolution in the Yukon River Flats, Alaska. The authors report a successful implementation of the framework for quantifying ALT. Higher resolution topography and geological data as well as a larger amount of field observations could thereby improve future modelling results [442]. In a publication by Schaefer et al. [169] the Remotely Sensed Active Layer Thickness (ReSALT) algorithm was applied on L-band InSAR data from ALOS PALSAR to retrieve ALT estimations around Barrow, Alaska. As stated by the authors, comparisons with in-situ observations revealed good agreement for $\sim 76\%$ of the study area, whereas ALT observed from ReSALT was underestimated in $\sim 23\%$ and overestimated in $\sim 1\%$ of the investigated region. Schaefer et al. [169] attributed underestimations of ALT to InSAR artifacts and unsaturated soils as well as the presence of gravel which reduces the porosity of soils. The integration of detailed soil moisture data and information about gravel size/distribution are recommended for improving ALT measurements in future studies by using the ReSALT algorithm [169]. Widhalm et al. [260] on the other hand used X-band SAR data from TerraSAR-X for ALT estimations on a 10 m spatial resolution for a region with deep ALT in central Yamal, Russia. The authors reported hereby a positive correlation between ALT and the corresponding backscatter signal. Uncertainty factors mentioned by Widhalm et al. [260] are soil moisture, surface roughness and sub-pixel heterogeneity in vegetation cover. It was further hypothesized that polarimetric SAR might be useful in differentiating between different scattering mechanisms and therefore addressing these issues [260].

Another frequently occurring subsurface environmental focus is “Freeze/Thaw Dynamics”. Li et al. [443] for example, used daily SSM/I passive RADAR data to investigate changes in the freeze/thaw cycle across the QTP. The study revealed an overall decrease of 10–50 frozen days over the time-span 1988–2007. Furthermore, the authors reported earlier soil thawing dates by 14.3 ± 13.0 days and delayed soil freezing dates by 10.1 ± 11.2 days. Increasing air temperatures especially during the winter months are hypothesized to be the driving factor behind these changes, however, the impacts of ecological and hydrological conditions on the freeze-thaw cycle need to be further investigated [443]. In a study by Roy et al. [444], weekly L-band passive RADAR imagery was used to assess its applicability for monitoring freeze-thaw dynamics over Canada. Strong agreements between the satellite-based freeze-thaw detection for all reference data sets could be observed by the authors. Nonetheless, vegetation growth as well as liquid water content in snow and ice cover during the transition phase proved to be limiting factors for accurate freeze-thaw retrievals [444]. A more recently published article by Hu et al. [166] presented a global and continuous record on near-surface soil freeze/thaw conditions based on Advanced Microwave Scanning Radiometer-Earth Observing System (AMSR-E) and Advanced Microwave Scanning Radiometer 2 (AMSR2) passive RADAR data. As stated by the authors, modelled freeze/thaw dynamics showed good agreement with in-situ observations. Data fusion with other remote sensing products of higher spatial resolution could thereby potentially increase the spatial resolution for freeze-thaw analyses in future investigations [166].

Other commonly studied topics are the dynamics in groundwater storage volume (e.g., [209,433]), assessment of ice wedge volumes (e.g., [139,193,439]) and soil carbon or nitrogen stocks (e.g., [445,446]).

3.5. Applied Spatio-Temporal Resolutions of Reviewed Articles

Almost half (47%) of all reviewed articles were applying a time series analysis in their research. 28% of analyses are unitemporal, 4% are bitemporal and 21% are multitemporal. A slight trend towards a prolongation of the time series length could be observed across the articles published between 2000 and 2020, since more recent studies had access to longer satellite records. Furthermore, the majority (53%) of time series studies cover a period of less than 10 years, 39% of which are even less than 5 years. Of the time series, 47% are longer than 10 years and roughly one fifth (21%) cover more than 20 years. Time series range from less than a year to 44 years with a median length of 9 years. Figure 10 depicts the overall distribution of temporal resolutions (Figure 10a) as well as the development of the length of time series studies from older to more recent publications (Figure 10b). Further visualization of the time-series length can be found in the supplementary data under Figure S2.

Complementary to the temporal resolution, the investigated scales and applied spatial resolutions of the reviewed articles are visualized in Figure 11. Most studies investigated permafrost related features and processes on a local scale (62%), followed by small regional (16%) and large regional (12%) scales. Only 8% of articles applied their analysis on a circumpolar extent and just 1% of articles carried out their research on a national level. Thus, the majority of studies focus on local and small scale investigations (Figure 11a).

Looking at the spatial resolutions applied within each scale reveals roughly half (52%) of articles which conducted their analysis on an area smaller $10,000 \text{ km}^2$ utilized high resolution remote sensing data. On the same scale, another 38% applied medium high resolution imagery, 6% medium low and only 4% included satellite data with a pixel size larger 1 km^2 . Small regional studies also cover all resolution categories, however the amount of articles that incorporated high resolution imagery is significantly lower with 11%, whereas medium high resolution imagery is the dominant class with 57%. Studies with large regional or national scales did not utilize high resolution data at all. Also, the proportion of low resolution data increases with larger scales, which results in circum-Artic studies being predominantly (74%) conducted based on low resolution satellite imagery. In contrast, two articles investigated their circumpolar analysis on a medium high and

another four articles on a medium low spatial resolution. A single study applied high resolution aerial and satellite imagery in order to map ponds and lakes on a circum-Arctic scale [156]. Generally speaking, a strong relationship between the study area size and spatial resolution could be observed, with studies applied on larger areas featuring lower spatial resolutions and vice versa (Figure 11b).

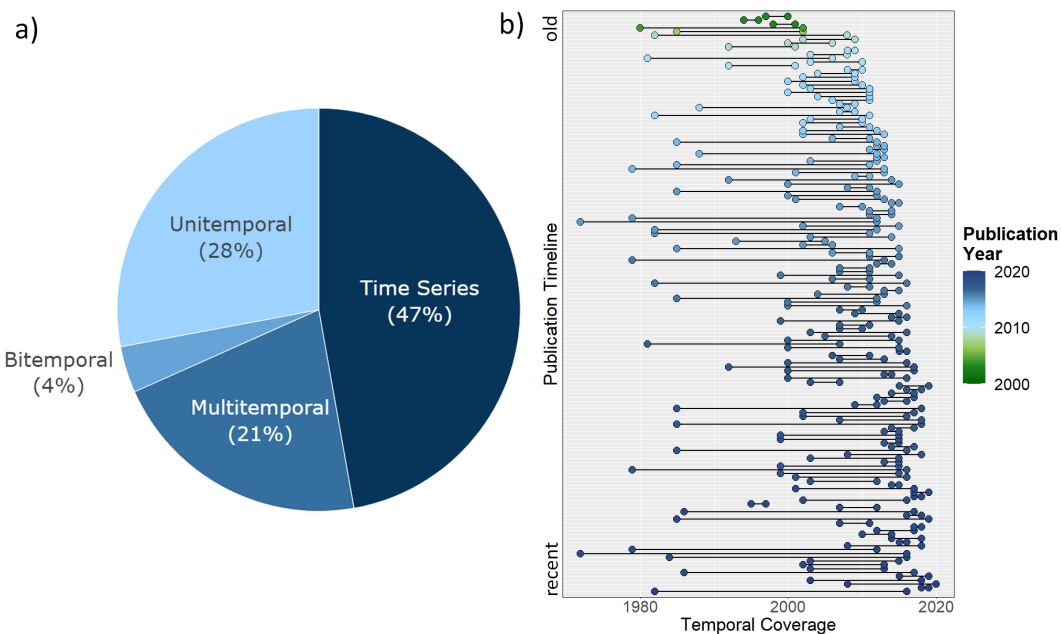


Figure 10. (a) Distribution of the temporal resolution across all reviewed articles. In the context of this review, “multitemporal” describes analyses which use 3–9 time steps, whereas a “time series” is defined to cover 10 time steps or more. (b) Timeline visualizing the time series length of articles that employed a time series analysis over the course of publication years. The x-axis shows the temporal coverage of applied time-series, the y-axis visualizes the temporal order in which articles that utilized time-series were published. The color gradient refers to the published year. The majority of studies which employed a time series analysis was published during the last decade.

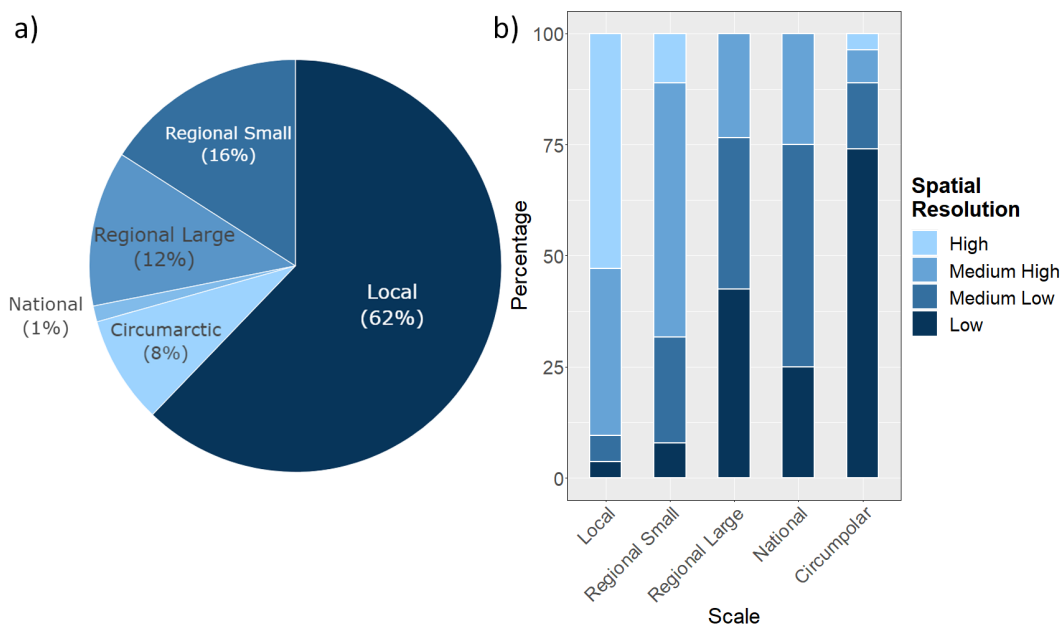


Figure 11. (a) Distribution of investigated spatial scales across the reviewed articles. The scales are categorized as local ($<10,000 \text{ km}^2$), regional small ($10,000\text{--}250,000 \text{ km}^2$), regional large ($>250,000 \text{ km}^2$), national or circum-Arctic. (b) Applied spatial resolutions within each scale. Spatial resolutions are categorized as high ($<10 \text{ m}$), medium high ($10\text{--}100 \text{ m}$), medium low ($100\text{--}1000 \text{ m}$) or low ($>1000 \text{ m}$).

The spatio-temporal resolution, time series length and area coverage for the top 20 most frequent environmental topics is visualized in Figure 12. The study area size covers for the most part relatively small regions ($<100 \text{ km}^2$ or $100\text{--}10,000 \text{ km}^2$). Especially the topics frost heave/thaw settlement, rock glaciers, thaw slumps, coastal erosion and ice wedge volumes are mainly studied on smaller spatial scales. On the other hand, more than half of the publications with a focus on freeze/thaw dynamics, are conducted on a large ($>1 \text{ Mio. km}^2$) or even circumpolar scale (Figure 12a).

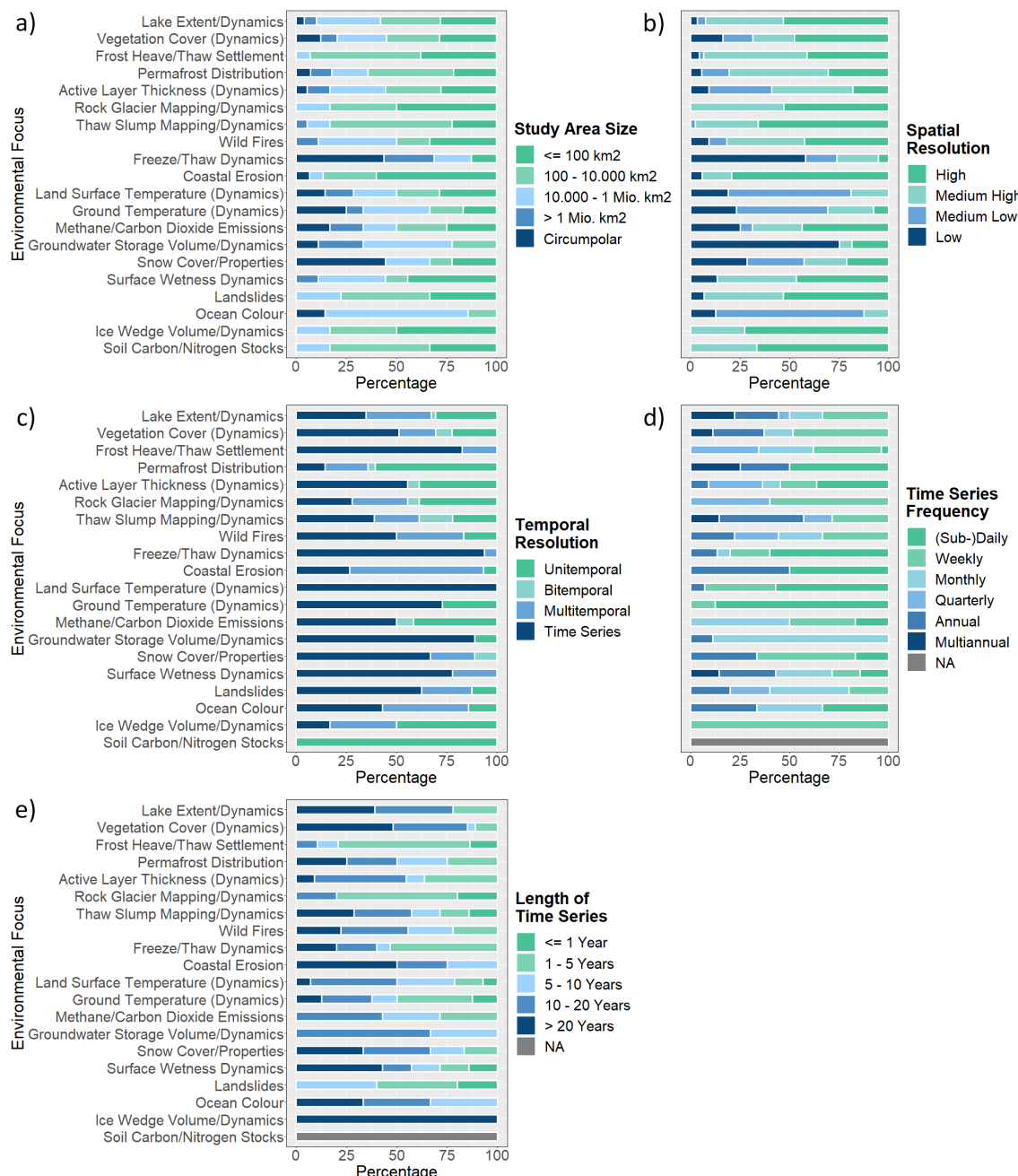


Figure 12. Distribution of spatial and temporal resolutions for the top 20 most frequent environmental topics within the reviewed articles. The y-axis is ordered by topic frequency. (a) Size of the study area. (b) Spatial resolution that is either high ($<10 \text{ m}$), medium high ($10\text{--}100 \text{ m}$), medium low ($100\text{--}1000 \text{ m}$) or low ($>1000 \text{ m}$). (c) Temporal resolution of studies. If ten or more time steps are used it is considered a time series within this review. (d) Temporal resolution applied within time series studies. (e) Length of time series for studies that conducted a time series analysis.

An analysis on the applied spatial resolution reveals a vast majority of studies utilized high (<10 m) to medium-high (10–100 m) resolutions for their research. Especially lake extent, rock glacier dynamics, thaw slumps, coastal erosion, ice wedges and soil carbon/nitrogen stocks are largely analyzed with high resolution remote sensing data which corresponds to the previously mentioned smaller study areas. Similarly, studies that are executed on larger spatial scales generally also utilized lower spatial resolution data (e.g., freeze/thaw dynamics and ground water storage volume dynamics) (Figure 12b).

As already stated, almost half of all reviewed articles applied a time series analysis for their research which is also reflected in the top 20 individual topics. All of the top 20 environmental topics featured articles that utilized time series analyses, except for soil carbon/nitrogen stock investigations. The environmental topics freeze/thaw dynamics, ground water storage volume dynamics and frost heave/thaw settlement are hereby almost exclusively studied via a time series. Environmental foci that feature predominantly untemporal studies are related to the distribution of permafrost, ice wedge/volume and soil carbon/nitrogen stocks (Figure 12c).

The frequency of time steps by which time series analyses were conducted varies across different topics. While some environmental foci feature a roughly even distribution of different time series frequencies (e.g., lake extent dynamics and vegetation cover dynamics), others are primarily conducted with higher frequencies on either a daily or weekly basis (e.g., freeze/thaw dynamics, land surface and ground temperature dynamics). Only one reviewed article applied a time series to investigate ice wedges [432] (Figure 12d).

Similar to the time series frequency, the length of time series per environmental topic is shown to be quite diverse. Albeit some topics mainly employ time series which cover 10 or more years (e.g., lake extent dynamics, vegetation cover dynamics, active layer thickness, coastal erosion and ice wedge volume), others mostly cover shorter time periods of less than 10 years, with some topics even encompass only 5 or less years in the majority of their time series analyses (e.g., frost heave/thaw settlement, rock glaciers or landslides). The environmental focus ice wedge volume features hereby 100% of its time series to cover more than 20 years, however, as already mentioned there was only a single study which performed a time series analysis for this topic [432] within this review (Figure 12e).

3.6. Platform and Sensor Distribution Across Reviewed Articles

Figure 13 displays the platform and sensor type distribution across all reviewed articles. Overall, data of optical nature is predominantly used with 55% throughout permafrost related investigations, followed by SAR (20%) and Thermal (9%) data. Noteworthy is also passive RADAR imagery, which makes up 7% of all sensor types.

Even though airborne-only studies were excluded from this review process, the most common platform is still of the type aerial (31% of all studies). The dominant sensor type is hereby optical, whereas some studies also carried out airborne RADAR, LiDAR and electromagnetic surveys.

The most frequent satellite platforms are from the Landsat mission (27% of all studies). Again, mainly optical imagery was applied, with only a few studies taking advantage of the thermal capabilities.

Next to the Landsat mission, the Terra and Aqua satellites are commonly used platforms. For both satellites, thermal data is a major focus accompanied by the optical imagery of the MODIS and ASTER sensors. In case of Aqua, some publications also worked with passive RADAR data via the AMSR-E sensor.

Several high-resolution optical satellites feature widespread occurrences in permafrost related studies. In particular images from the satellites Worldview-1/2/3, QuickBird-2, IKONOS, GeoEye-1, the Satellite Pour l’Observation de la Terre (SPOT) family, the RapidEye constellation and Gaofen-1/2 are commonly applied. The most frequent SAR-only platforms are (in the following order) TerraSAR-X, RADARSAT-1/2 and Sentinel-1.

ALOS is another frequently applied platform. For the most part the satellite is utilized thanks to its SAR data from the PALSAR sensor. In addition, optical imagery from both sen-

sors Advanced Visible and Near Infrared Radiometer Type 2 (AVNIR-2) and Panchromatic Remote-sensing Instrument for Stereo Mapping (PRISM) were employed in a few articles.

Data of various natures from the Environmental Satellite (Envisat) was used. SAR data by the Advanced Synthetic Aperture Radar (ASAR) sensor was hereby the most dominant data type, followed by optical data from the Medium Resolution Imaging Spectrometer (MERIS), thermal data from the Advanced Along Track Scanning Radiometer (AATSR) and altimetric data by the Radar Altimeter 2 (RA-2). Additionally, one study analyzed atmospheric trace gases via the SCIAMACHY sensor.

Also worth mentioning is the Defense Meteorological Satellite Program (DMSP), which was exclusively used for its passive RADAR capabilities from the SSM/I sensor. Furthermore, a handful of studies exploited the gravimetric products of the GRACE mission. Moreover, historical optical imagery of the CORONA program was utilized for long time series or as a historical reference point for change detection analyses.

Only a total of eight studies were working with optical imagery from the Sentinel-2 satellites, which could be explained by the relatively recent launch of Sentinel-2A in 2015 and Sentinel-2B in 2017 [447].

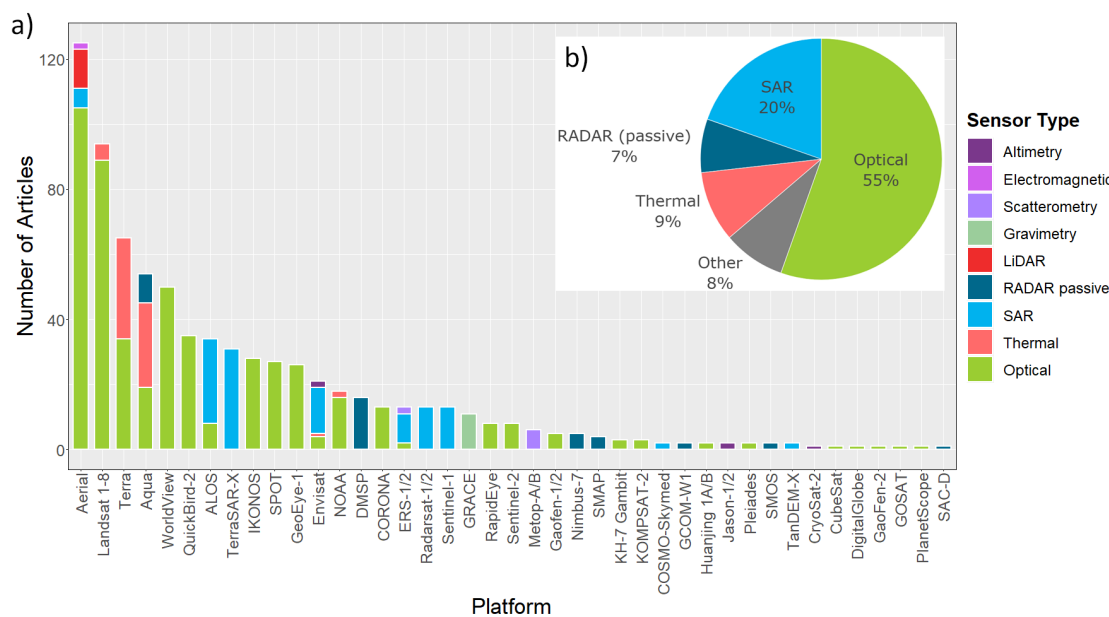


Figure 13. Remote sensing platforms utilized within the reviewed articles (a). Several platforms carry multiple sensors. The frequency of applied sensor types is therefore shown for each platform (a) as well as the overall distribution of sensor types (b). “Aerial” was also considered for the platform frequency analysis since many articles employed aerial imagery either as a historical reference, for validation or other complementary use with satellite data and is therefore included for completeness.

The increase in the number of publications per year is also reflected in the frequency of used satellite platforms over time (Figure 14a). Almost every year features one or several studies that incorporated aerial imagery next to satellite data (except for the years 2006 and 2007), which demonstrates its continuous relevance in the context of permafrost related research. Earliest analyses based on ALOS data could be observed for 2010 with a consistent usage since then. First efforts in using Aqua imagery for permafrost related investigations were applied in 2009, with higher publication counts in 2018 and 2019. Similar to Aqua, initial studies using Terra data already began in 2002, with spikes in 2018 and 2019, as well. Historical imagery from the CORONA satellites was sporadically applied since 2005. Similar to CORONA, DMSP was also used sporadically throughout the years without any positive or negative trend in frequency. First analyses on images taken by Envisat were published in 2010, whereby the highest publication count could

be observed in 2012 with no clear trend in the number of applications. Earliest usage of GeoEye-1 data occurred in 2013 with a peak in 2018. Other high resolution optical data by IKONOS was already incorporated in 2003 and features a sporadic recurrence throughout the following years. 2018 displays hereby an exceptional amount of articles with a total of seven studies working on IKONOS images. The application of Landsat data can be found in almost every year since 2001 (exceptions are 2002, 2004 and 2008) and demonstrates an overall steady increase in frequency over the years. Imagery from the National Oceanic and Atmospheric Administration (NOAA)-6 to -19 satellites was regularly implemented since 2003. Initial investigations on QuickBird imagery has taken place in 2005 with regular implementation since 2010. Studies based on SPOT data began in 2009, while most articles which utilized SPOT imagery were published in 2018. The majority of publications working with TerraSAR-X images appeared between 2017–2018. Lastly, efforts in studying WorldView data in the context of permafrost started in 2014, followed by frequent recurrences since then which reflects its position as the most commonly used high resolution optical satellite (Figure 13).

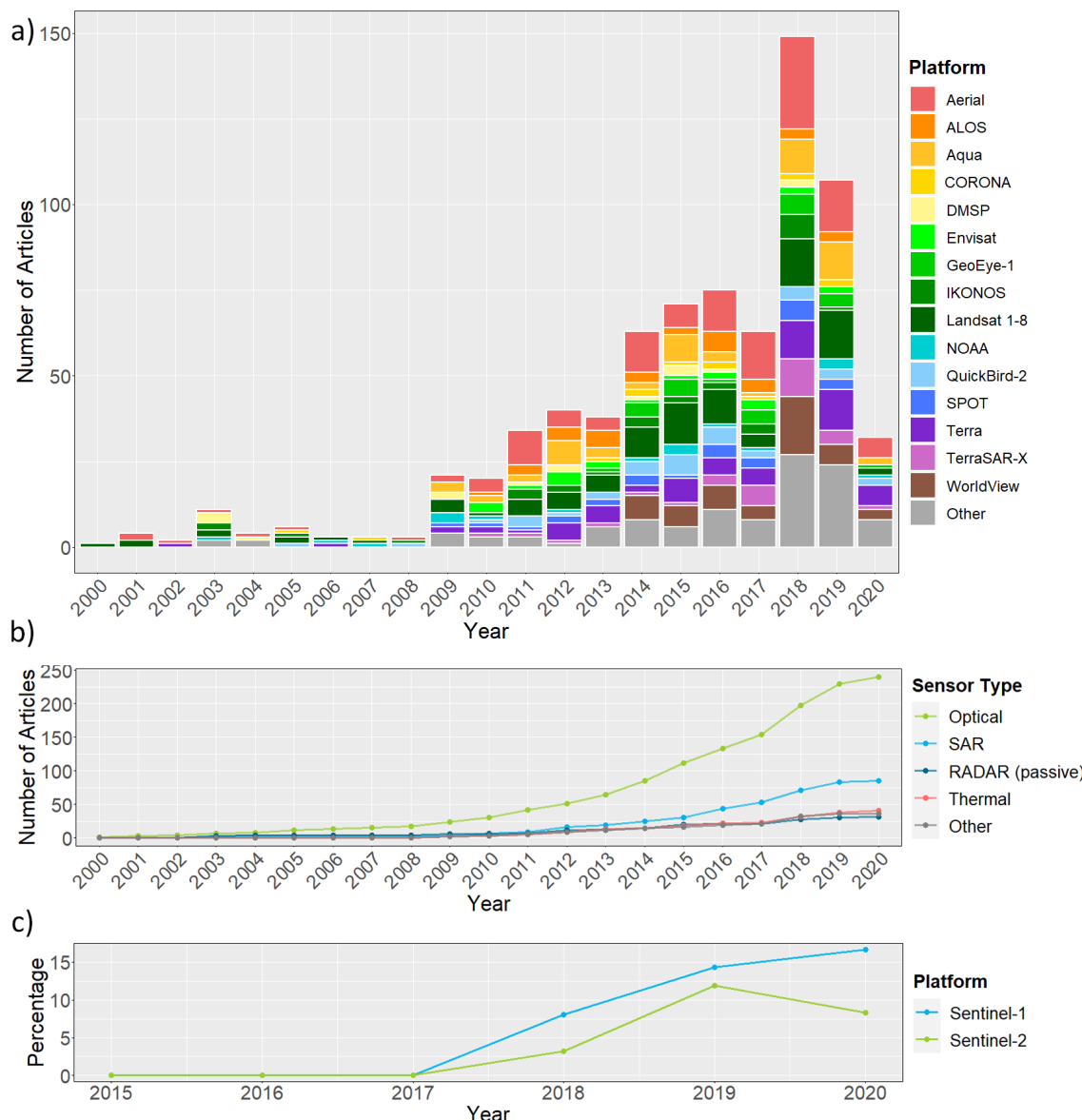


Figure 14. (a) Temporal development of the top 15 utilized remote sensing platforms within the reviewed articles over the past two decades. Several articles used data from multiple platforms. (b) Cumulative sum of applied sensor types over the past two decades. (c) Percentage of articles per year that utilized Sentinel imagery during the last five years.

Imagery from the Sentinel-fleet was first applied in 2018, with a growing percentage of articles per year including data from those satellite since then (Figure 14c). Sentinel-2 features hereby a slight decrease for the year 2020; however, only articles from the first two months of said year were analyzed. Therefore, the actual relative distribution for the complete year of 2020 might deviate. None of the reviewed publications took advantage of the Sentinel satellites prior to 2018, even though Sentinel-1A was already launched in 2014 and Sentinel-2A in 2015 [447,448].

The cumulative sum of applied sensor types is visualized in Figure 14b). Similar to Figure 14a), a continuous growing trend of publication frequency for all sensor types can be depicted during the last decade, with an exceptional increase since 2018. Strongest growth can thereby be observed for optical imagery, followed by SAR data. Thermal, passive RADAR and other sensor types feature relatively weak growing rates compared to optical and SAR sensor types.

Figure 15 provides further details on the sensor combinations applied on a per study basis. A differentiation between airborne and spaceborne sensors was hereby performed. With a total of 107 studies, roughly one third of all articles used exclusively optical satellite data. The first actual combination comes in at second place (49 articles; ~15%), which is comprised of optical satellite and airborne optical data. Aerial imagery serves thereby commonly either for increasing the temporal frequency of observations, as a means to analyse small scale patterns and changes which requires very high spatial resolution, or as a historical reference point. The third most common combination is again not a combination but 37 SAR-only studies (~11%). Next up is the joint use of optical and thermal satellite imagery, followed by 15 publication which applied only passive RADAR data. Other combinations such as optical + airborne optical + SAR, optical + SAR, thermal-only and airborne optical + SAR were commonly observed throughout the reviewed articles (13, 12, 11 and 10 articles, respectively). Noteworthy are also six articles that combined airborne LiDAR, airborne optical and optical satellite imagery for their analyses. Furthermore, ~15% of the reviewed permafrost related research articles applied different sensor combinations as the ones already mentioned which highlights the potential and possibilities of working with various remote sensing data products.

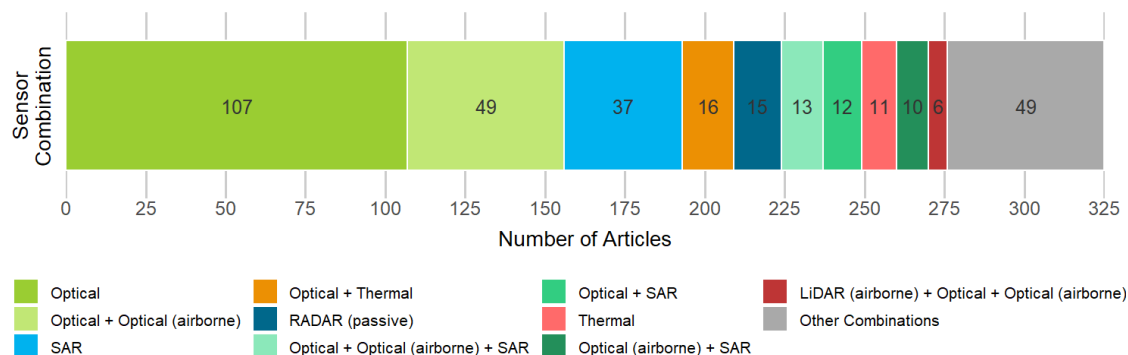


Figure 15. Frequency of the top ten most frequent sensor combinations analyzed within the reviewed articles. A differentiation between airborne and spaceborne sensor types was applied.

3.7. Relevant and Openly-Available Products for Permafrost-Related Analyses

A variety of openly available data sets which are relevant for Earth observation of permafrost are listed in Table 4. Atmospheric data for example, is provided by the international Cooperative Global Air Sampling Network through air flask samples for various greenhouse gases, including carbon monoxide, carbon dioxide and methane [104,449]. Information about snow cover duration are available via the Global SnowPack on a daily basis and a 500 m spatial resolution [450]. Further data for snow extent and snow water equivalent are provided by the ESA GlobSnow Snow Extent (SE) and GlobSnow Snow

Water Equivalent (SWE), with a daily frequency and 1 and 20 km spatial resolution, respectively [451,452]. Pekel et al. [453] used three million Landsat satellite images to globally map surface water on a 30 m spatial scale and a monthly temporal resolution since 1984. A coarser spatial but higher temporal resolution of surface water areas are publicly available through the Global WaterPack, which is based on daily MODIS data with a 250 m resolution [454]. In addition, Muster et al. [156] employed high resolution airborne and spaceborne imagery in a circum-Arctic mapping effort in order to delineate ponds and lakes with a resolution of 5 m or better. The Arctic Coastal Dynamics Database divided ~101,447 km of Arctic coastline into 1,315 segments and associated them with coastal erosion rates [73]. A number of different satellite derived land cover databases are available, including ESA CCI land cover, MODIS land cover, GlobeLand30, GLC2000 and the CAVM Raster Version [162,455–459]. A recent article by Liang et al. [161] compared four commonly used global land cover products. The authors hereby reported ESA CCI land cover to have the highest accuracy in Arctic regions (63.6%), closely followed by Glob-Land30 (62.2%). Global Land Cover by the National Mapping Organization (GLCNMO) and MODIS land cover products featured accuracies of 48.8% and 29.5%, respectively, and were therefore not recommended for studies related to the Arctic [161]. According to a review on land cover mapping in NHL by Bartsch et al. [22], CAVM proved to be the most frequently used map for circumpolar issues. While providing sufficient thematic details for many Arctic investigations, the moderate resolution of 1 km, restrictions to non-forested areas and the missing separation of shrub- and lichen-dominated land cover categories are major limitations [22]. Next to land cover data sets, there also exist products of trends in land cover changes such as provided by Nitze et al. [179]. The product features trends of various multi-spectral indices based on Landsat time-series analysis for four regional transects within the pan-Arctic permafrost domain [179]. Commonly applied digital elevation data are from the Shuttle Radar Topography Mission (SRTM) product, which covers land areas between latitudes of 56° south and 60° north at a 30 m spatial resolution [460]. Identical in resolution but covering the whole globe is the ALOS Digital Surface Model (DSM) through optical stereoscopic observations of the PRISM sensor on-board ALOS [461]. Lastly, the ArcticDEM allows for high resolution topographic analyses in Arctic regions above 60° north on a 2 m pixel scale based on optical stereo-imagery from Worldview-1, 2 and 3 satellites [462]. The SoilGrids database on the other hand provides global information about soil pH value, organic carbon content, soil texture and other parameters on a 250 m spatial resolution [463]. Further details about soil carbon stocks can be extracted from the Northern Circumpolar Soil CarbonDatabase version 2 (NCSCDv2) between 0–300 cm depth [464]. Moreover, the spatial distribution of 15,000 soil mapping units on a 30-arc second resolution raster is provided by the Harmonized World Soil Database (HWSD) [465,466]. Daily global soil moisture observations are available through the combination of four passive and two SAR satellite sensors on a coarse resolution of 0.25° in the ESA CCI Soil Moisture product [467]. As part of the NASA Making Earth System Data Records for Use in Research Environments (MEaSUREs) program and based on passive RADAR satellite remote sensing, daily records of freeze-thaw conditions on a global scale and 25 km resolution are obtainable for the years 1979 to 2017 [468]. Annual in-situ reference data of active layer thickness and near-surface permafrost for over 125 sites, including mountainous regions over 1300 m, is being published since 1990 by the Circumpolar Active Layer Monitoring (CALM) network [107,469]. Further borehole measurements were made openly available by the Thermal State of Permafrost (TSP) program [95]. Lastly, the commonly cited permafrost map by Brown et al. [1] displays the distribution of different permafrost zones, categorized as continuous, discontinuous, sporadic and isolated on a 1:10,000,000 scale. As previously mentioned in Section 3.4.5, recent efforts in circum-Arctic and circum-Antarctic mapping of the permafrost distribution and MAGT on a 1 km spatial resolution were made [163,415]. A selection of databases storing various of the previously mentioned data sets are listed in Table 5. Furthermore, new tools such as the PIC v1.3

R package allow for operational computation of possible trends of permafrost over the QTP [470].

Table 4. Overview of a variety of permafrost related and openly available products. The column “Temporal Resolution” shows the covered time span and in parenthesis the temporal frequency of available data, if more than one scene is available within the time span.

Name	Spatial Resolution	Temporal Resolution	Reference
Greenhouse Gases			
Cooperative Global Air Sampling Network	in-situ observations	since 1967 (varies)	NOAA Earth System Research Laboratories [104]
Snow Cover and Snow Water Equivalent			
Global Snow Pack	500 m	since 2000 (daily)	Dietz et al. [450]
ESA GlobSnow SWE	20 km	since 1979 (daily)	Metsämäki et al. [451]
ESA GlobSnow SE	1 km	since 1995 (daily)	Larue et al. [452]
Surface Water			
Global WaterPack	250 m	since 2003 (daily)	Klein et al. [454]
Global Surface Water	30 m	since 1984 (monthly)	Pekel et al. [453]
Permafrost Region Pond and Lake (PeRL) database	<5 m	2002–2013	Muster et al. [156]
Coastal Dynamics			
Arctic Coastal Dynamics Database	varies	2012	Lantuit et al. [73]
Land Cover			
ESA CCI land cover	300 m	1992–2015 (annual)	Plummer et al. [455]
MODIS land cover	500 m	since 2001 (annual)	Friedl et al. [456]
GlobeLand30	30 m	2000, 2010	Jun et al. [457]
GLC2000	1 km	2000	Bartholome and Belward [458]
Circumpolar Arctic Vegetation Map (CAVM) Raster Version	1 km	2003	Raynolds et al. [162]
Trends of land surface change from Landsat	30 m	1999–2014	Nitze et al. [179]
Digital Elevation and Surface Models			
ArcticDEM	2 m	2016	Morin et al. [462]
SRTM	30 m	2000	Farr et al. [460]
ALOS DSM	30 m	2006–2011	Takaku et al. [461]

Table 4. *Cont.*

Name	Spatial Resolution	Temporal Resolution	Reference
Soil Properties			
SoilGrids	250 m	2017	Hengl et al. [463]
Harmonized World Soil Database	30 arc-seconds	2012	FAO et al. [465]
Northern Circumpolar Soil Carbon Database version 2 (NCSCDv2)	0.012 degrees	2013	Hugelius et al. [464]
ESA CCI Soil Moisture	0.25 degrees	1978–2019 (daily)	Dorigo et al. [467]
Freeze/Thaw Dynamics			
MEaSUREs Global Record of Daily Landscape Freeze/Thaw Status	25 km	1979–2017 (daily)	Kim et al. [468]
Active Layer Thickness			
Circumpolar Active Layer Monitoring (CALM) program	in-situ observations	since 1990 (annual)	Brown et al. [469]
Borehole Measurements			
Thermal State of Permafrost (TSP) program	in-situ observations	2007–2009	Biskaborn et al. [95]
Permafrost Extent and Ground Temperature Maps			
Circum-Arctic Map of Permafrost and Ground-Ice Conditions, Version 2	Scale of 1:10,000,000	2002	Brown et al. [1]
Permafrost Extent and Ground Temperature Map	1 km	2000–2016	Obu et al. [415]
Pan-Antarctic map of near-surface permafrost temperatures	1 km	2000–2017	Obu et al. [163]

Table 5. Overview of a variety of permafrost related databases for openly available data.

Name	Description	Reference
Databases		
GTN-P database	Active Layer Thaw Depth & Permafrost Temperatures	Biskaborn et al. [95]
The Permafrost Information System (PerSys)	Portal for GlobPermafrost products, related results and data sets-Including ground and surface temperature, permafrost extent, Freeze/Thaw dynamics and others	Haas et al. [471]
PANGAEA	Data publisher and library for Earth and environmental science	Diepenbroek et al. [472]
National Snow & Ice Data Center	Management and distribution of cryospheric data	National Snow and Ice Data Center (NSIDC) [473]

4. Discussion

A strong relationship between the first authors institutional affiliation and their investigated study areas could be observed in this review, likely caused by research funding, the location of field sites and the availability of local reference data. Distinct study clusters are located in the North Slope of Alaska, Mackenzie Delta, Yamal and Gydan peninsulas, the Lena Delta and the Beiluhe region within the QTP (Figure 5). Although Russia features the highest number of studies out of any country (Figure 4), large parts of the permafrost affected landscapes outside the Lena Delta or Yamal and Gydan peninsulas require remote-sensing specific attention. A similar situation can be observed in Canada, where many research efforts are concentrated around the Mackenzie Delta, however large portions of both the mainland and Arctic islands of the Nunavut territory are only sparsely

covered (Figure 5), despite being underlain by large amounts of continuous permafrost. Study locations on the Southern Hemisphere are fewer in number due to the confined distribution of permafrost in alpine regions for example, Andes and ice-free areas of the South Shetland Islands in the Antarctic. That said, thanks to products such as the pan-Antarctic map of near-surface permafrost temperatures by Obu et al. [163], more investigations on permafrost occurrences within the Southern Hemisphere can be expected in the future.

In order to fully assess global and long-term implications for land cover and atmosphere caused by degrading permafrost, analyses on large scales with high temporal and spatial resolutions as well as long temporal coverage are required. However, only 9% of the reviewed articles applied their analyses on a circum-Arctic scale thus far. In fact, the majority of articles (62%) concentrated their research efforts on local investigations (Figure 11a). In 60% of studies on coastal erosion the covered area is even less than 100 km^2 (Figure 12a). Despite almost half (47%) of studies applying a time-series analysis in their investigations, only 47% of said studies feature time-series lengths that exceed 10 years and just one fifth (21%) cover more than 20 years (Figure 10). Freely available tools for example, the recently launched cloud-based geospatial analysis platform Google Earth Engine (GEE) make it easier than it has ever been before to work with mass data and large time-series, even if the computational power of an individual is limited [474]. First efforts of exploiting the computational capabilities of GEE are demonstrated by for example, Nyland et al. [475], who processed dense Landsat time-series since 1985 in order to quantify land cover change for an $\sim 60.750\text{ km}^2$ area in the central Siberian Arctic. Another study by Nill et al. [204] used the cloud computing capabilities of GEE to identify changes in land surface temperature and spectral indices over the Mackenzie Delta, Canada. With increasing spatio-temporal coverage of available satellite data records and computational platforms (e.g., GEE) that allow for long-term analyses on larger scales, our knowledge of permafrost-related land cover dynamics is likely to improve in the upcoming years.

Only very few studies explored the potential of deep learning in studying permafrost related features thus far. Next to the previously mentioned study by Huang et al. [294], first successful deep learning implementations were undertaken by for example, Langford et al. [476] who applied a multi-sensor deep learning approach to map Arctic vegetation for an area in western Alaska covering $\sim 343\text{ km}^2$. A study by Zhang et al. [477] combined airborne and satellite remote sensing data together with a deep learning algorithm to map ice-wedge polygons. In another study by Zhang et al. [478], high resolution airborne imagery in combination with a deep learning approach was applied to correctly classify 95% of individual ice-wedge polygons for an area of 134 km^2 in northern Alaska. Bartsch et al. [479] mapped Arctic settlements in a recent study via the joint use of optical and SAR satellite imagery. The authors hereby compared the performance of a machine learning approach via Gradient Boosting Machines (GBM) and deep learning based segmentation. User accuracy revealed higher scores for the deep learning method, however, in order to achieve overall best possible results, a combination of GBM and deep learning is suggested [479]. Due to the large potential of deep learning algorithms an increase in study efforts for deep learning of permafrost related features can be expected in the future.

The categorization of applied study foci into five spheres revealed “Surface Land Features and Processes” to be the most studied category overall (43%) as well as the fastest growing category in terms of published articles per year. The categories “Surface Water Features and Processes” and “Subsurface Features and Processes” feature a similar overall distribution (25% and 21%) and temporal development over time. The two categories “Atmospheric Features and Processes” and “Thermal Features and Processes” feature lowest overall article numbers and weakest growing rates, with “Atmospheric Features and Processes” only making up $\sim 4\%$ of all reviewed articles (Figure 7). As stated by for example, Jackson et al. [334] and Dlugokencky et al. [335], as of right now the emission rates in the Arctic are significantly lower compared to other latitudes. However, due to the degradation of permafrost, increasing greenhouse gas emissions can be expected in the near

future [334,335]. This highlights the need for future satellite remote sensing investigations in this context. New collaborative community initiatives for example, AMPAC underline the importance of addressing this challenging issue and lay foundations for future study efforts [337,338]. Next to atmospheric analyses, the thermal capabilities of satellite sensors are relatively sparsely utilized, which is especially notable for the Landsat mission (Figure 13). Although thermal data is often included in the analysis of subsurface features (e.g., distribution of permafrost) as an additional proxy, few studies focus specifically on the potential of thermal imagery. Valuable insights through the exploitation of thermal sensors were already given by for example, Hachem et al. [175] and Batbaatar et al. [323]. Therefore, long-term thermal analyses might still hold unexplored potentials for future permafrost-related studies, especially by taking advantage of the temporal coverage and relatively high spatial resolution of Landsat thermal products.

Another important parameter about permafrost is its distribution not only on land, but also in marine areas. A global sea level rise of approximately 120 m since the Late Pleistocene led to a flooding of coastal land areas underlain by permafrost [480]. The inundation of these former land areas caused an increase in ground temperature and therefore a potential release of stored methane hydrates to the sea [481,482]. None of the reviewed articles dedicated their research to subsea-permafrost. While several studies focused their research to sea surface properties (e.g., [151,217–219,255,258,410]), submarine permafrost itself is largely invisible to satellite remote sensing which explains the lack of studies in this field of research [483].

Although strong advancements in both methodology and satellite technology were presented throughout this review, many limitations for current satellite remote sensing system in the context of permafrost related research still remain, aside from not being able to directly measure the sub-surface frozen ground. While satellite missions such as Landsat allow for regular and long term time-series analysis of surface spectral properties covering multiple decades, data before the year 2000 is relatively sparse, especially in the Arctic region [22]. Environmental Arctic conditions including steep sun angles, low light intensities (including polar night) and persistent cloud coverage are further challenges for passive satellite systems [93]. As mentioned by Myers-Smith et al. [484], the unique challenges of polar remote sensing are often under-emphasized. Active systems such as SAR on the other hand are largely independent from the mentioned limitations of passive systems, but at the same time do have their own constraints [134,135]. In the context of surface deformation analyses, decorrelation between SAR scenes caused by altering surface properties (changing snow cover, soil moisture, vegetation cover etc.) restrict the applicability and accuracy of D-InSAR studies [26,94]. In particular short wavelength SAR imagery (e.g., X-band), while usually offering a higher spatial resolution, feature stronger noise levels for long-term movement observations compared to longer wavelength SAR data (e.g., L-band) [231]. Furthermore, the limited accessibility to high spatial resolution imagery for monitoring small scale features and processes is another commonly mentioned obstacle [22,76,134].

Despite this reviews focus on satellite Earth observation, the most frequent platform across all reviewed articles was revealed to be of the type aerial (Figure 13). In order to fully capture the dynamics and processes of many permafrost related landscape features for example, patterned ground, coastal erosion or thaw slumps, both data of very high spatial and temporal resolution are required [76]. Therefore, airborne data is likely to continue being a relevant input parameter in the near future [76,137,485]. This puts further emphasis on the need for easy and open access to high-resolution satellite imagery on a single digit meter or even sub-meter scale for a wider audience.

Imagery from optical sensors are applied most commonly out of all sensor types and also feature fastest growing rates in terms of their application in permafrost related studies during the last 20 years, followed by SAR data. An increasing amount of openly available images from optical and SAR satellites, for example, Sentinel-1/2, are hereby likely the reason for the continuous acceleration in their application frequency. Thus far, imagery

taken by the Sentinel-satellites only make up a small portion of the remote sensing data based on the articles reviewed in this paper. This can partly be attributed to the relatively recent launch dates of the individual satellites compared to long living missions such as Landsat or Terra/Aqua. However, this review also demonstrated the expanding utilization of Sentinel data during the last few years. The spectral properties, spatial and temporal resolution capabilities as well as the continuous global coverage make them a valuable data source for future permafrost research. Moreover, the combination of data from sensors of the same (e.g., optical imagery from Sentinel-2 and Landsat-8) or different nature (e.g., optical & SAR) hold great potential, as demonstrated by Runge and Grosse [142] who examined the feasibility of combining Landsat-8 and Sentinel-2 imagery. The authors reported strong correlation of spectral values between the two satellites, however local adjustments are recommended over global parameters [142].

Many Arctic products are openly available to help investigate permafrost-related issues and are suitable for reference and validation (Table 4). However, especially land cover products still lack either in thematic detail, spatial resolution, spatial coverage and/or accuracy [161]. Thus, an accurate circum-Arctic land cover map with high spatial resolution and sufficient thematic detail has yet to be published [22]. Moreover, data collection of relevant parameters are often concentrated around specific areas across the ~23 million km permafrost domain on the Northern Hemisphere, due to the remoteness and limited accessibility of large portions of permafrost-landscapes [52].

In this review, the focus was put on satellite remote sensing of permafrost related features and processes. A total of 325 articles from 30 international journals were hereby analyzed. We are aware that other relevant studies may have been published in journals with a specific application focus, which were not covered in this paper. However, the inclusion of additional journals would go beyond the scope of this review. For the same reason, we refrained from including non-English articles. Furthermore, the applied filtering approach may also have led to the exclusion of some relevant articles. That said, by applying the mentioned filtering criteria, we believe to have investigated a representative sample of available articles related to this field of study. By covering 11 international journals with a focus and remote sensing as well as 19 non-remote sensing specific international journals we consider this approach to be a good compromise for a representative overview.

5. Conclusions

This review provides an extensive overview of satellite Earth observation of permafrost related analysis during the last 20 years. A total of 325 articles from 30 international journals were analyzed based on the study country and first author institution nationality, the geographical study hot-spots, the distribution of environmental foci, the spatio-temporal resolution and scale of applied satellite data as well as the frequency of utilized remote sensing platforms and sensor combinations. In addition, relevant and openly available geospatial products for permafrost-related analyses are presented. The following main conclusions can be drawn from this review:

- The frequency of satellite Earth observation of permafrost related publications increased over the past two decades, with a particular growth during the last 10 years. The total number of publications hereby more than doubled since 2015.
- A strong relationship between the studied country and the first authors institution nationality could be observed. 93% of articles with a study focus in China were conducted by Chinese institutions, 80% of studies carried out in the United States are associated with American institutions and 58% of investigations in Canada are linked to Canadian institutions.
- Most studies (75%) were conducted in Russia, China, the United States and Canada.
- While the majority of first authors are affiliated with American (28%), Chinese (18%), German (15%) or Canadian (14%) institutions, first authors from Russian institutions (2%) appear underrepresented, potentially due to the exclusion of non-English articles.

- Geographical focus regions across the reviewed articles are revealed to be the North Slope Borough and its Arctic Coastal Plain in Alaska, the Mackenzie Delta in Canada, the Lena Delta and Yamal and Gydan Peninsulas in Russia as well as the Beiluhe region on the Qinghai–Tibet Plateau (QTP) in China.
- Many remote areas especially in the continuous permafrost zone of Russia and the Nunavut territory in Canada are still only sparsely covered by satellite remote sensing studies.
- The majority of studies (94%) is distributed across the Northern Hemisphere, whereas only a few articles (6%) investigated the Southern Hemisphere due to the confined distribution of permafrost in alpine regions for example, Andes and ice-free areas for example, South Shetland Islands in the Antarctic.
- Almost half (43%) of all reviewed articles studied land surface features/processes, followed by surface water features/processes (25%) and subsurface features/processes (21%). Studies related to thermal features/processes and atmospheric features and processes appear heavily underrepresented with only 7% and 4% of all reviewed publications, respectively.
- The category land surface features/processes is also revealed to have the strongest growing rates of 85 publications during the last five years within the framework of this review, followed by surface water features/processes (48 publications during the last five years), subsurface features/processes (47 publications during the last five years), thermal features/processes (16 publications during the last five years) and atmospheric features/processes (7 publications during the last five years).
- A regional deviation of study foci could be observed, with Canada, Russia and the United States featuring lake extent dynamics as the most common research objective, whereas studies in China mostly focus on surface displacement measurements along the Qinghai–Tibet Railway (QTR).
- Although almost half of all articles employed a time series analysis (10 scenes or more), 39% of which cover less than five years and only 21% cover more than 20 years.
- The majority of studies (62%) are limited to local scales, with only 8% of articles applying their analyses on a circumpolar scale.
- A general trend towards coarser spatial resolutions with increasing study area sizes can be observed and thus, 74% of circumpolar studies conducted their research on spatial resolutions >1000 m.
- The applied spatio-temporal resolution varies across different research topics. Topics such as frost heave/thaw settlement, coastal erosion or thaw slumps are usually conducted on local scales and with high spatial resolution, whereas observations of for example, freeze/thaw dynamics feature large regional or circumpolar extents and lower spatial resolutions.
- More than half (55%) of studies applied optical imagery, followed by SAR (20%). The most frequent platform is hereby aerial (31% of articles), followed by the Landsat satellites (27% of articles). As of right now, imagery from the Sentinel-fleet makes up only a small fraction (6%) of used satellite systems thus far. However, a growing application rate could be observed during the last three years, with Sentinel-1 being applied in 14% and Sentinel-2 in 12% of studies in 2019. Although aerial-exclusive studies have been excluded from this review, it still proved to be the most common platform. A complementary usage of airborne remote-sensing either as a historical reference, for validation or for the analysis of small scale features in conjunction with high-resolution satellite data are thereby explanations.
- Openly available Arctic products enable detailed analysis and validation of many permafrost related parameters. However, many products still lack either in thematic detail, spatial and temporal coverage and/or resolution are often concentrated around specific key regions.

New methodologies in terms of data combination/fusion and deep learning algorithms might improve classification accuracies and are expected to be the focus of several

upcoming permafrost-related investigations. There is a need for wider and free accessibility of very high resolution (single digit meter to sub-meter scale) satellite remote sensing data in order to fully capture the dynamics and processes of many small scale permafrost related landscape features for example, patterned ground, coastal erosion or thaw slumps. Next to that, long-term and large to circum-Arctic scale analyses of permafrost-related features are required to fully understand the current situation and future implications of degrading permafrost. Studies related to Arctic greenhouse gas emissions are underrepresented and will likely be a heavy focus in the upcoming years. Especially the Sentinel-5P mission and the Methane Remote Sensing LiDAR Mission (Merlin) are hereby promising data sources for future analyses. Furthermore, Landsat will continue to be a valuable satellite data source for long time series analyses and thanks to cloud computing capabilities through for example, Google Earth Engine (GEE), circum-Arctic analysis on a 30 m scale is easier than it has ever been before. Especially the potential of the thermal band(s) of Landsat sensors are under-utilized. Lastly, imagery from the Sentinel-fleet will likely be applied frequently in future studies, due to their spatial and temporal resolutions, global coverage, freely available data policy and the increasing potential for time-series investigations.

Supplementary Materials: The following are available online at www.mdpi.com/xxx/s1, Figure S1: Relationship of the first author institution nationality and study country. Figure S2: Discrete categorization of the time-series length across all reviewed studies that worked with time series data.

Author Contributions: Conceptualization, M.P. and C.K.; writing—original draft preparation, M.P.; writing—review and editing, M.P., A.D., S.B. and C.K.; visualization, M.P.; supervision, C.K. All authors have read and agreed to the published version of the manuscript.

Funding: This publication was supported by the Open Access Publication Fund of the University of Wuerzburg.

Acknowledgments: We would like to thank three anonymous reviewers for their helpful comments on this manuscript.

Conflicts of Interest: The authors declare no conflict of interest. The funders had no role in the design of the study; in the collection, analyses, or interpretation of data; in the writing of the manuscript, or in the decision to publish the results.

References

1. Brown, J.; Ferrians, O.; Heginbottom, J.; Melnikov, E. *Circum-Arctic Map of Permafrost and Ground-Ice Conditions*, Version 2; National Snow and Ice Data Center: Boulder, CO, USA, 2002. [[CrossRef](#)]
2. Schuur, E.A.; McGuire, A.D.; Schädel, C.; Grosse, G.; Harden, J.; Hayes, D.J.; Hugelius, G.; Koven, C.D.; Kuhry, P.; Lawrence, D.M.; et al. Climate change and the permafrost carbon feedback. *Nature* **2015**, *520*, 171–179. [[CrossRef](#)]
3. Pörtner, H.O.; Roberts, D.C.; Masson-Delmotte, V.; Zhai, P.; Tignor, M.; Poloczanska, E.; Mintenbeck, K.; Nicolai, M.; Okem, A.; Petzold, J.; et al. *IPCC Special Report on the Ocean and Cryosphere in a Changing Climate*; IPCC Intergovernmental Panel on Climate Change (IPCC): 2019, in press.
4. Whiteman, G.; Hope, C.; Wadhams, P. Vast costs of Arctic change. *Nature* **2013**, *499*, 401–403. [[CrossRef](#)] [[PubMed](#)]
5. Arenson, L.U.; Jakob, M. Periglacial geohazard risks and ground temperature increases. In *Engineering Geology for Society and Territory-Volume 1*; Springer: Berlin, Germany, 2015; pp. 233–237.
6. Farquharson, L.M.; Romanovsky, V.E.; Cable, W.L.; Walker, D.A.; Kokelj, S.V.; Nicolsky, D. Climate change drives widespread and rapid thermokarst development in very cold permafrost in the Canadian High Arctic. *Geophys. Res. Lett.* **2019**, *46*, 6681–6689. [[CrossRef](#)]
7. Zhang, X.; Zhang, H.; Wang, C.; Tang, Y.; Zhang, B.; Wu, F.; Wang, J.; Zhang, Z. Time-series InSAR monitoring of permafrost freeze-thaw seasonal displacement over Qinghai–Tibetan Plateau using Sentinel-1 data. *Remote Sens.* **2019**, *11*, 1000. [[CrossRef](#)]
8. Rudy, A.C.; Lamoureux, S.F.; Treitz, P.; Short, N.; Brisco, B. Seasonal and multi-year surface displacements measured by DInSAR in a High Arctic permafrost environment. *Int. J. Appl. Earth Obs. Geoinf.* **2018**, *64*, 51–61. [[CrossRef](#)]
9. Wang, C.; Zhang, Z.; Zhang, H.; Wu, Q.; Zhang, B.; Tang, Y. Seasonal deformation features on Qinghai–Tibet railway observed using time-series InSAR technique with high-resolution TerraSAR-X images. *Remote Sens. Lett.* **2017**, *8*, 1–10. [[CrossRef](#)]
10. Isaev, V.; Koshurnikov, A.; Pogorelov, A.; Amangurov, R.; Podchasov, O.; Sergeev, D.; Buldovich, S.; Aleksyutina, D.; Grishakina, E.; Kioka, A. Cliff retreat of permafrost coast in south-west Baydaratskaya Bay, Kara Sea, during 2005–2016. *Permafr. Periglac. Process.* **2019**, *30*, 35–47. [[CrossRef](#)]

11. Cunliffe, A.M.; Tanski, G.; Radosavljevic, B.; Palmer, W.F.; Sachs, T.; Lantuit, H.; Kerby, J.T.; Myers-Smith, I.H. Rapid retreat of permafrost coastline observed with aerial drone photogrammetry. *Cryosphere* **2019**, *13*, 1513–1528. [[CrossRef](#)]
12. Jones, B.M.; Farquharson, L.M.; Baughman, C.A.; Buzard, R.M.; Arp, C.D.; Grosse, G.; Bull, D.L.; Günther, F.; Nitze, I.; Urban, F.; et al. A decade of remotely sensed observations highlight complex processes linked to coastal permafrost bluff erosion in the Arctic. *Environ. Res. Lett.* **2018**, *13*, 115001. [[CrossRef](#)]
13. Song, C.; Xu, X.; Sun, X.; Tian, H.; Sun, L.; Miao, Y.; Wang, X.; Guo, Y. Large methane emission upon spring thaw from natural wetlands in the northern permafrost region. *Environ. Res. Lett.* **2012**, *7*, 034009. [[CrossRef](#)]
14. Watts, J.D.; Kimball, J.S.; Bartsch, A.; McDonald, K.C. Surface water inundation in the boreal-Arctic: Potential impacts on regional methane emissions. *Environ. Res. Lett.* **2014**, *9*, 075001. [[CrossRef](#)]
15. Curasi, S.R.; Loranty, M.M.; Natali, S.M. Water track distribution and effects on carbon dioxide flux in an eastern Siberian upland tundra landscape. *Environ. Res. Lett.* **2016**, *11*, 045002. [[CrossRef](#)]
16. Cohen, J.; Screen, J.A.; Furtado, J.C.; Barlow, M.; Whittleston, D.; Coumou, D.; Francis, J.; Dethloff, K.; Entekhabi, D.; Overland, J.; et al. Recent Arctic amplification and extreme mid-latitude weather. *Nat. Geosci.* **2014**, *7*, 627–637. [[CrossRef](#)]
17. Serreze, M.C.; Barry, R.G. Processes and impacts of Arctic amplification: A research synthesis. *Glob. Planet. Chang.* **2011**, *77*, 85–96. [[CrossRef](#)]
18. Brown, R.D.; Robinson, D.A. Northern Hemisphere spring snow cover variability and change over 1922–2010 including an assessment of uncertainty. *Cryosphere* **2011**, *5*, 219. [[CrossRef](#)]
19. Kim, Y.; Kimball, J.S.; Zhang, K.; McDonald, K.C. Satellite detection of increasing Northern Hemisphere non-frozen seasons from 1979 to 2008: Implications for regional vegetation growth. *Remote Sens. Environ.* **2012**, *121*, 472–487. [[CrossRef](#)]
20. Pearson, R.G.; Phillips, S.J.; Loranty, M.M.; Beck, P.S.; Damoulas, T.; Knight, S.J.; Goetz, S.J. Shifts in Arctic vegetation and associated feedbacks under climate change. *Nat. Clim. Chang.* **2013**, *3*, 673–677. [[CrossRef](#)]
21. Van Everdingen, R.O. *Multi-Language Glossary of Permafrost and Related Ground-Ice Terms in Chinese, English, French, German, Icelandic, Italian, Norwegian, Polish, Romanian, Russian, Spanish, and Swedish*; Arctic Inst. of North America University of Calgary, 2005. Available online: https://globalcryospherewatch.org/reference/glossary_docs/Glossary_of_Permafrost_and_Ground-Ice_IPA_2005.pdf (accessed on 14 January 2021).
22. Bartsch, A.; Höfler, A.; Kroisleitner, C.; Trofaier, A.M. Land cover mapping in northern high latitude permafrost regions with satellite data: Achievements and remaining challenges. *Remote Sens.* **2016**, *8*, 979. [[CrossRef](#)]
23. Trofaier, A.M.; Westermann, S.; Bartsch, A. Progress in space-borne studies of permafrost for climate science: Towards a multi-ECV approach. *Remote Sens. Environ.* **2017**, *203*, 55–70. [[CrossRef](#)]
24. Duguay, C.R.; Zhang, T.; Leverington, D.W.; Romanovsky, V.E. Satellite remote sensing of permafrost and seasonally frozen ground. *Geophys.-Monogr.-Am. Geophys. Union* **2005**, *163*, 91.
25. Chen, W.; Zhang, Y.; Cihlar, J.; Smith, S.L.; Riseborough, D.W. Changes in soil temperature and active layer thickness during the twentieth century in a region in western Canada. *J. Geophys. Res. Atmos.* **2003**, *108*, 4696–4708. [[CrossRef](#)]
26. Westermann, S.; Duguay, C.R.; Grosse, G.; Kääb, A., Remote sensing of permafrost and frozen ground. In *Remote Sensing of the Cryosphere*; John Wiley & Sons, Ltd.: Hoboken, NJ, USA, 2014; pp. 307–344. Chapter 13. [[CrossRef](#)]
27. Stephani, E.; Drage, J.; Miller, D.; Jones, B.M.; Kanevskiy, M. Taliks, cryopegs, and permafrost dynamics related to channel migration, Colville River Delta, Alaska. *Permafro. Periglac. Process.* **2020**, *31*, 239–254. [[CrossRef](#)]
28. Romanovsky, V.E.; Smith, S.L.; Christiansen, H.H. Permafrost thermal state in the polar Northern Hemisphere during the international polar year 2007–2009: A synthesis. *Permafro. Periglac. Process.* **2010**, *21*, 106–116. [[CrossRef](#)]
29. Slater, A.G.; Lawrence, D.M. Diagnosing present and future permafrost from climate models. *J. Clim.* **2013**, *26*, 5608–5623. [[CrossRef](#)]
30. Pastick, N.J.; Jorgenson, M.T.; Wylie, B.K.; Nield, S.J.; Johnson, K.D.; Finley, A.O. Distribution of near-surface permafrost in Alaska: Estimates of present and future conditions. *Remote Sens. Environ.* **2015**, *168*, 301–315. [[CrossRef](#)]
31. Zhao, S.; Zhang, S.; Cheng, W.; Zhou, C. Model simulation and prediction of Decadal Mountain permafrost distribution based on remote sensing data in the Qilian Mountains from the 1990s to the 2040s. *Remote Sens.* **2019**, *11*, 183. [[CrossRef](#)]
32. Subcommittee, P. Glossary of permafrost and related ground-ice terms. *Assoc. Comm. Geotech. Res. Natl. Res. Counc. Can. Ott.* **1988**, *142*, 156.
33. Nassar, R.; Sioris, C.E.; Jones, D.B.; McConnell, J.C. Satellite observations of CO₂ from a highly elliptical orbit for studies of the Arctic and boreal carbon cycle. *J. Geophys. Res. Atmos.* **2014**, *119*, 2654–2673. [[CrossRef](#)]
34. Hartley, I.P.; Hill, T.C.; Wade, T.J.; Clement, R.J.; Moncrieff, J.B.; Prieto-Blanco, A.; Disney, M.I.; Huntley, B.; Williams, M.; Howden, N.J.; et al. Quantifying landscape-level methane fluxes in subarctic Finland using a multiscale approach. *Glob. Chang. Biol.* **2015**, *21*, 3712–3725. [[CrossRef](#)]
35. Jørgensen, C.J.; Johansen, K.M.L.; Westergaard-Nielsen, A.; Elberling, B. Net regional methane sink in High Arctic soils of northeast Greenland. *Nat. Geosci.* **2015**, *8*, 20–23. [[CrossRef](#)]
36. Anthony, K.W.; Daanen, R.; Anthony, P.; von Deimling, T.S.; Ping, C.L.; Chanton, J.P.; Grosse, G. Methane emissions proportional to permafrost carbon thawed in Arctic lakes since the 1950s. *Nat. Geosci.* **2016**, *9*, 679–682. [[CrossRef](#)]
37. Anthony, K.W.; von Deimling, T.S.; Nitze, I.; Froliking, S.; Emond, A.; Daanen, R.; Anthony, P.; Lindgren, P.; Jones, B.; Grosse, G. 21st-century modeled permafrost carbon emissions accelerated by abrupt thaw beneath lakes. *Nat. Commun.* **2018**, *9*, 1–11.

38. Schneider, J.; Grosse, G.; Wagner, D. Land cover classification of tundra environments in the Arctic Lena Delta based on Landsat 7 ETM+ data and its application for upscaling of methane emissions. *Remote Sens. Environ.* **2009**, *113*, 380–391. [[CrossRef](#)]
39. Barnhart, K.; Overeem, I.; Anderson, R. The effect of changing sea ice on the physical vulnerability of Arctic coasts. *Cryosphere* **2014**, *8*, 1777–1799. [[CrossRef](#)]
40. Novikova, A.; Belova, N.; Baranskaya, A.; Alekseyutina, D.; Maslakov, A.; Zelenin, E.; Shabanova, N.; Ogorodov, S. Dynamics of permafrost coasts of Baydaratskaya Bay (Kara Sea) based on multi-temporal remote sensing data. *Remote Sens.* **2018**, *10*, 1481. [[CrossRef](#)]
41. Obu, J.; Lantuit, H.; Grosse, G.; Günther, F.; Sachs, T.; Helm, V.; Fritz, M. Coastal erosion and mass wasting along the Canadian Beaufort Sea based on annual airborne LiDAR elevation data. *Geomorphology* **2017**, *293*, 331–346. [[CrossRef](#)]
42. Günther, F.; Overduin, P.P.; Sandakov, A.V.; Grosse, G.; Grigoriev, M.N. Short- and long-term thermo-erosion of ice-rich permafrost coasts in the Laptev Sea region. *Biogeosciences* **2013**, *10*, 4297–4318. [[CrossRef](#)]
43. Strozzi, T.; Antonova, S.; Günther, F.; Mätzler, E.; Vieira, G.; Wegmüller, U.; Westermann, S.; Bartsch, A. Sentinel-1 SAR interferometry for surface deformation monitoring in low-land permafrost areas. *Remote Sens.* **2018**, *10*, 1360. [[CrossRef](#)]
44. Antonova, S.; Sudhaus, H.; Strozzi, T.; Zwieback, S.; Kääb, A.; Heim, B.; Langer, M.; Bornemann, N.; Boike, J. Thaw subsidence of a yedoma landscape in northern Siberia, measured in situ and estimated from TerraSAR-X interferometry. *Remote Sens.* **2018**, *10*, 494. [[CrossRef](#)]
45. Hu, J.; Wang, Q.; Li, Z.; Zhao, R.; Sun, Q. Investigating the ground deformation and source model of the Yangbajing geothermal field in Tibet, China with the WLS InSAR technique. *Remote Sens.* **2016**, *8*, 191. [[CrossRef](#)]
46. Short, N.; LeBlanc, A.M.; Sladen, W.; Oldenborger, G.; Mathon-Dufour, V.; Brisco, B. RADARSAT-2 D-InSAR for ground displacement in permafrost terrain, validation from Iqaluit Airport, Baffin Island, Canada. *Remote Sens. Environ.* **2014**, *141*, 40–51. [[CrossRef](#)]
47. Kääb, A. Monitoring high-mountain terrain deformation from repeated air-and spaceborne optical data: Examples using digital aerial imagery and ASTER data. *ISPRS J. Photogramm. Remote Sens.* **2002**, *57*, 39–52. [[CrossRef](#)]
48. Hao, J.; Wu, T.; Wu, X.; Hu, G.; Zou, D.; Zhu, X.; Zhao, L.; Li, R.; Xie, C.; Ni, J.; et al. Investigation of a small landslide in the Qinghai-Tibet Plateau by InSAR and absolute deformation model. *Remote Sens.* **2019**, *11*, 2126. [[CrossRef](#)]
49. Kharuk, V.I.; Shushpanov, A.S.; Im, S.T.; Ranson, K.J. Climate-induced landsliding within the larch dominant permafrost zone of central Siberia. *Environ. Res. Lett.* **2016**, *11*, 045004. [[CrossRef](#)] [[PubMed](#)]
50. Jorgenson, M.; Osterkamp, T.E. Response of boreal ecosystems to varying modes of permafrost degradation. *Can. J. For. Res.* **2005**, *35*, 2100–2111. [[CrossRef](#)]
51. Park, H.; Kim, Y.; Kimball, J.S. Widespread permafrost vulnerability and soil active layer increases over the high northern latitudes inferred from satellite remote sensing and process model assessments. *Remote Sens. Environ.* **2016**, *175*, 349–358. [[CrossRef](#)]
52. Grosse, G.; Goetz, S.; McGuire, A.D.; Romanovsky, V.E.; Schuur, E.A. Changing permafrost in a warming world and feedbacks to the Earth system. *Environ. Res. Lett.* **2016**, *11*, 040201. [[CrossRef](#)]
53. Rey, D.M.; Walvoord, M.; Minsley, B.; Rover, J.; Singha, K. Investigating lake-area dynamics across a permafrost-thaw spectrum using airborne electromagnetic surveys and remote sensing time-series data in Yukon Flats, Alaska. *Environ. Res. Lett.* **2019**, *14*, 025001. [[CrossRef](#)]
54. Wang, L.; Jolivel, M.; Marzahn, P.; Bernier, M.; Ludwig, R. Thermokarst pond dynamics in subarctic environment monitoring with radar remote sensing. *Permafro. Periglac. Process.* **2018**, *29*, 231–245. [[CrossRef](#)]
55. Nitze, I.; Grosse, G.; Jones, B.M.; Arp, C.D.; Ulrich, M.; Fedorov, A.; Veremeeva, A. Landsat-based trend analysis of lake dynamics across northern permafrost regions. *Remote Sens.* **2017**, *9*, 640. [[CrossRef](#)]
56. Farquharson, L.; Mann, D.H.; Grosse, G.; Jones, B.M.; Romanovsky, V. Spatial distribution of thermokarst terrain in Arctic Alaska. *Geomorphology* **2016**, *273*, 116–133. [[CrossRef](#)]
57. Jones, B.M.; Grosse, G.; Arp, C.D.; Miller, E.; Liu, L.; Hayes, D.J.; Larsen, C.F. Recent Arctic tundra fire initiates widespread thermokarst development. *Sci. Rep.* **2015**, *5*, 1–13. [[CrossRef](#)] [[PubMed](#)]
58. Gibson, C.M.; Chasmer, L.E.; Thompson, D.K.; Quinton, W.L.; Flannigan, M.D.; Olefeldt, D. Wildfire as a major driver of recent permafrost thaw in boreal peatlands. *Nat. Commun.* **2018**, *9*, 1–9. [[CrossRef](#)] [[PubMed](#)]
59. Zhou, Z.; Liu, L.; Jiang, L.; Feng, W.; Samsonov, S.V. Using long-term SAR backscatter data to monitor post-fire vegetation recovery in tundra environment. *Remote Sens.* **2019**, *11*, 2230. [[CrossRef](#)]
60. Strozzi, T.; Caduff, R.; Jones, N.; Barboux, C.; Delaloye, R.; Bodin, X.; Kääb, A.; Mätzler, E.; Schrott, L. Monitoring Rock Glacier Kinematics with Satellite Synthetic Aperture Radar. *Remote Sens.* **2020**, *12*, 559. [[CrossRef](#)]
61. Brenning, A.; Long, S.; Fieguth, P. Detecting rock glacier flow structures using Gabor filters and IKONOS imagery. *Remote Sens. Environ.* **2012**, *125*, 227–237. [[CrossRef](#)]
62. Kartozia, A. Assessment of the ice wedge polygon current state by means of UAV imagery analysis (Samoylov Island, the Lena Delta). *Remote Sens.* **2019**, *11*, 1627. [[CrossRef](#)]
63. Lousada, M.; Pina, P.; Vieira, G.; Bandeira, L.; Mora, C. Evaluation of the use of very high resolution aerial imagery for accurate ice-wedge polygon mapping (Adventdalen, Svalbard). *Sci. Total Environ.* **2018**, *615*, 1574–1583. [[CrossRef](#)]
64. Luo, J.; Niu, F.; Lin, Z.; Liu, M.; Yin, G. Recent acceleration of thaw slumping in permafrost terrain of Qinghai-Tibet Plateau: An example from the Beiluhe Region. *Geomorphology* **2019**, *341*, 79–85. [[CrossRef](#)]

65. Swanson, D.K.; Nolan, M. Growth of retrogressive thaw slumps in the Noatak Valley, Alaska, 2010–2016. measured by airborne photogrammetry. *Remote Sens.* **2018**, *10*, 983. [[CrossRef](#)]
66. Segal, R.A.; Lantz, T.C.; Kokelj, S.V. Acceleration of thaw slump activity in glaciated landscapes of the Western Canadian Arctic. *Environ. Res. Lett.* **2016**, *11*, 034025. [[CrossRef](#)]
67. Jorgenson, M.T.; Harden, J.; Kanevskiy, M.; O'Donnell, J.; Wickland, K.; Ewing, S.; Manies, K.; Zhuang, Q.; Shur, Y.; Striegl, R.; et al. Reorganization of vegetation, hydrology and soil carbon after permafrost degradation across heterogeneous boreal landscapes. *Environ. Res. Lett.* **2013**, *8*, 035017. [[CrossRef](#)]
68. Jones, B.M.; Grosse, G.; Arp, C.; Jones, M.; Anthony, K.W.; Romanovsky, V. Modern thermokarst lake dynamics in the continuous permafrost zone, northern Seward Peninsula, Alaska. *J. Geophys. Res. Biogeosci.* **2011**, *116*, G00M03. [[CrossRef](#)]
69. Yoshikawa, K.; Hinzman, L.D. Shrinking thermokarst ponds and groundwater dynamics in discontinuous permafrost near Council, Alaska. *Permafro. Periglac. Process.* **2003**, *14*, 151–160. [[CrossRef](#)]
70. Hinzman, L.D.; Bettez, N.D.; Bolton, W.R.; Chapin, F.S.; Dyrgerov, M.B.; Fastie, C.L.; Griffith, B.; Hollister, R.D.; Hope, A.; Huntington, H.P.; et al. Evidence and implications of recent climate change in northern Alaska and other arctic regions. *Clim. Chang.* **2005**, *72*, 251–298. [[CrossRef](#)]
71. Chen, F.; Lin, H.; Li, Z.; Chen, Q.; Zhou, J. Interaction between permafrost and infrastructure along the Qinghai–Tibet Railway detected via jointly analysis of C-and L-band small baseline SAR interferometry. *Remote Sens. Environ.* **2012**, *123*, 532–540. [[CrossRef](#)]
72. Hjort, J.; Karjalainen, O.; Aalto, J.; Westermann, S.; Romanovsky, V.E.; Nelson, F.E.; Etzelmüller, B.; Luoto, M. Degrading permafrost puts Arctic infrastructure at risk by mid-century. *Nat. Commun.* **2018**, *9*, 1–9. [[CrossRef](#)]
73. Lantuit, H.; Overduin, P.P.; Couture, N.; Wetterich, S.; Aré, F.; Atkinson, D.; Brown, J.; Cherkashov, G.; Drozdov, D.; Forbes, D.L.; et al. The Arctic coastal dynamics database: A new classification scheme and statistics on Arctic permafrost coastlines. *Estuaries Coasts* **2012**, *35*, 383–400. [[CrossRef](#)]
74. Radosavljevic, B.; Lantuit, H.; Pollard, W.; Overduin, P.; Couture, N.; Sachs, T.; Helm, V.; Fritz, M. Erosion and flooding—Threats to coastal infrastructure in the Arctic: A case study from Herschel Island, Yukon Territory, Canada. *Estuaries Coasts* **2016**, *39*, 900–915. [[CrossRef](#)]
75. Couture, N.J.; Irrgang, A.; Pollard, W.; Lantuit, H.; Fritz, M. Coastal erosion of permafrost soils along the Yukon Coastal Plain and fluxes of organic carbon to the Canadian Beaufort Sea. *J. Geophys. Res. Biogeosci.* **2018**, *123*, 406–422. [[CrossRef](#)]
76. Jorgenson, M.T.; Grosse, G. Remote sensing of landscape change in permafrost regions. *Permafro. Periglac. Process.* **2016**, *27*, 324–338. [[CrossRef](#)]
77. Schnabel, W.E.; Goering, D.J.; Dotson, A.D. Permafrost Engineering on Impermanent Frost. *Bridge* **2020**, *50*, 16–23.
78. Meredith, M.; Sommerkorn, M.; Cassotta, S.; Derksen, C.; Ekaykin, A.; Hollowed, A.; Kofinas, G.; Mackintosh, A.; Melbourne-Thomas, J.; Muelbert, M.; et al. Chapter 3: Polar Regions. In *IPCC Special Report on the Ocean and Cryosphere in a Changing Climate*; Pörtner, H.O., Roberts, D.C., Masson-Delmotte, V., Zhai, P., Tignor, M., Poloczanska, E., Mintenbeck, K., Nicolai, M., Okem, A., Petzold, J., et al., Eds.; IPCC Intergovernmental Panel on Climate Change (IPCC): 2019, in press.
79. Humlum, O.; Instanes, A.; Sollid, J.L. Permafrost in Svalbard: A review of research history, climatic background and engineering challenges. *Polar Res.* **2003**, *22*, 191–215. [[CrossRef](#)]
80. Qingbai, W.; Yongzhi, L.; Jianming, Z.; Changjiang, T. A review of recent frozen soil engineering in permafrost regions along Qinghai–Tibet Highway, China. *Permafro. Periglac. Process.* **2002**, *13*, 199–205. [[CrossRef](#)]
81. Cheng, G. Permafrost studies in the Qinghai–Tibet plateau for road construction. *J. Cold Reg. Eng.* **2005**, *19*, 19–29. [[CrossRef](#)]
82. Yang, M.; Nelson, F.E.; Shiklomanov, N.I.; Guo, D.; Wan, G. Permafrost degradation and its environmental effects on the Tibetan Plateau: A review of recent research. *Earth-Sci. Rev.* **2010**, *103*, 31–44. [[CrossRef](#)]
83. Voigt, C.; Lamprecht, R.E.; Marushchak, M.E.; Lind, S.E.; Novakovskiy, A.; Aurela, M.; Martikainen, P.J.; Biasi, C. Warming of subarctic tundra increases emissions of all three important greenhouse gases—Carbon dioxide, methane, and nitrous oxide. *Glob. Chang. Biol.* **2017**, *23*, 3121–3138. [[CrossRef](#)] [[PubMed](#)]
84. Abbott, B.W.; Jones, J.B.; Schuur, E.A.; Chapin III, F.S.; Bowden, W.B.; Bret-Harte, M.S.; Epstein, H.E.; Flannigan, M.D.; Harms, T.K.; Hollingsworth, T.N.; et al. Biomass offsets little or none of permafrost carbon release from soils, streams, and wildfire: An expert assessment. *Environ. Res. Lett.* **2016**, *11*, 034014. [[CrossRef](#)]
85. Kleinen, T.; Brovkin, V. Pathway-dependent fate of permafrost region carbon. *Environ. Res. Lett.* **2018**, *13*, 094001. [[CrossRef](#)]
86. Van Vuuren, D.P.; Edmonds, J.; Kainuma, M.; Riahi, K.; Thomson, A.; Hibbard, K.; Hurtt, G.C.; Kram, T.; Krey, V.; Lamarque, J.F.; et al. The representative concentration pathways: An overview. *Clim. Chang.* **2011**, *109*, 5–31. [[CrossRef](#)]
87. Koven, C.D.; Schuur, E.; Schädel, C.; Bohn, T.; Burke, E.; Chen, G.; Chen, X.; Ciais, P.; Grosse, G.; Harden, J.W.; et al. A simplified, data-constrained approach to estimate the permafrost carbon-Climate feedback. *Philos. Trans. R. Soc. A Math. Phys. Eng. Sci.* **2015**, *373*, 20140423. [[CrossRef](#)]
88. Koven, C.D.; Lawrence, D.M.; Riley, W.J. Permafrost carbon-climate feedback is sensitive to deep soil carbon decomposability but not deep soil nitrogen dynamics. *Proc. Natl. Acad. Sci. USA* **2015**, *112*, 3752–3757. [[CrossRef](#)]
89. Schaefer, K.; Lantuit, H.; Romanovsky, V.E.; Schuur, E.A.; Witt, R. The impact of the permafrost carbon feedback on global climate. *Environ. Res. Lett.* **2014**, *9*, 085003. [[CrossRef](#)]
90. University of Maryland Center for Environmental Science. IAN Symbol Libraries. Available online: <https://ian.umces.edu/symbols/> (accessed on 1 September 2020).

91. European Space Agency. Permafrost is a Phenomenon of the Subsurface Thermal State and is Defined as Ground at or Below the Freezing Point of Water for Two or More Years. Available online: <https://climate.esa.int/en/projects/permafrost/about/> (accessed on 11 September 2020).
92. Westermann, S.; Strozzi, T.; Wiesmann, A.; Aalstad, K.; Fiddes, J.; Kääb, A.; Obu, J.; Seifert, F.M.; Grosse, G.; Heim, B.; et al. Circumpolar mapping of permafrost temperature and thaw depth in the ESA Permafrost CCI project. In Proceedings of the AGU Fall Meeting 2018, Washington, DC, USA, 10–14 December 2018; AGU: Washington, DC, USA, 2018.
93. Duncan, B.N.; Ott, L.E.; Abshire, J.B.; Brucker, L.; Carroll, M.L.; Carton, J.; Comiso, J.C.; Dinnat, E.P.; Forbes, B.C.; Gonsamo, A.; et al. Space-Based Observations for Understanding Changes in the Arctic-Boreal Zone. *Rev. Geophys.* **2020**, *58*, e2019RG000652. [CrossRef]
94. Zwieback, S.; Liu, X.; Antonova, S.; Heim, B.; Bartsch, A.; Boike, J.; Hajnsek, I. A statistical test of phase closure to detect influences on DInSAR deformation estimates besides displacements and decorrelation noise: Two case studies in high-latitude regions. *IEEE Trans. Geosci. Remote Sens.* **2016**, *54*, 5588–5601. [CrossRef]
95. Biskaborn, B.K.; Lanckman, J.P.; Lantuit, H.; Elger, K.; Dmitry, S.; William, C.; Vladimir, R. The new database of the Global Terrestrial Network for Permafrost (GTN-P). *Earth Syst. Sci. Data* **2015**, *7*, 245–259. [CrossRef]
96. International Permafrost Association; Arctic Portal; Alfred-Wegener-Institut. About GTN-P. Available online: <https://gtnp.arcticportal.org/about-the-gtnp> (accessed on 16 November 2020).
97. Vonder Mühll, D.; Noetzli, J.; Roer, I. PERMOS—A comprehensive monitoring network of mountain permafrost in the Swiss Alps. In Proceedings of the 9th International Conference on Permafrost, Fairbanks, Alaska, 29 June–3 July 2008; pp. 1869–1874.
98. PERMOS. PERMOS-Swiss Permafrost Monitoring Network. Available online: <http://www.permos.ch/> (accessed on 16 November 2020).
99. Mair, V.; Zischg, A.P.; Lang, K.; Tonidandel, D.; Krainer, K.; Kellerer-Pirklbauer, A.; Deline, P.; Schoeneich, P.; Cremonese, E.; Pogliotti, P.; et al. *PermaNET, Permafrost Long-Term Monitoring Network*; International Research Society INTERPRAEVENT: Klagenfurt, Austria, 2011; pp. 1–28.
100. PermaNet Alpine Space. The PermaNET Project. Available online: <http://www.permanet-alpinespace.eu/project.html> (accessed on 16 November 2020).
101. Permafrost Carbon Network. Permafrost Carbon Network. Available online: <http://www.permafrostcarbon.org/index.html> (accessed on 28 October 2020).
102. ArcticNet. ArcticNet Annual Report 2019/2020. Available online: <https://arcticnet.ulaval.ca//pdf/media/arcticnet-ra-19-20-ang.pdf> (accessed on 28 October 2020).
103. ArcticNet. ArcticNET-about Us. Available online: <https://arcticnet.ulaval.ca/vision-and-mission/about-us> (accessed on 16 November 2020).
104. NOAA Earth System Research Laboratories. Cooperative Air Sampling Network. Available online: <https://www.esrl.noaa.gov/gmd/ccgg/flask.html> (accessed on 28 October 2020).
105. PAGE21. PAGE21-Changing Permafrost in the Arctic and Its Global Effects in the 21st Century. Available online: <https://www.page21.eu/> (accessed on 28 October 2020).
106. Shiklomanov, N.; Nelson, F.; Streletskev, D.; Hinkel, K.; Brown, J. The circumpolar active layer monitoring (CALM) program: Data collection, management, and dissemination strategies. In Proceedings of the Ninth International Conference on Permafrost, Institute of Northern Engineering, University of Alaska Fairbanks, Fairbanks, Alaska, 29 June–3 July 2008; Volume 29, pp. 1647–1652.
107. International Permafrost Association. Circumpolar Active Layer Monitoring Network (CALM). Available online: <https://ipa.arcticportal.org/products/gtn-p/calm> (accessed on 16 November 2020).
108. International Permafrost Association. Thermal State of Permafrost (TSP). Available online: <https://ipa.arcticportal.org/products/gtn-p/tsp> (accessed on 16 November 2020).
109. Hayman, G.; Bartsch, A.; Prigent, C.; Aires, F.; Buchwitz, M.; Burrows, J.; Schneising, O.; Blyth, E.; Clark, D.; O'Connor, F.; et al. Wetland extent and methane dynamics: An overview of the ESA ALANIS-methane project. In Proceedings of the ESA-iLEAPS-EGU Earth Observation for Land-Atmosphere Interaction Science Conference, Frascati, Rome, Italy, 3–5 November 2010.
110. Marconcini, M.; Fernandez-Prieto, D.; Pinnock, S.; Hayman, G.; Helbert, J.; de Leeuw, G. ALANIS: A Joint ESA-Ileaps Atmosphere-Land Interaction Study over Boreal Eurasia. *iLEAPS Newslett.* **2010**, *10*, 28–33.
111. Heim, B.; Bartsch, A.; Elger, K.; Lantuit, H.; Boike, J.; Muster, S.; Langer, M.; Duguay, C.; Hachem, S.; Soliman, A.; et al. ESA DUE Permafrost: An Earth observation (EO) permafrost monitoring system. *EARSeL eProc.* **2011**, *10*, 73–82.
112. European Space Agency. Permafrost-Information System on Permafrost. Available online: http://due.esrin.esa.int/page_project116.php (accessed on 16 November 2020).
113. Bartsch, A.; Grosse, G.; Kääb, A.; Westermann, S.; Strozzi, T.; Wiesmann, A.; Duguay, C.; Seifert, F.M.; Obu, J.; Golser, R. GlobPermafrost—How space-based earth observation supports understanding of permafrost. In Proceedings of the ESA Living Planet Symposium, Prague, Czech Republic, 9–13 May 2016; pp. 9–13.
114. European Space Agency. GlobPermafrost- A Service for Global Permafrost Monitoring. Available online: http://due.esrin.esa.int/page_project161.php (accessed on 16 November 2020).

115. Miller, C.; Griffith, P.; Goetz, S.; Hoy, E.; Pinto, N.; McCubbin, I.; Thorpe, A.; Hofton, M.; Hodkinson, D.; Hansen, C.; et al. An overview of ABoVE airborne campaign data acquisitions and science opportunities. *Environ. Res. Lett.* **2019**, *14*, 080201. [[CrossRef](#)]
116. National Aeronautics and Space Administration (NASA). Earth Expeditions: ABoVE. Available online: <https://www.nasa.gov/content/earth-expeditions-above> (accessed on 16 November 2020).
117. Allison, I.; Barry, R.G.; Goodison, B.E. *Climate and Cryosphere (CliC) Project Science and Co-Ordination Plan: Version 1*; Joint Planning Staff for WCRP; World Meteorological Organization: Geneva, Switzerland, 2001; Volume 114.
118. Climate and Cryosphere (CliC). About CliC. Available online: <http://www.climate-cryosphere.org/about> (accessed on 16 November 2020).
119. Wullschleger, S.; Hinzman, L.; Wilson, C. Planning the Next Generation of Arctic Ecosystem Experiments. *Eos Trans. Am. Geophys. Union* **2011**, *90*. [[CrossRef](#)]
120. Wullschleger, S.D. *Support for Next-Generation Ecosystem Experiments (NGEE Arctic) Field Campaign Report*; United States; DOE Office of Science Atmospheric Radiation Measurement (ARM) Program: Washington, DC, USA, 2019.
121. Study of Environmental Change (SEARCH). Study of Environmental Arctic Change: Plans for Implementation During the International Polar Year and Beyond. 2005. Available online: https://www.arcus.org/files/publication/23146/siw_report_final.pdf (accessed on 28 October 2020).
122. SEARCH. SEARCH-Vision and Mission. Available online: <https://www.searcharcticscience.org/vision> (accessed on 16 November 2020).
123. Antonova, S.; Beck, I.; Marx, S.; Anders, K.; Boike, J.; Höfle, B. PermaSAR: Entwicklung einer Methode zur Detektion von Subsidenz in Permafrostgebieten mit D-InSAR: Schlussbericht. 2019. Available online: <https://www.tib.eu/en/suchen/id/TIBKAT:167848864X/> (accessed on 13 January 2021).
124. University of Oslo-Department of Geosciences. SatPerm-Satellite-Based Permafrost Modeling across a Range of Scales. Available online: <https://www.mn.uio.no/geo/english/research/projects/satperm/> (accessed on 28 October 2020).
125. Central Institute for Meteorology and Geodynamics Section Climate Change Impacts. COLD Yamal-COMBining Remote Sensing and Field Studies for Assessment of Landform Dynamics and Permafrost State on Yamal. Available online: <http://cold.zgis.net/> (accessed on 28 October 2020).
126. Lantuit, H. Nunataryuk-Permafrost Thaw and the changing Arctic coast, science for socioeconomic adaptation. In Proceedings of the 5th YES Congress, Berlin, Germany, 9–13 September 2019.
127. NUNATARYUK. NUNATARYUK—The Project. Available online: <https://nunataryuk.org/about> (accessed on 16 November 2020).
128. Alfred-Wegener-Institute. Modular Observation Solutions for Earth Systems—MOSES. Available online: <https://www.awi.de/en/science/geosciences/permafrost-research/projects/moses.html> (accessed on 26 February 2021).
129. Alfred-Wegener-Institute. PETA-CARB: Rapid Permafrost Thaw in a Warming Arctic and Impacts on the Soil Organic Carbon Pool. Available online: <https://www.awi.de/en/science/junior-groups/peta-carb.html> (accessed on 26 February 2021).
130. Schwamborn, G.; Wetterich, S. Russian-German cooperation CARBOPERM: Field campaigns to Bol'shoy Lyakhovsky Island in 2014. *Berichte zur Polar- und Meeresforschung/Rep. Polar Mar. Res.* **2015**, *686*, 1–100.
131. KoPf. KoPf-Carbon in Permafrost. Available online: <http://www.kopf-permafrost.de/index.php?id=36> (accessed on 26 February 2021).
132. Alfred-Wegener-Institute. Changing Arctic Carbon Cycle in the cOastal Ocean Near-Shore-CACOON. Available online: <https://www.awi.de/forschung/geowissenschaften/permafrostforschung/projekte/cacoon.html> (accessed on 26 February 2021).
133. Zhang, T.; Barry, R.G.; Armstrong, R.L. Application of satellite remote sensing techniques to frozen ground studies. *Polar Geogr.* **2004**, *28*, 163–196. [[CrossRef](#)]
134. Kääb, A.; Huggel, C.; Fischer, L.; Guex, S.; Paul, F.; Roer, I.; Salzmann, N.; Schlaefli, S.; Schmutz, K.; Schneider, D.; et al. Remote sensing of glacier- and permafrost-related hazards in high mountains: An overview. *Nat. Hazards Earth Syst. Sci.* **2005**, *5*, 527–554. [[CrossRef](#)]
135. Kääb, A. Remote sensing of permafrost-related problems and hazards. *Permafro. Periglac. Process.* **2008**, *19*, 107–136. [[CrossRef](#)]
136. National Research Council. *Opportunities to Use Remote Sensing in Understanding Permafrost and Related Ecological Characteristics: Report of a Workshop*; National Academies Press: Washington, DC, USA, 2014.
137. Arenson, L.U.; Kääb, A.; O'Sullivan, A. Detection and analysis of ground deformation in permafrost environments. *Permafro. Periglac. Process.* **2016**, *27*, 339–351. [[CrossRef](#)]
138. André, C.; Ottlé, C.; Royer, A.; Maignan, F. Land surface temperature retrieval over circumpolar Arctic using SSM/I-SSMIS and MODIS data. *Remote Sens. Environ.* **2015**, *162*, 1–10. [[CrossRef](#)]
139. Ulrich, M.; Grosse, G.; Strauss, J.; Schirrmeyer, L. Quantifying wedge-ice volumes in Yedoma and thermokarst basin deposits. *Permafro. Periglac. Process.* **2014**, *25*, 151–161. [[CrossRef](#)]
140. Godin, E.; Osinski, G.R.; Harrison, T.N.; Pontefract, A.; Zanetti, M. Geomorphology of Gullies at Thomas Lee Inlet, Devon Island, Canadian High Arctic. *Permafro. Periglac. Process.* **2019**, *30*, 19–34. [[CrossRef](#)]
141. Boyle, S.A.; Kennedy, C.M.; Torres, J.; Colman, K.; Pérez-Estigarribia, P.E.; Noé, U. High-resolution satellite imagery is an important yet underutilized resource in conservation biology. *PLoS ONE* **2014**, *9*, e86908. [[CrossRef](#)]

142. Runge, A.; Grosse, G. Comparing Spectral Characteristics of Landsat-8 and Sentinel-2 Same-Day Data for Arctic-Boreal Regions. *Remote Sens.* **2019**, *11*, 1730. [[CrossRef](#)]
143. Clarivate Analytics. Web of Science. Available online: <https://apps.webofknowledge.com/> (accessed on 13 September 2020).
144. Gallerman, T.; Haas, U.; Teipel, U.; von Poschinger, A.; Wagner, B.; Mahr, M.; Bäse, F. *Permafrost Messstation am Zugspitzgipfel: Ergebnisse und Modellberechnungen*; Bayerisches Landesamt für Umwelt: Bavaria, Germany, 2017.
145. Oelke, C.; Zhang, T.; Serreze, M.C.; Armstrong, R.L. Regional-scale modeling of soil freeze/thaw over the Arctic drainage basin. *J. Geophys. Res. Atmos.* **2003**, *108*, 4314. [[CrossRef](#)]
146. Oelke, C.; Zhang, T. A model study of circum-Arctic soil temperatures. *Permafro. Periglac. Process.* **2004**, *15*, 103–121. [[CrossRef](#)]
147. Euskirchen, E.; McGuire, A.D.; Kicklighter, D.W.; Zhuang, Q.; Clein, J.S.; Dargaville, R.; Dye, D.; Kimball, J.S.; McDonald, K.C.; Melillo, J.M.; et al. Importance of recent shifts in soil thermal dynamics on growing season length, productivity, and carbon sequestration in terrestrial high-latitude ecosystems. *Glob. Chang. Biol.* **2006**, *12*, 731–750. [[CrossRef](#)]
148. Epstein, H.E.; Raynolds, M.K.; Walker, D.A.; Bhatt, U.S.; Tucker, C.J.; Pinzon, J.E. Dynamics of aboveground phytomass of the circumpolar Arctic tundra during the past three decades. *Environ. Res. Lett.* **2012**, *7*, 015506. [[CrossRef](#)]
149. Soliman, A.; Duguay, C.; Saunders, W.; Hachem, S. Pan-arctic land surface temperature from MODIS and AATSR: Product development and intercomparison. *Remote Sens.* **2012**, *4*, 3833–3856. [[CrossRef](#)]
150. Watts, J.D.; Kimball, J.S.; Jones, L.A.; Schroeder, R.; McDonald, K.C. Satellite Microwave remote sensing of contrasting surface water inundation changes within the Arctic–Boreal Region. *Remote Sens. Environ.* **2012**, *127*, 223–236. [[CrossRef](#)]
151. Fichot, C.G.; Kaiser, K.; Hooker, S.B.; Amon, R.M.; Babin, M.; Bélanger, S.; Walker, S.A.; Benner, R. Pan-Arctic distributions of continental runoff in the Arctic Ocean. *Sci. Rep.* **2013**, *3*, 1–6. [[CrossRef](#)]
152. Kim, Y.; Kimball, J.S.; Robinson, D.; Derksen, C. New satellite climate data records indicate strong coupling between recent frozen season changes and snow cover over high northern latitudes. *Environ. Res. Lett.* **2015**, *10*, 084004. [[CrossRef](#)]
153. Paltan, H.; Dash, J.; Edwards, M. A refined mapping of Arctic lakes using Landsat imagery. *Int. J. Remote Sens.* **2015**, *36*, 5970–5982. [[CrossRef](#)]
154. Yi, Y.; Kimball, J.S.; Rawlins, M.A.; Moghaddam, M.; Euskirchen, E.S. The role of snow cover affecting boreal–arctic soil freeze–thaw and carbon dynamics. *Biogeosciences* **2015**, *12*, 5811–5829. [[CrossRef](#)]
155. Bartsch, A.; Pointner, G.; Leibman, M.O.; Dvornikov, Y.A.; Khomutov, A.V.; Trofaier, A.M. Circumpolar mapping of ground-fast lake ice. *Front. Earth Sci.* **2017**, *5*, 12. [[CrossRef](#)]
156. Muster, S.; Roth, K.; Langer, M.; Lange, S.; Cresto Aleina, F.; Bartsch, A.; Morgenstern, A.; Grosse, G.; Jones, B.; Sannel, A.B.K.; et al. PeRL: A circum-Arctic permafrost region pond and lake database. *Earth Syst. Sci. Data* **2017**, *9*, 317–348. [[CrossRef](#)]
157. Xia, J.; McGuire, A.D.; Lawrence, D.; Burke, E.; Chen, G.; Chen, X.; Delire, C.; Koven, C.; MacDougall, A.; Peng, S.; et al. Terrestrial ecosystem model performance in simulating productivity and its vulnerability to climate change in the northern permafrost region. *J. Geophys. Res. Biogeosci.* **2017**, *122*, 430–446. [[CrossRef](#)]
158. Kroisleitner, C.; Bartsch, A.; Bergstedt, H. Circumpolar patterns of potential mean annual ground temperature based on surface state obtained from microwave satellite data. *Cryosphere* **2018**, *12*, 2349–2370. [[CrossRef](#)]
159. Lyu, Z.; Zhuang, Q. Quantifying the effects of snowpack on soil thermal and carbon dynamics of the Arctic terrestrial ecosystems. *J. Geophys. Res. Biogeosci.* **2018**, *123*, 1197–1212. [[CrossRef](#)]
160. Suzuki, K.; Matsuo, K.; Yamazaki, D.; Ichii, K.; Iijima, Y.; Papa, F.; Yanagi, Y.; Hiyama, T. Hydrological variability and changes in the Arctic circumpolar tundra and the three largest pan-Arctic river basins from 2002 to 2016. *Remote Sens.* **2018**, *10*, 402. [[CrossRef](#)]
161. Liang, L.; Liu, Q.; Liu, G.; Li, H.; Huang, C. Accuracy Evaluation and Consistency Analysis of Four Global Land Cover Products in the Arctic Region. *Remote Sens.* **2019**, *11*, 1396. [[CrossRef](#)]
162. Raynolds, M.K.; Walker, D.A.; Balser, A.; Bay, C.; Campbell, M.; Cherosov, M.M.; Daniëls, F.J.; Eidesen, P.B.; Ermokhina, K.A.; Frost, G.V.; et al. A raster version of the Circumpolar Arctic Vegetation Map (CAVM). *Remote Sens. Environ.* **2019**, *232*, 111297. [[CrossRef](#)]
163. Obu, J.; Westermann, S.; Vieira, G.; Abramov, A.; Balks, M.R.; Bartsch, A.; Hrbáček, F.; Kääb, A.; Ramos, M. Pan-Antarctic map of near-surface permafrost temperatures at 1 km 2 scale. *Cryosphere* **2020**, *14*, 497–519. [[CrossRef](#)]
164. Naeimi, V.; Paulik, C.; Bartsch, A.; Wagner, W.; Kidd, R.; Park, S.E.; Elger, K.; Boike, J. ASCAT Surface State Flag (SSF): Extracting information on surface freeze/thaw conditions from backscatter data using an empirical threshold-analysis algorithm. *IEEE Trans. Geosci. Remote Sens.* **2012**, *50*, 2566–2582. [[CrossRef](#)]
165. Forkel, M.; Migliavacca, M.; Thonicke, K.; Reichstein, M.; Schaphoff, S.; Weber, U.; Carvalhais, N. Codominant water control on global interannual variability and trends in land surface phenology and greenness. *Glob. Chang. Biol.* **2015**, *21*, 3414–3435. [[CrossRef](#)]
166. Hu, T.; Zhao, T.; Zhao, K.; Shi, J. A continuous global record of near-surface soil freeze/thaw status from AMSR-E and AMSR2 data. *Int. J. Remote Sens.* **2019**, *40*, 6993–7016. [[CrossRef](#)]
167. Frost, G.V.; Christopherson, T.; Jorgenson, M.T.; Liljedahl, A.K.; Macander, M.J.; Walker, D.A.; Wells, A.F. Regional patterns and asynchronous onset of ice-wedge degradation since the Mid-20th Century in Arctic Alaska. *Remote Sens.* **2018**, *10*, 1312. [[CrossRef](#)]
168. Engram, M.; Arp, C.D.; Jones, B.M.; Ajadi, O.A.; Meyer, F.J. Analyzing floating and bedfast lake ice regimes across Arctic Alaska using 25 years of space-borne SAR imagery. *Remote Sens. Environ.* **2018**, *209*, 660–676. [[CrossRef](#)]

169. Schaefer, K.; Liu, L.; Parsekian, A.; Jafarov, E.; Chen, A.; Zhang, T.; Gusmeroli, A.; Panda, S.; Zebker, H.A.; Schaefer, T. Remotely sensed active layer thickness (ReSALT) at Barrow, Alaska using interferometric synthetic aperture radar. *Remote Sens.* **2015**, *7*, 3735–3759. [[CrossRef](#)]
170. Lyons, E.A.; Sheng, Y.; Smith, L.C.; Li, J.; Hinkel, K.M.; Lenters, J.D.; Wang, J. Quantifying sources of error in multitemporal multisensor lake mapping. *Int. J. Remote Sens.* **2013**, *34*, 7887–7905. [[CrossRef](#)]
171. Hinkel, K.; Eisner, W.; Kim, C. Detection of tundra trail damage near Barrow, Alaska using remote imagery. *Geomorphology* **2017**, *293*, 360–367. [[CrossRef](#)]
172. Frohn, R.C.; Hinkel, K.M.; Eisner, W.R. Satellite remote sensing classification of thaw lakes and drained thaw lake basins on the North Slope of Alaska. *Remote Sens. Environ.* **2005**, *97*, 116–126. [[CrossRef](#)]
173. Kuplik, M.; Witmer, F.D.; MacLeod, E.A.; Wang, C.; Ravens, T. Gaussian Process Regression for Arctic Coastal Erosion Forecasting. *IEEE Trans. Geosci. Remote Sens.* **2018**, *57*, 1256–1264. [[CrossRef](#)]
174. Iwahana, G.; Uchida, M.; Liu, L.; Gong, W.; Meyer, F.J.; Guritz, R.; Yamanokuchi, T.; Hinzman, L. InSAR detection and field evidence for thermokarst after a tundra wildfire, using ALOS-PALSAR. *Remote Sens.* **2016**, *8*, 218. [[CrossRef](#)]
175. Hachem, S.; Duguay, C.; Allard, M. Comparison of MODIS-derived land surface temperatures with ground surface and air temperature measurements in continuous permafrost terrain. *Cryosphere* **2012**, *6*, 51. [[CrossRef](#)]
176. Raynolds, M.K.; Walker, D.A. Increased wetness confounds Landsat-derived NDVI trends in the central Alaska North Slope region, 1985–2011. *Environ. Res. Lett.* **2016**, *11*, 085004. [[CrossRef](#)]
177. Marchand, N.; Royer, A.; Krinner, G.; Roy, A.; Langlois, A.; Vargel, C. Snow-Covered Soil Temperature Retrieval in Canadian Arctic Permafrost Areas, Using a Land Surface Scheme Informed with Satellite Remote Sensing Data. *Remote Sens.* **2018**, *10*, 1703. [[CrossRef](#)]
178. Liu, L.; Schaefer, K.; Gusmeroli, A.; Grosse, G.; Jones, B.M.; Zhang, T.; Parsekian, A.; Zebker, H.A. Seasonal thaw settlement at drained thermokarst lake basins, Arctic Alaska. *Cryosphere* **2014**, *8*, 815–826. [[CrossRef](#)]
179. Nitze, I.; Grosse, G.; Jones, B.M.; Romanovsky, V.E.; Boike, J. Remote sensing quantifies widespread abundance of permafrost region disturbances across the Arctic and Subarctic. *Nat. Commun.* **2018**, *9*, 1–11. [[CrossRef](#)]
180. Tape, K.D.; Jones, B.M.; Arp, C.D.; Nitze, I.; Grosse, G. Tundra be dammed: Beaver colonization of the Arctic. *Glob. Chang. Biol.* **2018**, *24*, 4478–4488. [[CrossRef](#)] [[PubMed](#)]
181. Gangodagamage, C.; Rowland, J.C.; Hubbard, S.S.; Brumby, S.P.; Liljedahl, A.K.; Wainwright, H.; Wilson, C.J.; Altmann, G.L.; Dafflon, B.; Peterson, J.; et al. Extrapolating active layer thickness measurements across Arctic polygonal terrain using LiDAR and NDVI data sets. *Water Resour. Res.* **2014**, *50*, 6339–6357. [[CrossRef](#)] [[PubMed](#)]
182. Lara, M.J.; Nitze, I.; Grosse, G.; Martin, P.; McGuire, A.D. Reduced arctic tundra productivity linked with landform and climate change interactions. *Sci. Rep.* **2018**, *8*, 1–10. [[CrossRef](#)]
183. Muster, S.; Riley, W.J.; Roth, K.; Langer, M.; Cresto Aleina, F.; Koven, C.D.; Lange, S.; Bartsch, A.; Grosse, G.; Wilson, C.J.; et al. Size distributions of Arctic waterbodies reveal consistent relations in their statistical moments in space and time. *Front. Earth Sci.* **2019**, *7*, 5. [[CrossRef](#)]
184. Piliouras, A.; Rowland, J.C. Arctic river delta morphologic variability and implications for riverine fluxes to the coast. *J. Geophys. Res. Earth Surf.* **2020**, *125*, e2019JF005250. [[CrossRef](#)]
185. Höglström, E.; Heim, B.; Bartsch, A.; Bergstedt, H.; Pointner, G. Evaluation of a MetOp ASCAT-Derived Surface Soil Moisture Product in Tundra Environments. *J. Geophys. Res. Earth Surf.* **2018**, *123*, 3190–3205. [[CrossRef](#)]
186. Liu, L.; Schaefer, K.; Chen, A.; Gusmeroli, A.; Zebker, H.; Zhang, T. Remote sensing measurements of thermokarst subsidence using InSAR. *J. Geophys. Res. Earth Surf.* **2015**, *120*, 1935–1948. [[CrossRef](#)]
187. Andresen, C.G.; Lougheed, V.L. Disappearing Arctic tundra ponds: Fine-scale analysis of surface hydrology in drained thaw lake basins over a 65 year period (1948–2013). *J. Geophys. Res. Biogeosci.* **2015**, *120*, 466–479. [[CrossRef](#)]
188. Balser, A.W.; Jones, J.B.; Gens, R. Timing of retrogressive thaw slump initiation in the Noatak Basin, northwest Alaska, USA. *J. Geophys. Res. Earth Surf.* **2014**, *119*, 1106–1120. [[CrossRef](#)]
189. Tape, K.D.; Verbyla, D.; Welker, J.M. Twentieth century erosion in Arctic Alaska foothills: The influence of shrubs, runoff, and permafrost. *J. Geophys. Res. Biogeosci.* **2011**, *116*, G04024. [[CrossRef](#)]
190. Ping, C.L.; Michaelson, G.J.; Guo, L.; Jorgenson, M.T.; Kanevskiy, M.; Shur, Y.; Dou, F.; Liang, J. Soil carbon and material fluxes across the eroding Alaska Beaufort Sea coastline. *J. Geophys. Res. Biogeosci.* **2011**, *116*, G02004. [[CrossRef](#)]
191. Liu, L.; Zhang, T.; Wahr, J. InSAR measurements of surface deformation over permafrost on the North Slope of Alaska. *J. Geophys. Res. Earth Surf.* **2010**, *115*, F03023. [[CrossRef](#)]
192. Kim, E.; England, A. A yearlong comparison of plot-scale and satellite footprint-scale 19 and 37 GHz brightness of the Alaskan North Slope. *J. Geophys. Res. Atmos.* **2003**, *108*, 4388. [[CrossRef](#)]
193. Liljedahl, A.K.; Boike, J.; Daanen, R.P.; Fedorov, A.N.; Frost, G.V.; Grosse, G.; Hinzman, L.D.; Iijima, Y.; Jorgenson, J.C.; Matveyeva, N.; et al. Pan-Arctic ice-wedge degradation in warming permafrost and its influence on tundra hydrology. *Nat. Geosci.* **2016**, *9*, 312–318. [[CrossRef](#)]
194. Regmi, P.; Grosse, G.; Jones, M.C.; Jones, B.M.; Anthony, K.W. Characterizing post-drainage succession in thermokarst lake basins on the Seward Peninsula, Alaska with TerraSAR-X backscatter and Landsat-based NDVI data. *Remote Sens.* **2012**, *4*, 3741–3765. [[CrossRef](#)]

195. Iwahana, G.; Harada, K.; Uchida, M.; Tsuyuzaki, S.; Saito, K.; Narita, K.; Kushida, K.; Hinzman, L.D. Geomorphological and geochemistry changes in permafrost after the 2002 tundra wildfire in Kougarok, Seward Peninsula, Alaska. *J. Geophys. Res. Earth Surf.* **2016**, *121*, 1697–1715. [[CrossRef](#)]
196. Jones, M.C.; Grosse, G.; Jones, B.M.; Walter Anthony, K. Peat accumulation in drained thermokarst lake basins in continuous, ice-rich permafrost, northern Seward Peninsula, Alaska. *J. Geophys. Res. Biogeosci.* **2012**, *117*, G00M07. [[CrossRef](#)]
197. Whitley, M.A.; Frost, G.V.; Jorgenson, M.T.; Macander, M.J.; Maio, C.V.; Winder, S.G. Assessment of LiDAR and spectral techniques for high-resolution mapping of sporadic permafrost on the Yukon-Kuskokwim Delta, Alaska. *Remote Sens.* **2018**, *10*, 258. [[CrossRef](#)]
198. Jorgenson, M.T.; Frost, G.V.; Dissing, D. Drivers of landscape changes in coastal ecosystems on the Yukon-Kuskokwim Delta, Alaska. *Remote Sens.* **2018**, *10*, 1280. [[CrossRef](#)]
199. Michaelides, R.J.; Schaefer, K.; Zebker, H.A.; Parsekian, A.; Liu, L.; Chen, J.; Natali, S.; Ludwig, S.; Schaefer, S.R. Inference of the impact of wildfire on permafrost and active layer thickness in a discontinuous permafrost region using the remotely sensed active layer thickness (ReSALT) algorithm. *Environ. Res. Lett.* **2019**, *14*, 035007. [[CrossRef](#)]
200. Brenning, A. Benchmarking classifiers to optimally integrate terrain analysis and multispectral remote sensing in automatic rock glacier detection. *Remote Sens. Environ.* **2009**, *113*, 239–247. [[CrossRef](#)]
201. Evans, S.G.; Ge, S.; Voss, C.I.; Molotchk, N.P. The role of frozen soil in groundwater discharge predictions for warming alpine watersheds. *Water Resour. Res.* **2018**, *54*, 1599–1615. [[CrossRef](#)]
202. Zhang, T.; Armstrong, R.; Smith, J. Investigation of the near-surface soil freeze-thaw cycle in the contiguous United States: Algorithm development and validation. *J. Geophys. Res. Atmos.* **2003**, *108*, 8860. [[CrossRef](#)]
203. Natural Earth. Natural Earth I with Shaded Relief and Water. Available online: <https://www.naturalearthdata.com/downloads/10m-raster-data/10m-natural-earth-1/> (accessed on 28 August 2020).
204. Nill, L.; Ullmann, T.; Kneisel, C.; Sobiech-Wolf, J.; Baumhauer, R. Assessing Spatiotemporal Variations of Landsat Land Surface Temperature and Multispectral Indices in the Arctic Mackenzie Delta Region between 1985 and 2018. *Remote Sens.* **2019**, *11*, 2329. [[CrossRef](#)]
205. Nguyen, T.N.; Burn, C.R.; King, D.J.; Smith, S. Estimating the extent of near-surface permafrost using remote sensing, Mackenzie Delta, Northwest Territories. *Permafro. Periglac. Process.* **2009**, *20*, 141–153. [[CrossRef](#)]
206. Zwieback, S.; Kokelj, S.V.; Günther, F.; Boike, J.; Grosse, G.; Hajnsek, I. Sub-seasonal thaw slump mass wasting is not consistently energy limited at the landscape scale. *Cryosphere* **2018**, *12*, 549–564. [[CrossRef](#)]
207. Samsonov, S.V.; Lantz, T.C.; Kokelj, S.V.; Zhang, Y. Growth of a young pingo in the Canadian Arctic observed by RADARSAT-2 interferometric satellite radar. *Cryosphere* **2016**, *10*, 799–810. [[CrossRef](#)]
208. Olthof, I.; Fraser, R.H.; Schmitt, C. Landsat-based mapping of thermokarst lake dynamics on the Tuktoyaktuk Coastal Plain, Northwest Territories, Canada since 1985. *Remote Sens. Environ.* **2015**, *168*, 194–204. [[CrossRef](#)]
209. Muskett, R.R.; Romanovsky, V.E. Groundwater storage changes in arctic permafrost watersheds from GRACE and in situ measurements. *Environ. Res. Lett.* **2009**, *4*, 045009. [[CrossRef](#)]
210. Brooker, A.; Fraser, R.H.; Olthof, I.; Kokelj, S.V.; Lacelle, D. Mapping the activity and evolution of retrogressive thaw slumps by tasseled cap trend analysis of a Landsat satellite image stack. *Permafro. Periglac. Process.* **2014**, *25*, 243–256. [[CrossRef](#)]
211. Fraser, R.H.; Olthof, I.; Kokelj, S.V.; Lantz, T.C.; Lacelle, D.; Brooker, A.; Wolfe, S.; Schwarz, S. Detecting landscape changes in high latitude environments using landsat trend analysis: 1. Visualization. *Remote Sens.* **2014**, *6*, 11533–11557. [[CrossRef](#)]
212. Kokelj, S.; Tunnicliffe, J.; Lacelle, D.; Lantz, T.; Chin, K.; Fraser, R. Increased precipitation drives mega slump development and destabilization of ice-rich permafrost terrain, northwestern Canada. *Glob. Planet. Chang.* **2015**, *129*, 56–68. [[CrossRef](#)]
213. Kohnert, K.; Juhls, B.; Muster, S.; Antonova, S.; Serafimovich, A.; Metzger, S.; Hartmann, J.; Sachs, T. Toward understanding the contribution of waterbodies to the methane emissions of a permafrost landscape on a regional scale—A case study from the Mackenzie delta, Canada. *Glob. Chang. Biol.* **2018**, *24*, 3976–3989. [[CrossRef](#)]
214. Vesakoski, J.M.; Nylén, T.; Arheimer, B.; Gustafsson, D.; Isberg, K.; Holopainen, M.; Hyppä, J.; Alho, P. Arctic Mackenzie Delta channel planform evolution during 1983–2013 utilising Landsat data and hydrological time series. *Hydrol. Process.* **2017**, *31*, 3979–3995. [[CrossRef](#)]
215. Beighley, R.; Eggert, K.; Wilson, C.; Rowland, J.; Lee, H. A hydrologic routing model suitable for climate-scale simulations of arctic rivers: Application to the Mackenzie River Basin. *Hydrol. Process.* **2015**, *29*, 2751–2768. [[CrossRef](#)]
216. Zwieback, S.; Westermann, S.; Langer, M.; Boike, J.; Marsh, P.; Berg, A. Improving permafrost modeling by assimilating remotely sensed soil moisture. *Water Resour. Res.* **2019**, *55*, 1814–1832. [[CrossRef](#)]
217. Fouest, V.L.; Matsuoka, A.; Manizza, M.; Shernetsky, M.; Tremblay, B.; Babin, M. Towards an assessment of riverine dissolved organic carbon in surface waters of the western Arctic Ocean based on remote sensing and biogeochemical modeling. *Biogeosciences* **2018**, *15*, 1335–1346. [[CrossRef](#)]
218. Doxaran, D.; Devred, E.; Babin, M. A 50% increase in the mass of terrestrial particles delivered by the Mackenzie River into the Beaufort Sea (Canadian Arctic Ocean) over the last 10 years. *Biogeosciences* **2015**, *12*, 3551–3565. [[CrossRef](#)]
219. Doxaran, D.; Ehn, J.; Bélanger, S.; Matsuoka, A.; Hooker, S.; Babin, M. Optical characterisation of suspended particles in the Mackenzie River plume (Canadian Arctic Ocean) and implications for ocean colour remote sensing. *Biogeosciences* **2012**, *9*, 3213–3229. [[CrossRef](#)]

220. Zhang, Y.; Olthof, I.; Fraser, R.; Wolfe, S.A. A new approach to mapping permafrost and change incorporating uncertainties in ground conditions and climate projections. *Cryosphere* **2014**, *8*, 2177–2194. [[CrossRef](#)]
221. Chasmer, L.; Hopkinson, C.; Veness, T.; Quinton, W.; Baltzer, J. A decision-tree classification for low-lying complex land cover types within the zone of discontinuous permafrost. *Remote Sens. Environ.* **2014**, *143*, 73–84. [[CrossRef](#)]
222. Chasmer, L.; Quinton, W.; Hopkinson, C.; Petrone, R.; Whittington, P. Vegetation canopy and radiation controls on permafrost plateau evolution within the discontinuous permafrost zone, Northwest Territories, Canada. *Permafro. Periglac. Process.* **2011**, *22*, 199–213. [[CrossRef](#)]
223. Carpino, O.A.; Berg, A.A.; Quinton, W.L.; Adams, J.R. Climate change and permafrost thaw-induced boreal forest loss in northwestern Canada. *Environ. Res. Lett.* **2018**, *13*, 084018. [[CrossRef](#)]
224. Quinton, W.; Hayashi, M.; Chasmer, L. Permafrost-thaw-induced land-cover change in the Canadian subarctic: Implications for water resources. *Hydrol. Process.* **2011**, *25*, 152–158. [[CrossRef](#)]
225. Chasmer, L.; Hopkinson, C. Threshold loss of discontinuous permafrost and landscape evolution. *Glob. Chang. Biol.* **2017**, *23*, 2672–2686. [[CrossRef](#)]
226. Helbig, M.; Wischnewski, K.; Kljun, N.; Chasmer, L.E.; Quinton, W.L.; Dettlo, M.; Sonnentag, O. Regional atmospheric cooling and wetting effect of permafrost thaw-induced boreal forest loss. *Glob. Chang. Biol.* **2016**, *22*, 4048–4066. [[CrossRef](#)]
227. Connan, R.F.; Quinton, W.L.; Craig, J.R.; Hayashi, M. Changing hydrologic connectivity due to permafrost thaw in the lower Liard River valley, NWT, Canada. *Hydrol. Process.* **2014**, *28*, 4163–4178. [[CrossRef](#)]
228. Quinton, W.; Hayashi, M.; Pietroniro, A. Connectivity and storage functions of channel fens and flat bogs in northern basins. *Hydrol. Process.* **2003**, *17*, 3665–3684. [[CrossRef](#)]
229. Abis, B.; Brovkin, V. Environmental conditions for alternative tree-cover states in high latitudes. *Biogeosciences* **2017**, *14*, 511–527. [[CrossRef](#)]
230. Morse, P.; Wolfe, S. Geological and meteorological controls on icing (aufeis) dynamics (1985 to 2014) in subarctic Canada. *J. Geophys. Res. Earth Surf.* **2015**, *120*, 1670–1686. [[CrossRef](#)]
231. Short, N.; Brisco, B.; Couture, N.; Pollard, W.; Murnaghan, K.; Budkewitsch, P. A comparison of TerraSAR-X, RADARSAT-2 and ALOS-PALSAR interferometry for monitoring permafrost environments, case study from Herschel Island, Canada. *Remote Sens. Environ.* **2011**, *115*, 3491–3506. [[CrossRef](#)]
232. Obu, J.; Lantuit, H.; Myers-Smith, I.; Heim, B.; Wolter, J.; Fritz, M. Effect of terrain characteristics on soil organic carbon and total nitrogen stocks in soils of Herschel Island, Western Canadian Arctic. *Permafro. Periglac. Process.* **2017**, *28*, 92–107. [[CrossRef](#)]
233. Lantuit, H.; Pollard, W. Fifty years of coastal erosion and retrogressive thaw slump activity on Herschel Island, southern Beaufort Sea, Yukon Territory, Canada. *Geomorphology* **2008**, *95*, 84–102. [[CrossRef](#)]
234. Ramage, J.L.; Irrgang, A.M.; Morgenstern, A.; Lantuit, H. Increasing coastal slump activity impacts the release of sediment and organic carbon into the Arctic Ocean. *Biogeosciences* **2018**, *15*, 1483–1495. [[CrossRef](#)]
235. Coch, C.; Ramage, J.; Lamoureux, S.; Meyer, H.; Knoblauch, C.; Lantuit, H. Spatial variability of dissolved organic carbon, solutes, and suspended sediment in disturbed Low Arctic coastal watersheds. *J. Geophys. Res. Biogeosci.* **2020**, *125*, e2019JG005505. [[CrossRef](#)]
236. Irrgang, A.M.; Lantuit, H.; Manson, G.K.; Günther, F.; Grosse, G.; Overduin, P.P. Variability in rates of coastal change along the Yukon coast, 1951 to 2015. *J. Geophys. Res. Earth Surf.* **2018**, *123*, 779–800. [[CrossRef](#)]
237. Ramage, J.L.; Irrgang, A.M.; Herzschuh, U.; Morgenstern, A.; Couture, N.; Lantuit, H. Terrain controls on the occurrence of coastal retrogressive thaw slumps along the Yukon Coast, Canada. *J. Geophys. Res. Earth Surf.* **2017**, *122*, 1619–1634. [[CrossRef](#)]
238. Wang, L.; Marzahn, P.; Bernier, M.; Jacome, A.; Poulin, J.; Ludwig, R. Comparison of TerraSAR-X and ALOS PALSAR differential interferometry with multisource DEMs for monitoring ground displacement in a discontinuous permafrost region. *IEEE J. Sel. Top. Appl. Earth Obs. Remote Sens.* **2017**, *10*, 4074–4093. [[CrossRef](#)]
239. Freitas, P.; Vieira, G.; Canário, J.; Folhas, D.; Vincent, W.F. Identification of a Threshold Minimum Area for Reflectance Retrieval from Thermokarst Lakes and Ponds Using Full-Pixel Data from Sentinel-2. *Remote Sens.* **2019**, *11*, 657. [[CrossRef](#)]
240. Beck, I.; Ludwig, R.; Bernier, M.; Lévesque, E.; Boike, J. Assessing permafrost degradation and land cover changes (1986–2009) using remote sensing data over Umiujaq, sub-arctic Québec. *Permafro. Periglac. Process.* **2015**, *26*, 129–141. [[CrossRef](#)]
241. Wang, L.; Marzahn, P.; Bernier, M.; Ludwig, R. Mapping permafrost landscape features using object-based image classification of multi-temporal SAR images. *ISPRS J. Photogramm. Remote Sens.* **2018**, *141*, 10–29. [[CrossRef](#)]
242. Watanabe, S.; Laurion, I.; Chokmani, K.; Pienitz, R.; Vincent, W.F. Optical diversity of thaw ponds in discontinuous permafrost: A model system for water color analysis. *J. Geophys. Res. Biogeosci.* **2011**, *116*, G02003. [[CrossRef](#)]
243. Morgenstern, A.; Grosse, G.; Günther, F.; Fedorova, I.; Schirrmeyer, L. Spatial analyses of thermokarst lakes and basins in Yedoma landscapes of the Lena Delta. *Cryosphere Discuss.* **2011**, *5*, 1495–1545.
244. Antonova, S.; Käab, A.; Heim, B.; Langer, M.; Boike, J. Spatio-temporal variability of X-band radar backscatter and coherence over the Lena River Delta, Siberia. *Remote Sens. Environ.* **2016**, *182*, 169–191. [[CrossRef](#)]
245. Langer, M.; Westermann, S.; Boike, J. Spatial and temporal variations of summer surface temperatures of wet polygonal tundra in Siberia—implications for MODIS LST based permafrost monitoring. *Remote Sens. Environ.* **2010**, *114*, 2059–2069. [[CrossRef](#)]
246. Langer, M.; Westermann, S.; Heikenfeld, M.; Dorn, W.; Boike, J. Satellite-based modeling of permafrost temperatures in a tundra lowland landscape. *Remote Sens. Environ.* **2013**, *135*, 12–24. [[CrossRef](#)]

247. Nitze, I.; Grosse, G. Detection of landscape dynamics in the Arctic Lena Delta with temporally dense Landsat time-series stacks. *Remote Sens. Environ.* **2016**, *181*, 27–41. [[CrossRef](#)]
248. Chen, J.; Günther, F.; Grosse, G.; Liu, L.; Lin, H. Sentinel-1 InSAR Measurements of Elevation Changes over Yedoma Uplands on Sobo-Sise Island, Lena Delta. *Remote Sens.* **2018**, *10*, 1152. [[CrossRef](#)]
249. Stettner, S.; Beamish, A.L.; Bartsch, A.; Heim, B.; Grosse, G.; Roth, A.; Lantuit, H. Monitoring inter-and intra-seasonal dynamics of rapidly degrading ice-rich permafrost riverbanks in the Lena Delta with TerraSAR-X time series. *Remote Sens.* **2018**, *10*, 51. [[CrossRef](#)]
250. Reschke, J.; Bartsch, A.; Schlaffer, S.; Schepaschenko, D. Capability of C-band SAR for operational wetland monitoring at high latitudes. *Remote Sens.* **2012**, *4*, 2923–2943. [[CrossRef](#)]
251. Morgenstern, A.; Ulrich, M.; Günther, F.; Roessler, S.; Fedorova, I.V.; Rudaya, N.A.; Wetterich, S.; Boike, J.; Schirrmeister, L. Evolution of thermokarst in East Siberian ice-rich permafrost: A case study. *Geomorphology* **2013**, *201*, 363–379. [[CrossRef](#)]
252. Grosse, G.; Schirrmeister, L.; Siegert, C.; Kunitsky, V.V.; Slagoda, E.A.; Andreev, A.A.; Dereviagyn, A.Y. Geological and geomorphological evolution of a sedimentary periglacial landscape in Northeast Siberia during the Late Quaternary. *Geomorphology* **2007**, *86*, 25–51. [[CrossRef](#)]
253. Westermann, S.; Peter, M.; Langer, M.; Schwamborn, G.; Schirrmeister, L.; Etzelmüller, B.; Boike, J. Transient modeling of the ground thermal conditions using satellite data in the Lena River delta, Siberia. *Cryosphere* **2017**, *11*, 1441–1463. [[CrossRef](#)]
254. Grosse, G.; Schirrmeister, L.; Kunitsky, V.V.; Hubberten, H.W. The use of CORONA images in remote sensing of periglacial geomorphology: An illustration from the NE Siberian coast. *Permafrosl. Periglac. Process.* **2005**, *16*, 163–172. [[CrossRef](#)]
255. Juhls, B.; Overduin, P.P.; Hölemann, J.; Hieronymi, M.; Matsuoka, A.; Heim, B.; Fischer, J. Dissolved organic matter at the fluvial–marine transition in the Laptev Sea using in situ data and ocean colour remote sensing. *Biogeosciences* **2019**, *16*, 2693–2713. [[CrossRef](#)]
256. Mikola, J.; Virtanen, T.; Linkosalmi, M.; Vähä, E.; Nyman, J.; Postanogova, O.; Räsänen, A.; Kotze, D.J.; Laurila, T.; Juutinen, S.; et al. Spatial variation and linkages of soil and vegetation in the Siberian Arctic tundra–coupling field observations with remote sensing data. *Biogeosciences* **2018**, *15*, 2781–2801. [[CrossRef](#)]
257. Fuchs, M.; Grosse, G.; Strauss, J.; Günther, F.; Grigoriev, M.; Maximov, G.M.; Hugelius, G. Carbon and nitrogen pools in thermokarst-affected permafrost landscapes in Arctic Siberia. *Biogeosciences* **2018**, *15*, 953–971. [[CrossRef](#)]
258. Heim, B.; Abramova, E.; Doerffer, R.; Günther, F.; Hölemann, J.; Kraberg, A.; Lantuit, H.; Loginova, A.; Martynov, F.; Overduin, P.P.; et al. Ocean colour remote sensing in the southern Laptev Sea: Evaluation and applications. *Biogeosciences* **2014**, *11*, 4191–4210. [[CrossRef](#)]
259. Walker, D.; Leibman, M.; Epstein, H.; Forbes, B.; Bhatt, U.; Raynolds, M.; Comiso, J.; Gubarkov, A.; Khomutov, A.; Jia, G.; et al. Spatial and temporal patterns of greenness on the Yamal Peninsula, Russia: Interactions of ecological and social factors affecting the Arctic normalized difference vegetation index. *Environ. Res. Lett.* **2009**, *4*, 045004. [[CrossRef](#)]
260. Widhalm, B.; Bartsch, A.; Leibman, M.; Khomutov, A. Active-layer thickness estimation from X-band SAR backscatter intensity. *Cryosphere* **2017**, *11*, 483–496. [[CrossRef](#)]
261. Dvornikov, Y.; Leibman, M.; Heim, B.; Bartsch, A.; Herzschuh, U.; Skorospekhova, T.; Fedorova, I.; Khomutov, A.; Widhalm, B.; Gubarkov, A.; et al. Terrestrial CDOM in lakes of Yamal peninsula: Connection to lake and lake catchment properties. *Remote Sens.* **2018**, *10*, 167. [[CrossRef](#)]
262. Bartsch, A.; Leibman, M.; Strozzi, T.; Khomutov, A.; Widhalm, B.; Babkina, E.; Mullanurov, D.; Ermokhina, K.; Kroisleitner, C.; Bergstedt, H. Seasonal progression of ground displacement identified with satellite radar interferometry and the impact of unusually warm conditions on permafrost at the Yamal Peninsula in 2016. *Remote Sens.* **2019**, *11*, 1865. [[CrossRef](#)]
263. Kizyakov, A.; Khomutov, A.; Zimin, M.; Khairullin, R.; Babkina, E.; Dvornikov, Y.; Leibman, M. Microrelief associated with gas emission craters: Remote-sensing and field-based study. *Remote Sens.* **2018**, *10*, 677. [[CrossRef](#)]
264. Trofaiar, A.; Bartsch, A.; Rees, W.; Leibman, M. Assessment of spring floods and surface water extent over the Yamalo-Nenets Autonomous District. *Environ. Res. Lett.* **2013**, *8*, 045026. [[CrossRef](#)]
265. Frost, G.V.; Epstein, H.E.; Walker, D.A. Regional and landscape-scale variability of Landsat-observed vegetation dynamics in northwest Siberian tundra. *Environ. Res. Lett.* **2014**, *9*, 025004. [[CrossRef](#)]
266. Frost, G.V.; Epstein, H.E. Tall shrub and tree expansion in Siberian tundra ecotones since the 1960s. *Glob. Chang. Biol.* **2014**, *20*, 1264–1277. [[CrossRef](#)]
267. Forbes, B.C.; Fauria, M.M.; Zetterberg, P. Russian Arctic warming and ‘greening’ are closely tracked by tundra shrub willows. *Glob. Chang. Biol.* **2010**, *16*, 1542–1554. [[CrossRef](#)]
268. Flessa, H.; Rodionov, A.; Guggenberger, G.; Fuchs, H.; Magdon, P.; Shibistova, O.; Zrazhevskaya, G.; Mikheyeva, N.; Kasansky, O.A.; Blodau, C. Landscape controls of CH₄ fluxes in a catchment of the forest tundra ecotone in northern Siberia. *Glob. Chang. Biol.* **2008**, *14*, 2040–2056. [[CrossRef](#)]
269. Bohn, T.J.; Melton, J.R.; Ito, A.; Kleinen, T.; Spahni, R.; Stocker, B.; Zhang, B.; Zhu, X.; Schroeder, R.; Glagolet, M.V.; et al. WETCHIMP-WSL: Intercomparison of wetland methane emissions models over West Siberia. *Biogeosciences* **2015**, *12*, 3321–3349. [[CrossRef](#)]
270. Rawlins, M.A.; McGuire, A.D.; Kimball, J.S.; Dass, P.; Lawrence, D.; Burke, E.; Chen, X.; Delire, C.; Koven, C.; MacDougall, A.; et al. Assessment of model estimates of land-atmosphere CO₂ exchange across Northern Eurasia. *Biogeosciences* **2015**, *12*, 4385–4405. [[CrossRef](#)]

271. Sannel, A.; Kuhry, P. Warming-induced destabilization of peat plateau/thermokarst lake complexes. *J. Geophys. Res. Biogeosci.* **2011**, *116*, G03035. [[CrossRef](#)]
272. Sakai, T.; Matsunaga, T.; Maksyutov, S.; Gotovtsev, S.; Gagarin, L.; Hiyama, T.; Yamaguchi, Y. Climate-Induced Extreme Hydrologic Events in the Arctic. *Remote Sens.* **2016**, *8*, 971. [[CrossRef](#)]
273. Broderick, D.E.; Frey, K.E.; Rogan, J.; Alexander, H.D.; Zimov, N.S. Estimating upper soil horizon carbon stocks in a permafrost watershed of Northeast Siberia by integrating field measurements with Landsat-5 TM and WorldView-2 satellite data. *Gisci. Remote Sens.* **2015**, *52*, 131–157. [[CrossRef](#)]
274. Siewert, M.B.; Hanisch, J.; Weiss, N.; Kuhry, P.; Maximov, T.C.; Hugelius, G. Comparing carbon storage of Siberian tundra and taiga permafrost ecosystems at very high spatial resolution. *J. Geophys. Res. Biogeosci.* **2015**, *120*, 1973–1994. [[CrossRef](#)]
275. Loranty, M.M.; Natali, S.M.; Berner, L.T.; Goetz, S.J.; Holmes, R.M.; Davydov, S.P.; Zimov, N.S.; Zimov, S.A. Siberian tundra ecosystem vegetation and carbon stocks four decades after wildfire. *J. Geophys. Res. Biogeosci.* **2014**, *119*, 2144–2154. [[CrossRef](#)]
276. Griffin, C.G.; Frey, K.E.; Rogan, J.; Holmes, R.M. Spatial and interannual variability of dissolved organic matter in the Kolyma River, East Siberia, observed using satellite imagery. *J. Geophys. Res. Biogeosci.* **2011**, *116*, G03018. [[CrossRef](#)]
277. Park, S.E.; Bartsch, A.; Sabel, D.; Wagner, W.; Naeimi, V.; Yamaguchi, Y. Monitoring freeze/thaw cycles using ENVISAT ASAR Global Mode. *Remote Sens. Environ.* **2011**, *115*, 3457–3467. [[CrossRef](#)]
278. Dupeyrat, L.; Hurault, B.; Costard, F.; Marmo, C.; Gautier, E. Satellite image analysis and frozen cylinder experiments on thermal erosion of periglacial fluvial islands. *Permafro. Periglac. Process.* **2018**, *29*, 100–111. [[CrossRef](#)]
279. Séjourné, A.; Costard, F.; Fedorov, A.; Gargani, J.; Skorve, J.; Massé, M.; Mège, D. Evolution of the banks of thermokarst lakes in Central Yakutia (Central Siberia) due to retrogressive thaw slumps activity controlled by insolation. *Geomorphology* **2015**, *241*, 31–40. [[CrossRef](#)]
280. Chen, F.; Lin, H.; Zhou, W.; Hong, T.; Wang, G. Surface deformation detected by ALOS PALSAR small baseline SAR interferometry over permafrost environment of Beiluhe section, Tibet Plateau, China. *Remote Sens. Environ.* **2013**, *138*, 10–18. [[CrossRef](#)]
281. Song, Y.; Jin, L.; Wang, H. Vegetation changes along the Qinghai–Tibet Plateau engineering corridor since 2000 induced by climate change and human activities. *Remote Sens.* **2018**, *10*, 95. [[CrossRef](#)]
282. Wang, C.; Zhang, Z.; Paloscia, S.; Zhang, H.; Wu, F.; Wu, Q. Permafrost Soil Moisture Monitoring Using Multi-Temporal TerraSAR-X Data in Beiluhe of Northern Tibet, China. *Remote Sens.* **2018**, *10*, 1577. [[CrossRef](#)]
283. Niu, F.; Yin, G.; Luo, J.; Lin, Z.; Liu, M. Permafrost distribution along the Qinghai–Tibet Engineering Corridor, China using high-resolution statistical mapping and modeling integrated with remote sensing and GIS. *Remote Sens.* **2018**, *10*, 215. [[CrossRef](#)]
284. Yin, G.; Zheng, H.; Niu, F.; Luo, J.; Lin, Z.; Liu, M. Numerical mapping and modeling permafrost thermal dynamics across the Qinghai–Tibet engineering corridor, China integrated with remote sensing. *Remote Sens.* **2018**, *10*, 2069. [[CrossRef](#)]
285. Luo, J.; Yin, G.; Niu, F.; Lin, Z.; Liu, M. High spatial resolution modeling of climate change impacts on permafrost thermal conditions for the Beiluhe Basin, Qinghai–Tibet Plateau. *Remote Sens.* **2019**, *11*, 1294. [[CrossRef](#)]
286. Jia, Y.; Kim, J.W.; Shum, C.; Lu, Z.; Ding, X.; Zhang, L.; Erkan, K.; Kuo, C.Y.; Shang, K.; Tseng, K.H.; et al. Characterization of active layer thickening rate over the northern Qinghai–Tibetan plateau permafrost region using ALOS interferometric synthetic aperture radar data, 2007–2009. *Remote Sens.* **2017**, *9*, 84. [[CrossRef](#)]
287. Zhang, Z.; Wang, C.; Zhang, H.; Tang, Y.; Liu, X. Analysis of permafrost region coherence variation in the Qinghai–Tibet Plateau with a high-resolution TerraSAR-X image. *Remote Sens.* **2018**, *10*, 298. [[CrossRef](#)]
288. Tang, P.; Zhou, W.; Tian, B.; Chen, F.; Li, Z.; Li, G. Quantification of Temporal Decorrelation in X-, C-, and L-Band Interferometry for the Permafrost Region of the Qinghai–Tibet Plateau. *IEEE Geosci. Remote. Sens. Lett.* **2017**, *14*, 2285–2289. [[CrossRef](#)]
289. Xie, C.; Li, Z.; Xu, J.; Li, X. Analysis of deformation over permafrost regions of Qinghai–Tibet plateau based on permanent scatterers. *Int. J. Remote Sens.* **2010**, *31*, 1995–2008. [[CrossRef](#)]
290. Tian, B.; Li, Z.; Tang, P.; Zou, P.; Zhang, M.; Niu, F. Use of intensity and coherence of X-band SAR data to map thermokarst lakes on the Northern Tibetan Plateau. *IEEE J. Sel. Top. Appl. Earth Obs. Remote Sens.* **2016**, *9*, 3164–3176. [[CrossRef](#)]
291. Zhang, Z.; Wang, M.; Liu, X.; Wang, C.; Zhang, H.; Tang, Y.; Zhang, B. Deformation Feature Analysis of Qinghai–Tibet Railway Using TerraSAR-X and Sentinel-1A Time-Series Interferometry. *IEEE J. Sel. Top. Appl. Earth Obs. Remote Sens.* **2019**, *12*, 5199–5212. [[CrossRef](#)]
292. Tian, B.; Li, Z.; Zhang, M.; Huang, L.; Qiu, Y.; Li, Z.; Tang, P. Mapping thermokarst lakes on the Qinghai–Tibet Plateau using nonlocal active contours in Chinese GaoFen-2 multispectral imagery. *IEEE J. Sel. Top. Appl. Earth Obs. Remote Sens.* **2017**, *10*, 1687–1700. [[CrossRef](#)]
293. Wang, C.; Zhang, Z.; Zhang, H.; Zhang, B.; Tang, Y.; Wu, Q. Active layer thickness retrieval of Qinghai–Tibet permafrost using the TerraSAR-X InSAR technique. *IEEE J. Sel. Top. Appl. Earth Obs. Remote Sens.* **2018**, *11*, 4403–4413. [[CrossRef](#)]
294. Huang, L.; Luo, J.; Lin, Z.; Niu, F.; Liu, L. Using deep learning to map retrogressive thaw slumps in the Beiluhe region (Tibetan Plateau) from CubeSat images. *Remote Sens. Environ.* **2020**, *237*, 111534. [[CrossRef](#)]
295. Zou, D.; Zhao, L.; Wu, T.; Wu, X.; Pang, Q.; Wang, Z. Modeling ground surface temperature by means of remote sensing data in high-altitude areas: Test in the central Tibetan Plateau with application of moderate-resolution imaging spectroradiometer Terra/Aqua land surface temperature and ground-based infrared radiometer. *J. Appl. Remote Sens.* **2014**, *8*, 083516.
296. Chang, L.; Hanssen, R.F. Detection of permafrost sensitivity of the Qinghai–Tibet railway using satellite radar interferometry. *Int. J. Remote Sens.* **2015**, *36*, 691–700. [[CrossRef](#)]

297. Westermann, S.; Langer, M.; Boike, J. Systematic bias of average winter-time land surface temperatures inferred from MODIS at a site on Svalbard, Norway. *Remote Sens. Environ.* **2012**, *118*, 162–167. [[CrossRef](#)]
298. Westermann, S.; Langer, M.; Boike, J. Spatial and temporal variations of summer surface temperatures of high-arctic tundra on Svalbard—Implications for MODIS LST based permafrost monitoring. *Remote Sens. Environ.* **2011**, *115*, 908–922. [[CrossRef](#)]
299. Rouyet, L.; Lauknes, T.R.; Christiansen, H.H.; Strand, S.M.; Larsen, Y. Seasonal dynamics of a permafrost landscape, Adventdalen, Svalbard, investigated by InSAR. *Remote Sens. Environ.* **2019**, *231*, 111236. [[CrossRef](#)]
300. Eckerstorfer, M.; Malnes, E.; Christiansen, H. Freeze/thaw conditions at periglacial landforms in Kapp Linné, Svalbard, investigated using field observations, in situ, and radar satellite monitoring. *Geomorphology* **2017**, *293*, 433–447. [[CrossRef](#)]
301. Bernhardt, H.; Reiss, D.; Hiesinger, H.; Hauber, E.; Johnsson, A. Debris flow recurrence periods and multi-temporal observations of colluvial fan evolution in central Spitsbergen (Svalbard). *Geomorphology* **2017**, *296*, 132–141. [[CrossRef](#)]
302. Kasprzak, M.; Łopuch, M.; Glowacki, T.; Milczarek, W. Evolution of Near-Shore Outwash Fans and Permafrost Spreading Under Their Surface: A Case Study from Svalbard. *Remote Sens.* **2020**, *12*, 482. [[CrossRef](#)]
303. Woelders, L.; Lenaerts, J.T.; Hagemans, K.; Akkerman, K.; van Hoof, T.B.; Hoek, W.Z. Recent climate warming drives ecological change in a remote high-Arctic lake. *Sci. Rep.* **2018**, *8*, 1–8.
304. Bertone, A.; Zucca, F.; Marin, C.; Notarnicola, C.; Cuozzo, G.; Krainer, K.; Mair, V.; Riccardi, P.; Callegari, M.; Seppi, R. An unsupervised method to detect rock glacier activity by using Sentinel-1 SAR interferometric coherence: A regional-scale study in the eastern European Alps. *Remote Sens.* **2019**, *11*, 1711. [[CrossRef](#)]
305. Gruber, S.; Hoelzle, M. Statistical modelling of mountain permafrost distribution: Local calibration and incorporation of remotely sensed data. *Permafr. Periglac. Process.* **2001**, *12*, 69–77. [[CrossRef](#)]
306. Strozzi, T.; Kääb, A.; Frauenfelder, R. Detecting and quantifying mountain permafrost creep from in situ inventory, space-borne radar interferometry and airborne digital photogrammetry. *Int. J. Remote Sens.* **2004**, *25*, 2919–2931. [[CrossRef](#)]
307. Kenyi, L.W.; Kaufmann, V. Estimation of rock glacier surface deformation using SAR interferometry data. *IEEE Trans. Geosci. Remote Sens.* **2003**, *41*, 1512–1515. [[CrossRef](#)]
308. Ravanel, L.; Magnin, F.; Deline, P. Impacts of the 2003 and 2015 summer heatwaves on permafrost-affected rock-walls in the Mont Blanc massif. *Sci. Total Environ.* **2017**, *609*, 132–143. [[CrossRef](#)] [[PubMed](#)]
309. Strozzi, T.; Delaloye, R.; Kääb, A.; Ambrosi, C.; Perruchoud, E.; Wegmüller, U. Combined observations of rock mass movements using satellite SAR interferometry, differential GPS, airborne digital photogrammetry, and airborne photography interpretation. *J. Geophys. Res. Earth Surf.* **2010**, *115*, F01014. [[CrossRef](#)]
310. Eriksen, H.Ø.; Lauknes, T.R.; Larsen, Y.; Corner, G.D.; Bergh, S.G.; Dehls, J.; Kierulf, H.P. Visualizing and interpreting surface displacement patterns on unstable slopes using multi-geometry satellite SAR interferometry (2D InSAR). *Remote Sens. Environ.* **2017**, *191*, 297–312. [[CrossRef](#)]
311. Jagdhuber, T.; Stockamp, J.; Hajnsek, I.; Ludwig, R. Identification of soil freezing and thawing states using SAR polarimetry at C-band. *Remote Sens.* **2014**, *6*, 2008–2023. [[CrossRef](#)]
312. Torbick, N.; Persson, A.; Olefeldt, D.; Frolking, S.; Salas, W.; Hagen, S.; Crill, P.; Li, C. High resolution mapping of peatland hydroperiod at a high-latitude Swedish mire. *Remote Sens.* **2012**, *4*, 1974–1994. [[CrossRef](#)]
313. Gismås, K.; Etzelmüller, B.; Farbrot, H.; Schuler, T.; Westermann, S. CryoGRID 1.0: Permafrost distribution in Norway estimated by a spatial numerical model. *Permafr. Periglac. Process.* **2013**, *24*, 2–19. [[CrossRef](#)]
314. Etzelmüller, B.; Ødegård, R.S.; Berthling, I.; Sollid, J.L. Terrain parameters and remote sensing data in the analysis of permafrost distribution and periglacial processes: Principles and examples from southern Norway. *Permafr. Periglac. Process.* **2001**, *12*, 79–92. [[CrossRef](#)]
315. Westermann, S.; Elberling, B.; Højlund Pedersen, S.; Stendel, M.; Hansen, B.; Liston, G. Future permafrost conditions along environmental gradients in Zackenberg, Greenland. *Cryosphere* **2015**, *9*, 719–735. [[CrossRef](#)]
316. Westergaard-Nielsen, A.; Karami, M.; Hansen, B.U.; Westermann, S.; Elberling, B. Contrasting temperature trends across the ice-free part of Greenland. *Sci. Rep.* **2018**, *8*, 1–6. [[CrossRef](#)] [[PubMed](#)]
317. Finger Higgins, R.; Chipman, J.; Lutz, D.; Culler, L.; Virginia, R.; Ogden, L. Changing lake dynamics indicate a drier Arctic in Western Greenland. *J. Geophys. Res. Biogeosci.* **2019**, *124*, 870–883. [[CrossRef](#)]
318. Villarroel, C.D.; Tamburini Beliveau, G.; Forte, A.P.; Monserrat, O.; Morvillo, M. DInSAR for a Regional inventory of active rock glaciers in the dry andes mountains of argentina and chile with sentinel-1 data. *Remote Sens.* **2018**, *10*, 1588. [[CrossRef](#)]
319. Nagy, B.; Ignéczi, Á.; Kovács, J.; Szalai, Z.; Mari, L. Shallow ground temperature measurements on the highest volcano on Earth, Mt. Ojos del Salado, Arid Andes, Chile. *Permafr. Periglac. Process.* **2019**, *30*, 3–18. [[CrossRef](#)]
320. Monnier, S.; Kinnard, C.; Surazakov, A.; Bossy, W. Geomorphology, internal structure, and successive development of a glacier foreland in the semiarid Chilean Andes (Cerro Tapado, upper Elqui Valley, 30°08' S., 69°55' W.). *Geomorphology* **2014**, *207*, 126–140. [[CrossRef](#)]
321. Janke, J.R.; Ng, S.; Bellisario, A. An inventory and estimate of water stored in firn fields, glaciers, debris-covered glaciers, and rock glaciers in the Aconcagua River Basin, Chile. *Geomorphology* **2017**, *296*, 142–152. [[CrossRef](#)]
322. Brenning, A.; Peña, M.; Long, S.; Soliman, A. Thermal remote sensing of ice-debris landforms using ASTER: An example from the Chilean Andes. *Cryosphere* **2012**, *6*, 367. [[CrossRef](#)]
323. Batbaatar, J.; Gillespie, A.R.; Sletten, R.S.; Mushkin, A.; Amit, R.; Liaudat, D.T.; Liu, L.; Petrie, G. Toward the Detection of Permafrost Using Land-Surface Temperature Mapping. *Remote Sens.* **2020**, *12*, 695. [[CrossRef](#)]

324. Mink, S.; López-Martínez, J.; Maestro, A.; Garrote, J.; Ortega, J.A.; Serrano, E.; Durán, J.J.; Schmid, T. Insights into deglaciation of the largest ice-free area in the South Shetland Islands (Antarctica) from quantitative analysis of the drainage system. *Geomorphology* **2014**, *225*, 4–24. [[CrossRef](#)]
325. López-Martínez, J.; Serrano, E.; Schmid, T.; Mink, S.; Linés, C. Periglacial processes and landforms in the South Shetland Islands (northern Antarctic Peninsula region). *Geomorphology* **2012**, *155*, 62–79. [[CrossRef](#)]
326. Moura, P.A.; Francelino, M.R.; Schaefer, C.e.g., Simas, F.N.; de Mendonça, B.A. Distribution and characterization of soils and landform relationships in Byers Peninsula, Livingston Island, Maritime Antarctica. *Geomorphology* **2012**, *155*, 45–54. [[CrossRef](#)]
327. Vieira, G.; Mora, C.; Pina, P.; Schaefer, C.E. A proxy for snow cover and winter ground surface cooling: Mapping Usnea sp. communities using high resolution remote sensing imagery (maritime Antarctica). *Geomorphology* **2014**, *225*, 69–75. [[CrossRef](#)]
328. Miranda, V.; Pina, P.; Heleno, S.; Vieira, G.; Mora, C.; Schaefer, C.E. Monitoring recent changes of vegetation in Fildes Peninsula (King George Island, Antarctica) through satellite imagery guided by UAV surveys. *Sci. Total Environ.* **2020**, *704*, 135295. [[CrossRef](#)] [[PubMed](#)]
329. Bockheim, J.G. Distribution, properties and origin of viscous-flow features in the McMurdo Dry Valleys, Antarctica. *Geomorphology* **2014**, *204*, 114–122. [[CrossRef](#)]
330. Liu, J.; Chen, J.; Cihlar, J. Mapping evapotranspiration based on remote sensing: An application to Canada's landmass. *Water Resour. Res.* **2003**, *39*. [[CrossRef](#)]
331. Yang, W.; Wang, Y.; Liu, X.; Zhao, H.; Shao, R.; Wang, G. Evaluation of the rescaled complementary principle in the estimation of evaporation on the Tibetan Plateau. *Sci. Total Environ.* **2020**, *699*, 134367. [[CrossRef](#)] [[PubMed](#)]
332. Hammerling, D.M.; Kawa, S.R.; Schaefer, K.; Doney, S.; Michalak, A.M. Detectability of CO₂ flux signals by a space-based lidar mission. *J. Geophys. Res. Atmos.* **2015**, *120*, 1794–1807. [[CrossRef](#)]
333. Crowell, S.M.; Randolph Kawa, S.; Browell, E.V.; Hammerling, D.M.; Moore, B.; Schaefer, K.; Doney, S.C. On the ability of space-based passive and active remote sensing observations of CO₂ to detect flux perturbations to the carbon cycle. *J. Geophys. Res. Atmos.* **2018**, *123*, 1460–1477. [[CrossRef](#)]
334. Jackson, R.B.; Saunois, M.; Bousquet, P.; Canadell, J.G.; Poulter, B.; Stavert, A.R.; Bergamaschi, P.; Niwa, Y.; Segers, A.; Tsuruta, A. Increasing anthropogenic methane emissions arise equally from agricultural and fossil fuel sources. *Environ. Res. Lett.* **2020**, *15*, 071002. [[CrossRef](#)]
335. Dlugokencky, E.J.; Bruhwiler, L.; White, J.; Emmons, L.; Novelli, P.C.; Montzka, S.A.; Masarie, K.A.; Lang, P.M.; Crotwell, A.; Miller, J.B.; et al. Observational constraints on recent increases in the atmospheric CH₄ burden. *Geophys. Res. Lett.* **2009**, *36*, L18803. [[CrossRef](#)]
336. Elder, C.D.; Thompson, D.R.; Thorpe, A.K.; Hanke, P.; Walter Anthony, K.M.; Miller, C.E. Airborne mapping reveals emergent power law of arctic methane emissions. *Geophys. Res. Lett.* **2020**, *47*, e2019GL085707. [[CrossRef](#)]
337. European Space Agency. Arctic Methane and Permafrost Challenge (AMPC). Available online: <https://eo4society.esa.int/communities/scientists/arctic-methane-and-permafrost/> (accessed on 28 November 2020).
338. European Space Agency. A NASA and ESA Collaborative Community Initiative on Arctic Methane and Permafrost. 2020. Available online: <https://eo4society.esa.int/2020/09/01/a-nasa-and-es-a-collaborative-community-initiative-on-arctic-methane-and-permafrost/> (accessed on 28 November 2020).
339. Veefkind, J.; Aben, I.; McMullan, K.; Förster, H.; De Vries, J.; Otter, G.; Claas, J.; Eskes, H.; De Haan, J.; Kleipool, Q.; et al. TROPOMI on the ESA Sentinel-5 Precursor: A GMES mission for global observations of the atmospheric composition for climate, air quality and ozone layer applications. *Remote Sens. Environ.* **2012**, *120*, 70–83. [[CrossRef](#)]
340. Griffin, D.; Zhao, X.; McLinden, C.A.; Boersma, F.; Bourassa, A.; Dammers, E.; Degenstein, D.; Eskes, H.; Fehr, L.; Fioletov, V.; et al. High-resolution mapping of nitrogen dioxide with TROPOMI: First results and validation over the Canadian oil sands. *Geophys. Res. Lett.* **2019**, *46*, 1049–1060. [[CrossRef](#)]
341. Hu, H.; Landgraf, J.; Detmers, R.; Borsdorff, T.; Aan de Brugh, J.; Aben, I.; Butz, A.; Hasekamp, O. Toward global mapping of methane with TROPOMI: First results and intersatellite comparison to GOSAT. *Geophys. Res. Lett.* **2018**, *45*, 3682–3689. [[CrossRef](#)]
342. Lorente, A.; Borsdorff, T.; Butz, A.; Hasekamp, O.; Schneider, A.; Wu, L.; Hase, F.; Kivi, R.; Wunch, D.; Pollard, D.F.; et al. Methane retrieved from TROPOMI: Improvement of the data product and validation of the first 2 years of measurements. *Atmos. Meas. Tech.* **2021**, *14*, 665–684. [[CrossRef](#)]
343. Schneising, O.; Buchwitz, M.; Reuter, M.; Bovensmann, H.; Burrows, J.P.; Borsdorff, T.; Deutscher, N.M.; Feist, D.G.; Griffith, D.W.; Hase, F.; et al. A scientific algorithm to simultaneously retrieve carbon monoxide and methane from TROPOMI onboard Sentinel-5 Precursor. *Atmos. Meas. Tech.* **2019**, *12*, 6771–6802. [[CrossRef](#)]
344. Varon, D.; McKeever, J.; Jervis, D.; Maasakkers, J.; Pandey, S.; Houweling, S.; Aben, I.; Scarpelli, T.; Jacob, D. Satellite discovery of anomalously large methane point sources from oil/gas production. *Geophys. Res. Lett.* **2019**, *46*, 13507–13516. [[CrossRef](#)]
345. Ehret, G.; Bousquet, P.; Pierangelo, C.; Alpers, M.; Millet, B.; Abshire, J.B.; Bovensmann, H.; Burrows, J.P.; Chevallier, F.; Ciais, P.; et al. MERLIN: A French-German space lidar mission dedicated to atmospheric methane. *Remote Sens.* **2017**, *9*, 1052. [[CrossRef](#)]
346. Pierangelo, C.; Millet, B.; Esteve, F.; Alpers, M.; Ehret, G.; Flamant, P.; Berthier, S.; Gibert, F.; Chomette, O.; Edouart, D.; et al. Merlin (methane remote sensing Lidar mission): An overview. In Proceedings of the 27th International Laser Radar Conference (ILRC), New York, NY, USA, 5–10 July 2015; EPJ Web of Conferences: Les Ulis, France, 2016; Volume 119, p. 26001.

347. Stephan, C.; Alpers, M.; Millet, B.; Ehret, G.; Flamant, P.; Deniel, C. MERLIN: A space-based methane monitor. In Proceedings of the SPIE, Lidar Remote Sensing for Environmental Monitoring XII, San Diego, CA, USA, 21–22 August 2011; Volume 8159, pp. 815–908.
348. German Aerospace Centre (DLR). MERLIN—Die Deutsch-Französische Klimamission. Available online: https://www.dlr.de/rd/en/desktopdefault.aspx/tabcid-2440/3586_read-31672/ (accessed on 20 February 2021).
349. Yao, F.; Wang, J.; Yang, K.; Wang, C.; Walter, B.A.; Crétaux, J.F. Lake storage variation on the endorheic Tibetan Plateau and its attribution to climate change since the new millennium. *Environ. Res. Lett.* **2018**, *13*, 064011. [CrossRef]
350. Necsoiu, M.; Dinwiddie, C.L.; Walter, G.R.; Larsen, A.; Stothoff, S.A. Multi-temporal image analysis of historical aerial photographs and recent satellite imagery reveals evolution of water body surface area and polygonal terrain morphology in Kobuk Valley National Park, Alaska. *Environ. Res. Lett.* **2013**, *8*, 025007. [CrossRef]
351. Carroll, M.L.; Loboda, T.V. The sign, magnitude and potential drivers of change in surface water extent in Canadian tundra. *Environ. Res. Lett.* **2018**, *13*, 045009. [CrossRef]
352. Liu, J.; Wang, S.; Yu, S.; Yang, D.; Zhang, L. Climate warming and growth of high-elevation inland lakes on the Tibetan Plateau. *Glob. Planet. Chang.* **2009**, *67*, 209–217. [CrossRef]
353. Turner, K.W.; Wolfe, B.B.; Edwards, T.W.; Lantz, T.C.; Hall, R.I.; Larocque, G. Controls on water balance of shallow thermokarst lakes and their relations with catchment characteristics: A multi-year, landscape-scale assessment based on water isotope tracers and remote sensing in Old Crow Flats, Yukon (Canada). *Glob. Chang. Biol.* **2014**, *20*, 1585–1603. [CrossRef]
354. Duan, L.; Man, X.; Kurylyk, B.L.; Cai, T.; Li, Q. Distinguishing streamflow trends caused by changes in climate, forest cover, and permafrost in a large watershed in northeastern China. *Hydrol. Process.* **2017**, *31*, 1938–1951. [CrossRef]
355. Jepsen, S.M.; Walvoord, M.A.; Voss, C.I.; Rover, J. Effect of permafrost thaw on the dynamics of lakes recharged by ice-jam floods: Case study of Yukon Flats, Alaska. *Hydrol. Process.* **2016**, *30*, 1782–1795. [CrossRef]
356. Wanchang, Z.; Ogawa, K.; Besheng, Y.; Yamaguchi, Y. A monthly stream flow model for estimating the potential changes of river runoff on the projected global warming. *Hydrol. Process.* **2000**, *14*, 1851–1868. [CrossRef]
357. Gao, L.; Liao, J.; Shen, G. Monitoring lake-level changes in the Qinghai–Tibetan Plateau using radar altimeter data (2002–2012). *J. Appl. Remote Sens.* **2013**, *7*, 073470. [CrossRef]
358. Lantz, T.; Turner, K. Changes in lake area in response to thermokarst processes and climate in Old Crow Flats, Yukon. *J. Geophys. Res. Biogeosci.* **2015**, *120*, 513–524. [CrossRef]
359. Mętrak, M.; Szwarczewski, P.; Bińska, K.; Rojan, E.; Karasiński, J.; Górecki, G.; Suska-Malawska, M. Late Holocene development of Lake Rangkul (Eastern Pamir, Tajikistan) and its response to regional climatic changes. *Palaeogeogr. Palaeoclimatol. Palaeoecol.* **2019**, *521*, 99–113. [CrossRef]
360. Sjöberg, Y.; Hugelius, G.; Kuhry, P. Thermokarst lake morphometry and erosion features in two peat plateau areas of northeast European Russia. *Permafro. Periglac. Process.* **2013**, *24*, 75–81. [CrossRef]
361. Hinkel, K.M.; Frohn, R.; Nelson, F.; Eisner, W.; Beck, R. Morphometric and spatial analysis of thaw lakes and drained thaw lake basins in the western Arctic Coastal Plain, Alaska. *Permafro. Periglac. Process.* **2005**, *16*, 327–341. [CrossRef]
362. Karlsson, J.M.; Lyon, S.W.; Destouni, G. Temporal behavior of lake size-distribution in a thawing permafrost landscape in northwestern Siberia. *Remote Sens.* **2014**, *6*, 621–636. [CrossRef]
363. Mao, D.; Wang, Z.; Yang, H.; Li, H.; Thompson, J.R.; Li, L.; Song, K.; Chen, B.; Gao, H.; Wu, J. Impacts of climate change on Tibetan lakes: Patterns and processes. *Remote Sens.* **2018**, *10*, 358. [CrossRef]
364. Muster, S.; Heim, B.; Abnizova, A.; Boike, J. Water body distributions across scales: A remote sensing based comparison of three arctic tundra wetlands. *Remote Sens.* **2013**, *5*, 1498–1523. [CrossRef]
365. Lara, M.J.; Chipman, M.L.; Hu, F.S. Automated detection of thermoerosion in permafrost ecosystems using temporally dense Landsat image stacks. *Remote Sens. Environ.* **2019**, *221*, 462–473. [CrossRef]
366. Zakharova, E.A.; Kouraev, A.V.; Stephane, G.; Franck, G.; Desyatkin, R.V.; Desyatkin, A.R. Recent dynamics of hydro-ecosystems in thermokarst depressions in Central Siberia from satellite and in situ observations: Importance for agriculture and human life. *Sci. Total Environ.* **2018**, *615*, 1290–1304. [CrossRef]
367. Günther, F.; Overduin, P.P.; Yakshina, I.A.; Opel, T.; Baranskaya, A.V.; Grigoriev, M.N. Observing Muostakh disappear: Permafrost thaw subsidence and erosion of a ground-ice-rich island in response to arctic summer warming and sea ice reduction. *Cryosphere* **2015**, *9*, 151–178. [CrossRef]
368. Ulrich, M.; Matthes, H.; Schirrmeyer, L.; Schütze, J.; Park, H.; Iijima, Y.; Fedorov, A.N. Differences in behavior and distribution of permafrost-related lakes in Central Yakutia and their response to climatic drivers. *Water Resour. Res.* **2017**, *53*, 1167–1188. [CrossRef]
369. Surdu, C.M.; Duguay, C.R.; Fernández Prieto, D. Evidence of recent changes in the ice regime of lakes in the Canadian High Arctic from spaceborne satellite observations. *Cryosphere* **2016**, *10*, 941–960. [CrossRef]
370. Klinge, M.; Dulamsuren, C.; Erasmi, S.; Karger, D.N.; Hauck, M. Climate effects on vegetation vitality at the treeline of boreal forests of Mongolia. *Biogeosciences* **2018**, *15*, 1319–1333. [CrossRef]
371. Jones, M.K.W.; Pollard, W.H.; Jones, B.M. Rapid initialization of retrogressive thaw slumps in the Canadian high Arctic and their response to climate and terrain factors. *Environ. Res. Lett.* **2019**, *14*, 055006. [CrossRef]
372. Yi, S.; Zhou, Z.; Ren, S.; Xu, M.; Qin, Y.; Chen, S.; Ye, B. Effects of permafrost degradation on alpine grassland in a semi-arid basin on the Qinghai–Tibetan Plateau. *Environ. Res. Lett.* **2011**, *6*, 045403. [CrossRef]

373. Yu, Q.; Epstein, H.E.; Engstrom, R.; Shiklomanov, N.; Streletskeiy, D. Land cover and land use changes in the oil and gas regions of Northwestern Siberia under changing climatic conditions. *Environ. Res. Lett.* **2015**, *10*, 124020. [[CrossRef](#)]
374. Forkel, M.; Thonicke, K.; Beer, C.; Cramer, W.; Bartalev, S.; Schmullius, C. Extreme fire events are related to previous-year surface moisture conditions in permafrost-underlain larch forests of Siberia. *Environ. Res. Lett.* **2012**, *7*, 044021. [[CrossRef](#)]
375. Lu, X.; Zhuang, Q. Areal changes of land ecosystems in the Alaskan Yukon River Basin from 1984 to 2008. *Environ. Res. Lett.* **2011**, *6*, 034012. [[CrossRef](#)]
376. Bartsch, A.; Balzter, H.; George, C. The influence of regional surface soil moisture anomalies on forest fires in Siberia observed from satellites. *Environ. Res. Lett.* **2009**, *4*, 045021. [[CrossRef](#)]
377. Xue, X.; Guo, J.; Han, B.; Sun, Q.; Liu, L. The effect of climate warming and permafrost thaw on desertification in the Qinghai-Tibetan Plateau. *Geomorphology* **2009**, *108*, 182–190. [[CrossRef](#)]
378. Mohammadimaneesh, F.; Salehi, B.; Mahdianpari, M.; English, J.; Chamberland, J.; Alasset, P.J. Monitoring surface changes in discontinuous permafrost terrain using small baseline SAR interferometry, object-based classification, and geological features: A case study from Mayo, Yukon Territory, Canada. *GIScience Remote Sens.* **2019**, *56*, 485–510. [[CrossRef](#)]
379. Boike, J.; Grau, T.; Heim, B.; Günther, F.; Langer, M.; Muster, S.; Gouttevin, I.; Lange, S. Satellite-derived changes in the permafrost landscape of central Yakutia, 2000–2011: Wetting, drying, and fires. *Glob. Planet. Chang.* **2016**, *139*, 116–127. [[CrossRef](#)]
380. Pastick, N.J.; Jorgenson, M.T.; Goetz, S.J.; Jones, B.M.; Wylie, B.K.; Minsley, B.J.; Genet, H.; Knight, J.F.; Swanson, D.K.; Jorgenson, J.C. Spatiotemporal remote sensing of ecosystem change and causation across Alaska. *Glob. Chang. Biol.* **2019**, *25*, 1171–1189. [[CrossRef](#)]
381. Lara, M.J.; Genet, H.; McGuire, A.D.; Euskirchen, E.S.; Zhang, Y.; Brown, D.R.; Jorgenson, M.T.; Romanovsky, V.; Breen, A.; Bolton, W.R. Thermokarst rates intensify due to climate change and forest fragmentation in an Alaskan boreal forest lowland. *Glob. Chang. Biol.* **2016**, *22*, 816–829. [[CrossRef](#)]
382. Yamazaki, T.; Ohta, T.; Suzuki, R.; Ohata, T. Flux variation in a Siberian taiga forest near Yakutsk estimated by a one-dimensional model with routine data, 1986–2000. *Hydrol. Process. Int. J.* **2007**, *21*, 2009–2015. [[CrossRef](#)]
383. Chimitdorzhiev, T.N.; Dagurov, P.N.; Bykov, M.E.; Dmitriev, A.V.; Kirbizhekova, I.I. Comparison of ALOS PALSAR interferometry and field geodetic leveling for marshy soil thaw/freeze monitoring, case study from the Baikal lake region, Russia. *J. Appl. Remote Sens.* **2016**, *10*, 016006. [[CrossRef](#)]
384. Herzschuh, U.; Pestryakova, L.A.; Savelieva, L.A.; Heinecke, L.; Böhmer, T.; Biskaborn, B.K.; Andreev, A.; Ramisch, A.; Shinneman, A.L.; Birks, H.J.B. Siberian larch forests and the ion content of thaw lakes form a geochemically functional entity. *Nat. Commun.* **2013**, *4*, 1–8. [[CrossRef](#)]
385. Li, X.; Jin, H.; He, R.; Huang, Y.; Wang, H.; Luo, D.; Jin, X.; Lü, L.; Wang, L.; Li, W.; et al. Effects of forest fires on the permafrost environment in the northern Da Xing'anling (Hinggan) mountains, Northeast China. *Permafro. Periglac. Process.* **2019**, *30*, 163–177. [[CrossRef](#)]
386. Holloway, J.E.; Lamoureux, S.F.; Montross, S.N.; Lafrenière, M.J. Climate and terrain characteristics linked to mud ejection occurrence in the Canadian High Arctic. *Permafro. Periglac. Process.* **2016**, *27*, 204–218. [[CrossRef](#)]
387. Eshqi Molan, Y.; Kim, J.W.; Lu, Z.; Wylie, B.; Zhu, Z. Modeling wildfire-induced permafrost deformation in an alaskan boreal forest using InSAR observations. *Remote Sens.* **2018**, *10*, 405. [[CrossRef](#)]
388. Jorgenson, J.C.; Jorgenson, M.T.; Boldenow, M.L.; Orndahl, K.M. Landscape change detected over a half century in the Arctic National Wildlife Refuge using high-resolution aerial imagery. *Remote Sens.* **2018**, *10*, 1305. [[CrossRef](#)]
389. Sun, Z.; Wang, Q.; Xiao, Q.; Batkhishig, O.; Watanabe, M. Diverse responses of remotely sensed grassland phenology to interannual climate variability over frozen ground regions in Mongolia. *Remote Sens.* **2015**, *7*, 360–377. [[CrossRef](#)]
390. Meng, Y.; Lan, H.; Li, L.; Wu, Y.; Li, Q. Characteristics of surface deformation detected by X-band SAR Interferometry over Sichuan-Tibet grid connection project area, China. *Remote Sens.* **2015**, *7*, 12265–12281. [[CrossRef](#)]
391. Kizyakov, A.; Zimin, M.; Sonyushkin, A.; Dvornikov, Y.; Khomutov, A.; Leibman, M. Comparison of gas emission crater geomorphodynamics on Yamal and Gydan Peninsulas (Russia), based on repeat very-high-resolution stereopairs. *Remote Sens.* **2017**, *9*, 1023. [[CrossRef](#)]
392. Shi, X.; Liao, M.; Wang, T.; Zhang, L.; Shan, W.; Wang, C. Expressway deformation mapping using high-resolution TerraSAR-X images. *Remote Sens. Lett.* **2014**, *5*, 194–203. [[CrossRef](#)]
393. Necsoiu, M.; Onaca, A.; Wigginton, S.; Urdea, P. Rock glacier dynamics in Southern Carpathian Mountains from high-resolution optical and multi-temporal SAR satellite imagery. *Remote Sens. Environ.* **2016**, *177*, 21–36. [[CrossRef](#)]
394. Gong, W.; Darrow, M.M.; Meyer, F.J.; Daanen, R.P. Reconstructing movement history of frozen debris lobes in northern Alaska using satellite radar interferometry. *Remote Sens. Environ.* **2019**, *221*, 722–740. [[CrossRef](#)]
395. Zhao, R.; Li, Z.W.; Feng, G.C.; Wang, Q.J.; Hu, J. Monitoring surface deformation over permafrost with an improved SBAS-InSAR algorithm: With emphasis on climatic factors modeling. *Remote Sens. Environ.* **2016**, *184*, 276–287. [[CrossRef](#)]
396. Dini, B.; Daout, S.; Manconi, A.; Loew, S. Classification of slope processes based on multitemporal DInSAR analyses in the Himalaya of NW Bhutan. *Remote Sens. Environ.* **2019**, *233*, 111408. [[CrossRef](#)]
397. Juszak, I.; Erb, A.M.; Maximov, T.C.; Schaepman-Strub, G. Arctic shrub effects on NDVI, summer albedo and soil shading. *Remote Sens. Environ.* **2014**, *153*, 79–89. [[CrossRef](#)]
398. Ulrich, M.; Grosse, G.; Chabriat, S.; Schirrmeyer, L. Spectral characterization of periglacial surfaces and geomorphological units in the Arctic Lena Delta using field spectrometry and remote sensing. *Remote Sens. Environ.* **2009**, *113*, 1220–1235. [[CrossRef](#)]

399. Xu, M.; Kang, S.; Chen, X.; Wu, H.; Wang, X.; Su, Z. Detection of hydrological variations and their impacts on vegetation from multiple satellite observations in the Three-River Source Region of the Tibetan Plateau. *Sci. Total Environ.* **2018**, *639*, 1220–1232. [[CrossRef](#)]
400. Nagai, H.; Fujita, K.; Nuimura, T.; Sakai, A. Southwest-facing slopes control the formation of debris-covered glaciers in the Bhutan Himalaya. *Cryosphere* **2013**, *7*, 1303–1314. [[CrossRef](#)]
401. Yi, Y.; Kimball, J.S.; Chen, R.H.; Moghaddam, M.; Miller, C.E. Sensitivity of active-layer freezing process to snow cover in Arctic Alaska. *Cryosphere* **2019**, *13*, 197–218. [[CrossRef](#)]
402. Wang, X.; Liu, L.; Zhao, L.; Wu, T.; Li, Z.; Liu, G. Mapping and inventorying active rock glaciers in the northern Tien Shan of China using satellite SAR interferometry. *Cryosphere* **2017**, *11*, 997–1014. [[CrossRef](#)]
403. Belshe, E.; Schuur, E.; Grosse, G. Quantification of upland thermokarst features with high resolution remote sensing. *Environ. Res. Lett.* **2013**, *8*, 035016. [[CrossRef](#)]
404. Veremeeva, A.; Gubin, S. Modern tundra landscapes of the Kolyma Lowland and their evolution in the Holocene. *Permafro. Periglac. Process.* **2009**, *20*, 399–406. [[CrossRef](#)]
405. Davidson, S.J.; Santos, M.J.; Sloan, V.L.; Watts, J.D.; Phoenix, G.K.; Oechel, W.C.; Zona, D. Mapping Arctic tundra vegetation communities using field spectroscopy and multispectral satellite data in North Alaska, USA. *Remote Sens.* **2016**, *8*, 978. [[CrossRef](#)]
406. Kharuk, V.I.; Ranson, K.J.; Im, S.T.; Il'ya, A.P. Climate-induced larch growth response within the central Siberian permafrost zone. *Environ. Res. Lett.* **2015**, *10*, 125009. [[CrossRef](#)]
407. Brown, D.; Jorgenson, M.T.; Kielland, K.; Verbyla, D.L.; Prakash, A.; Koch, J.C. Landscape effects of wildfire on permafrost distribution in interior Alaska derived from remote sensing. *Remote Sens.* **2016**, *8*, 654. [[CrossRef](#)]
408. Li, C.; Lu, H.; Leung, L.R.; Yang, K.; Li, H.; Wang, W.; Han, M.; Chen, Y. Improving land surface temperature simulation in CoLM over the Tibetan Plateau through fractional vegetation cover derived from a remotely sensed clumping index and model-simulated leaf area index. *J. Geophys. Res. Atmos.* **2019**, *124*, 2620–2642. [[CrossRef](#)]
409. Hachem, S.; Allard, M.; Duguay, C. Using the MODIS land surface temperature product for mapping permafrost: An application to Northern Quebec and Labrador, Canada. *Permafro. Periglac. Process.* **2009**, *20*, 407–416. [[CrossRef](#)]
410. Klein, K.P.; Lantuit, H.; Heim, B.; Fell, F.; Doxaran, D.; Irrgang, A.M. Long-term high-resolution sediment and sea surface temperature spatial patterns in Arctic nearshore waters retrieved using 30-year landsat archive imagery. *Remote Sens.* **2019**, *11*, 2791. [[CrossRef](#)]
411. Muster, S.; Langer, M.; Abnizova, A.; Young, K.L.; Boike, J. Spatio-temporal sensitivity of MODIS land surface temperature anomalies indicates high potential for large-scale land cover change detection in Arctic permafrost landscapes. *Remote Sens. Environ.* **2015**, *168*, 1–12. [[CrossRef](#)]
412. Ran, Y.; Li, X.; Cheng, G. Climate warming over the past half century has led to thermal degradation of permafrost on the Qinghai–Tibet Plateau. *Cryosphere* **2018**, *12*, 595–608. [[CrossRef](#)]
413. Smith, M.W.; Riseborough, D.W. Permafrost monitoring and detection of climate change. *Permafro. Periglac. Process.* **1996**, *7*, 301–309. [[CrossRef](#)]
414. Westermann, S.; Østby, T.; Gisnås, K.; Schuler, T.; Etzelmüller, B. A ground temperature map of the North Atlantic permafrost region based on remote sensing and reanalysis data. *Cryosphere* **2015**, *9*, 1303–1319. [[CrossRef](#)]
415. Obu, J.; Westermann, S.; Bartsch, A.; Berdnikov, N.; Christiansen, H.H.; Dashtseren, A.; Delaloye, R.; Elberling, B.; Etzelmüller, B.; Kholodov, A.; et al. Northern Hemisphere permafrost map based on TTOP modelling for 2000–2016 at 1 km² scale. *Earth-Sci. Rev.* **2019**, *193*, 299–316. [[CrossRef](#)]
416. Haq, M.A.; Baral, P. Study of permafrost distribution in Sikkim Himalayas using Sentinel-2 satellite images and logistic regression modelling. *Geomorphology* **2019**, *333*, 123–136. [[CrossRef](#)]
417. Panda, S.; Prakash, A.; Jorgenson, M.; Solie, D. Near-surface permafrost distribution mapping using logistic regression and remote sensing in Interior Alaska. *GIScience Remote Sens.* **2012**, *49*, 346–363. [[CrossRef](#)]
418. Dulamsuren, C.; Klinge, M.; Degener, J.; Khishigjargal, M.; Chenlemuge, T.; Bat-Enerel, B.; Yeruult, Y.; Saindovdon, D.; Ganbaatar, K.; Tsogtbaatar, J.; et al. Carbon pool densities and a first estimate of the total carbon pool in the Mongolian forest-steppe. *Glob. Chang. Biol.* **2016**, *22*, 830–844. [[CrossRef](#)] [[PubMed](#)]
419. Xu, M.; Kang, S.; Wang, X.; Pepin, N.; Wu, H. Understanding changes in the water budget driven by climate change in cryospheric-dominated watershed of the northeast Tibetan Plateau, China. *Hydrol. Process.* **2019**, *33*, 1040–1058. [[CrossRef](#)]
420. Ou, C.; Leblon, B.; Zhang, Y.; LaRocque, A.; Webster, K.; McLaughlin, J. Modelling and mapping permafrost at high spatial resolution using Landsat and Radarsat images in northern Ontario, Canada: Part 1—model calibration. *Int. J. Remote Sens.* **2016**, *37*, 2727–2750. [[CrossRef](#)]
421. Ou, C.; LaRocque, A.; Leblon, B.; Zhang, Y.; Webster, K.; McLaughlin, J. Modelling and mapping permafrost at high spatial resolution using Landsat and Radarsat-2 images in Northern Ontario, Canada: Part 2—regional mapping. *Int. J. Remote Sens.* **2016**, *37*, 2751–2779. [[CrossRef](#)]
422. Bibi, S.; Wang, L.; Li, X.; Zhang, X.; Chen, D. Response of groundwater storage and recharge in the Qaidam Basin (Tibetan Plateau) to climate variations from 2002 to 2016. *J. Geophys. Res. Atmos.* **2019**, *124*, 9918–9934. [[CrossRef](#)]
423. Landerer, F.W.; Dickey, J.O.; Güntner, A. Terrestrial water budget of the Eurasian pan-Arctic from GRACE satellite measurements during 2003–2009. *J. Geophys. Res. Atmos.* **2010**, *115*, D23115. [[CrossRef](#)]

424. Pastick, N.J.; Jorgenson, M.T.; Wylie, B.K.; Rose, J.R.; Rigge, M.; Walvoord, M.A. Spatial variability and landscape controls of near-surface permafrost within the Alaskan Yukon River basin. *J. Geophys. Res. Biogeosci.* **2014**, *119*, 1244–1265. [[CrossRef](#)]
425. Kremer, M.; Lewkowicz, A.G.; Bonnaventure, P.P.; Sawada, M.C. Utility of classification and regression tree analyses and vegetation in mountain permafrost models, Yukon, Canada. *Permafr. Periglac. Process.* **2011**, *22*, 163–178. [[CrossRef](#)]
426. Hugelius, G.; Kuhry, P.; Tarnocai, C.; Virtanen, T. Soil organic carbon pools in a periglacial landscape: A case study from the central Canadian Arctic. *Permafr. Periglac. Process.* **2010**, *21*, 16–29. [[CrossRef](#)]
427. Panda, S.K.; Prakash, A.; Solie, D.N.; Romanovsky, V.E.; Jorgenson, M.T. Remote sensing and field-based mapping of permafrost distribution along the Alaska Highway corridor, interior Alaska. *Permafr. Periglac. Process.* **2010**, *21*, 271–281. [[CrossRef](#)]
428. Cao, B.; Zhang, T.; Wu, Q.; Sheng, Y.; Zhao, L.; Zou, D. Permafrost zonation index map and statistics over the Qinghai–Tibet Plateau based on field evidence. *Permafr. Periglac. Process.* **2019**, *30*, 178–194. [[CrossRef](#)]
429. Etzelmüller, B.; Heggem, E.S.F.; Sharkhuu, N.; Frauenfelder, R.; Käab, A.; Goulden, C. Mountain permafrost distribution modelling using a multi-criteria approach in the Hövsgöl area, northern Mongolia. *Permafr. Periglac. Process.* **2006**, *17*, 91–104. [[CrossRef](#)]
430. Bai, X.; Yang, J.; Tao, B.; Ren, W. Spatio-Temporal Variations of Soil Active Layer Thickness in Chinese Boreal Forests from 2000 to 2015. *Remote Sens.* **2018**, *10*, 1225. [[CrossRef](#)]
431. Shi, Y.; Niu, F.; Yang, C.; Che, T.; Lin, Z.; Luo, J. Permafrost presence/absence mapping of the Qinghai–Tibet Plateau based on multi-source remote sensing data. *Remote Sens.* **2018**, *10*, 309. [[CrossRef](#)]
432. Fraser, R.H.; Kokelj, S.V.; Lantz, T.C.; McFarlane-Winchester, M.; Olthof, I.; Lacelle, D. Climate sensitivity of high Arctic permafrost terrain demonstrated by widespread ice-wedge thermokarst on Banks Island. *Remote Sens.* **2018**, *10*, 954. [[CrossRef](#)]
433. Muskett, R.R.; Romanovsky, V.E. Alaskan permafrost groundwater storage changes derived from GRACE and ground measurements. *Remote Sens.* **2011**, *3*, 378–397. [[CrossRef](#)]
434. Gagarin, L.; Wu, Q.; Melnikov, A.; Volgusheva, N.; Tananaev, N.; Jin, H.; Zhang, Z.; Zhizhin, V. Morphometric Analysis of Groundwater Icings: Intercomparison of Estimation Techniques. *Remote Sens.* **2020**, *12*, 692. [[CrossRef](#)]
435. Zheng, G.; Yang, Y.; Yang, D.; Dafflon, B.; Lei, H.; Yang, H. Satellite-based simulation of soil freezing/thawing processes in the northeast Tibetan Plateau. *Remote Sens. Environ.* **2019**, *231*, 111269. [[CrossRef](#)]
436. Wang, J.; Jiang, L.; Cui, H.; Wang, G.; Yang, J.; Liu, X.; Su, X. Evaluation and analysis of SMAP, AMSR2 and MEaSUREs freeze/thaw products in China. *Remote Sens. Environ.* **2020**, *242*, 111734. [[CrossRef](#)]
437. Yin, G.; Niu, F.; Lin, Z.; Luo, J.; Liu, M. Effects of local factors and climate on permafrost conditions and distribution in Beiluhe basin, Qinghai–Tibet Plateau, China. *Sci. Total Environ.* **2017**, *581*, 472–485. [[CrossRef](#)]
438. Yi, Y.; Kimball, J.S.; Chen, R.H.; Moghaddam, M.; Reichle, R.H.; Mishra, U.; Zona, D.; Oechel, W.C. Characterizing permafrost active layer dynamics and sensitivity to landscape spatial heterogeneity in Alaska. *Cryosphere* **2018**, *12*, 145–161. [[CrossRef](#)]
439. Bernard-Grand'Maison, C.; Pollard, W. An estimate of ice wedge volume for a High Arctic polar desert environment, Fosheim Peninsula, Ellesmere Island. *Cryosphere* **2018**, *12*, 3589–3604. [[CrossRef](#)]
440. Jones, B.M.; Baughman, C.A.; Romanovsky, V.E.; Parsekian, A.D.; Babcock, E.L.; Stephani, E.; Jones, M.C.; Grosse, G.; Berg, E.E. Presence of rapidly degrading permafrost plateaus in south-central Alaska. *Cryosphere* **2016**, *10*, 2673–2692. [[CrossRef](#)]
441. Riseborough, D.; Shiklomanov, N.; Etzelmüller, B.; Gruber, S.; Marchenko, S. Recent advances in permafrost modelling. *Permafr. Periglac. Process.* **2008**, *19*, 137–156. [[CrossRef](#)]
442. Pastick, N.J.; Jorgenson, M.T.; Wylie, B.K.; Minsley, B.J.; Ji, L.; Walvoord, M.A.; Smith, B.D.; Abraham, J.D.; Rose, J.R. Extending airborne electromagnetic surveys for regional active layer and permafrost mapping with remote sensing and ancillary data, Yukon Flats Ecoregion, Central Alaska. *Permafr. Periglac. Process.* **2013**, *24*, 184–199. [[CrossRef](#)]
443. Li, X.; Jin, R.; Pan, X.; Zhang, T.; Guo, J. Changes in the near-surface soil freeze–thaw cycle on the Qinghai–Tibetan Plateau. *Int. J. Appl. Earth Obs. Geoinf.* **2012**, *17*, 33–42. [[CrossRef](#)]
444. Roy, A.; Royer, A.; Derksen, C.; Brucker, L.; Langlois, A.; Mialon, A.; Kerr, Y.H. Evaluation of spaceborne L-band radiometer measurements for terrestrial freeze/thaw retrievals in Canada. *IEEE J. Sel. Top. Appl. Earth Obs. Remote Sens.* **2015**, *8*, 4442–4459. [[CrossRef](#)]
445. Fuchs, M.; Lenz, J.; Jock, S.; Nitze, I.; Jones, B.M.; Strauss, J.; Günther, F.; Grosse, G. Organic carbon and nitrogen stocks along a thermokarst lake sequence in Arctic Alaska. *J. Geophys. Res. Biogeosci.* **2019**, *124*, 1230–1247. [[CrossRef](#)]
446. Zubrzycki, S.; Kutzbach, L.; Grosse, G.; Desyatkin, A.; Pfeiffer, E.M. Organic carbon and total nitrogen stocks in soils of the Lena River Delta. *Biogeosciences* **2013**, *10*, 3507–3524. [[CrossRef](#)]
447. European Space Agency. Sentinel-2 Mission Details. Available online: <https://earth.esa.int/web/guest/missions/esa-operational-eo-missions/sentinel-2> (accessed on 1 September 2020).
448. European Space Agency. Copernicus: Sentinel-1-The SAR Imaging Constellation for Land and Ocean Services. Available online: <https://directory.eoportal.org/web/eoportal/satellite-missions/c-missions/copernicus-sentinel-1> (accessed on 1 September 2020).
449. NOAA Earth System Research Laboratories. NOAA Cooperative Global Air Sampling Network-Greenhouse Gases. Available online: <https://www.esrl.noaa.gov/gmd/obop/mlo/programs/esrl/ccg/ccg.html> (accessed on 28 October 2020).
450. Dietz, A.J.; Kuenzer, C.; Dech, S. Global SnowPack: A new set of snow cover parameters for studying status and dynamics of the planetary snow cover extent. *Remote Sens. Lett.* **2015**, *6*, 844–853. [[CrossRef](#)]

451. Metsämäki, S.; Pulliainen, J.; Salminen, M.; Luojuus, K.; Wiesmann, A.; Solberg, R.; Böttcher, K.; Hiltunen, M.; Ripper, E. Introduction to GlobSnow Snow Extent products with considerations for accuracy assessment. *Remote Sens. Environ.* **2015**, *156*, 96–108. [CrossRef]
452. Larue, F.; Royer, A.; De Sève, D.; Langlois, A.; Roy, A.; Brucker, L. Validation of GlobSnow-2 snow water equivalent over Eastern Canada. *Remote Sens. Environ.* **2017**, *194*, 264–277. [CrossRef]
453. Pekel, J.F.; Cottam, A.; Gorelick, N.; Belward, A.S. High-resolution mapping of global surface water and its long-term changes. *Nature* **2016**, *540*, 418–422. [CrossRef]
454. Klein, I.; Gessner, U.; Dietz, A.J.; Kuenzer, C. Global WaterPack—A 250 m resolution dataset revealing the daily dynamics of global inland water bodies. *Remote Sens. Environ.* **2017**, *198*, 345–362. [CrossRef]
455. Plummer, S.; Lecomte, P.; Doherty, M. The ESA climate change initiative (CCI): A European contribution to the generation of the global climate observing system. *Remote Sens. Environ.* **2017**, *203*, 2–8. [CrossRef]
456. Friedl, M.A.; McIver, D.K.; Hodges, J.C.; Zhang, X.Y.; Muchoney, D.; Strahler, A.H.; Woodcock, C.E.; Gopal, S.; Schneider, A.; Cooper, A.; et al. Global land cover mapping from MODIS: Algorithms and early results. *Remote Sens. Environ.* **2002**, *83*, 287–302. [CrossRef]
457. Jun, C.; Ban, Y.; Li, S. Open access to Earth land-cover map. *Nature* **2014**, *514*, 434–434. [CrossRef] [PubMed]
458. Bartholome, E.; Belward, A.S. GLC2000: A new approach to global land cover mapping from Earth observation data. *Int. J. Remote Sens.* **2005**, *26*, 1959–1977. [CrossRef]
459. Walker, D.A.; Raynolds, M.K.; Daniëls, F.J.; Einarsson, E.; Elvebakk, A.; Gould, W.A.; Katenin, A.E.; Kholod, S.S.; Markon, C.J.; Melnikov, E.S.; et al. The circumpolar Arctic vegetation map. *J. Veg. Sci.* **2005**, *16*, 267–282. [CrossRef]
460. Farr, T.G.; Rosen, P.A.; Caro, E.; Crippen, R.; Duren, R.; Hensley, S.; Kobrick, M.; Paller, M.; Rodriguez, E.; Roth, L.; et al. The shuttle radar topography mission. *Rev. Geophys.* **2007**, *45*, RG2004. [CrossRef]
461. Takaku, J.; Tadono, T.; Tsutsui, K.; Ichikawa, M. Validation of “AW3D” global DSM generated from Alos Prism. *ISPRS Ann. Photogramm. Remote Sens. Spat. Inf. Sci.* **2016**, *3*, 25. [CrossRef]
462. Morin, P.; Porter, C.; Cloutier, M.; Howat, I.; Noh, M.J.; Willis, M.; Bates, B.; Williamson, C.; Peterman, K. ArcticDEM; a publically available, high resolution elevation model of the Arctic. In Proceedings of the EGU General Assembly 2016, Vienna, Austria, 17–22 April 2016; p. EPSC2016-8396.
463. Hengl, T.; Mendes de Jesus, J.; Heuvelink, G.B.; Ruiperez Gonzalez, M.; Kilibarda, M.; Blagotić, A.; Shangguan, W.; Wright, M.N.; Geng, X.; Bauer-Marschallinger, B.; et al. SoilGrids250m: Global gridded soil information based on machine learning. *PLoS ONE* **2017**, *12*, e0169748. [CrossRef]
464. Hugelius, G.; Bockheim, J.G.; Camill, P.; Elberling, B.; Grosse, G.; Harden, J.W.; Johnson, K.; Jorgenson, T.; Koven, C.; Kuhry, P.; et al. A new data set for estimating organic carbon storage to 3 m depth in soils of the northern circumpolar permafrost region. *Earth Syst. Sci. Data (Online)* **2013**, *5*, 393–402. [CrossRef]
465. FAO; IIASA; ISRIC; ISSCAS; JRC. Harmonized World Soil Database (version 1.2). FAO, Rome, Italy and IIASA, Laxenburg, Austria. 2012. Available online: http://webarchive.iiasa.ac.at/Research/LUC/External-World-soil-database/HTML/HWSD_Data.html?sb=4 (accessed on 11 September 2020).
466. FAO; IIASA.; ISRIC.; ISSCAS.; JRC. Harmonized World Soil Database v 1.2. 2020. Available online: <http://www.fao.org/soils-portal/soil-survey/soil-maps-and-databases/harmonized-world-soil-database-v12/en/> (accessed on 11 September 2020).
467. Dorigo, W.; Gruber, A.; De Jeu, R.; Wagner, W.; Stacke, T.; Loew, A.; Albergel, C.; Brocca, L.; Chung, D.; Parinussa, R.; et al. Evaluation of the ESA CCI soil moisture product using ground-based observations. *Remote Sens. Environ.* **2015**, *162*, 380–395. [CrossRef]
468. Kim, Y.; Kimball, J.S.; Glassy, J.M.; Du, J. An extended global Earth system data record on daily landscape freeze–thaw status determined from satellite passive microwave remote sensing. *Earth Syst. Sci. Data* **2017**, *9*, 133–147. [CrossRef]
469. Brown, J.; Hinkel, K.M.; Nelson, F. The circumpolar active layer monitoring (CALM) program: Research designs and initial results. *Polar Geogr.* **2000**, *24*, 166–258. [CrossRef]
470. Luo, L.; Zhang, Z.; Ma, W.; Yi, S.; Zhuang, Y. PIC v1. 3: Comprehensive R package for computing permafrost indices with daily weather observations and atmospheric forcing over the Qinghai–Tibet Plateau. *Geosci. Model Dev.* **2018**, *11*, 2475–2491. [CrossRef]
471. Haas, A.; Grosse, G.; Heim, B.; Schäfer-Neth, C.; Laboor, S.; Nitze, I.; Bartsch, A.; Seifert, F.M. PerSYS—Permafrost Information System Web-GIS: Visualization of permafrost-related Remote Sensing products for ESA GlobPermafrost. In Proceedings of the 2nd Asian Conference On Permafrost, Hokkaido University, Sapporo, Japan, 2–6 July 2017.
472. Diepenbroek, M.; Grobe, H.; Reinke, M.; Schindler, U.; Schlitzer, R.; Sieger, R.; Wefer, G. PANGAEA—An information system for environmental sciences. *Comput. Geosci.* **2002**, *28*, 1201–1210. [CrossRef]
473. National Snow and Ice Data Center (NSIDC). National Snow and Ice Data Center. 2020. Available online: <https://nsidc.org/> (accessed on 25 September 2020).
474. Gorelick, N.; Hancher, M.; Dixon, M.; Ilyushchenko, S.; Thau, D.; Moore, R. Google Earth Engine: Planetary-scale geospatial analysis for everyone. *Remote Sens. Environ.* **2017**, *202*, 18–27. [CrossRef]
475. Nyland, K.E.; Gunn, G.E.; Shiklomanov, N.I.; Engstrom, R.N.; Streletskiy, D.A. Land cover change in the lower Yenisei River using dense stacking of landsat imagery in Google Earth Engine. *Remote Sens.* **2018**, *10*, 1226. [CrossRef]
476. Langford, Z.L.; Kumar, J.; Hoffman, F.M.; Breen, A.L.; Iversen, C.M. Arctic vegetation mapping using unsupervised training datasets and convolutional neural networks. *Remote Sens.* **2019**, *11*, 69. [CrossRef]

477. Zhang, W.; Liljedahl, A.K.; Kanevskiy, M.; Epstein, H.E.; Jones, B.M.; Jorgenson, M.T.; Kent, K. Transferability of the Deep Learning Mask R-CNN Model for Automated Mapping of Ice-Wedge Polygons in High-Resolution Satellite and UAV Images. *Remote Sens.* **2020**, *12*, 1085. [[CrossRef](#)]
478. Zhang, W.; Witharana, C.; Liljedahl, A.K.; Kanevskiy, M. Deep convolutional neural networks for automated characterization of arctic ice-wedge polygons in very high spatial resolution aerial imagery. *Remote Sens.* **2018**, *10*, 1487. [[CrossRef](#)]
479. Bartsch, A.; Pointner, G.; Ingeman-Nielsen, T.; Lu, W. Towards Circumpolar Mapping of Arctic Settlements and Infrastructure Based on Sentinel-1 and Sentinel-2. *Remote Sens.* **2020**, *12*, 2368. [[CrossRef](#)]
480. Brothers, L.L.; Hart, P.E.; Ruppel, C.D. Minimum distribution of subsea ice-bearing permafrost on the US Beaufort Sea continental shelf. *Geophys. Res. Lett.* **2012**, *39*, L15501. [[CrossRef](#)]
481. Taylor, A.E. Marine transgression, shoreline emergence: Evidence in seabed and terrestrial ground temperatures of changing relative sea levels, Arctic Canada. *J. Geophys. Res. Solid Earth* **1991**, *96*, 6893–6909. [[CrossRef](#)]
482. Rachold, V.; Bolshiyanov, D.Y.; Grigoriev, M.N.; Hubberten, H.W.; Junker, R.; Kunitsky, V.V.; Merker, F.; Overduin, P.; Schneider, W. Nearshore Arctic subsea permafrost in transition. *Eos Trans. Am. Geophys. Union* **2007**, *88*, 149–150. [[CrossRef](#)]
483. Angelopoulos, M.; Overduin, P.P.; Miesner, F.; Grigoriev, M.N.; Vasiliev, A.A. Recent advances in the study of Arctic submarine permafrost. *Permafr. Periglac. Process.* **2020**, *31*, 442–453. [[CrossRef](#)]
484. Myers-Smith, I.H.; Kerby, J.T.; Phoenix, G.K.; Bjerke, J.W.; Epstein, H.E.; Assmann, J.J.; John, C.; Andreu-Hayles, L.; Angers-Blondin, S.; Beck, P.S.; et al. Complexity revealed in the greening of the Arctic. *Nat. Clim. Chang.* **2020**, *10*, 106–117. [[CrossRef](#)]
485. Kokelj, S.V.; Jorgenson, M. Advances in thermokarst research. *Permafr. Periglac. Process.* **2013**, *24*, 108–119. [[CrossRef](#)]